DISSERTATION

PHOTOPROTECTIVE ACCLIMATION OF XANTHOPHYLL PIGMENTS TO HIGH LIGHT IN MARINE DIATOMS

2015

SOKA UNIVERSITY

GRADUATE SCHOOL OF ENGINEERING

TOMOYO KATAYAMA

PHOTOPROTECTIVE ACCLIMATION OF XANTHOPHYLL PIGMENTS TO HIGH LIGHT IN MARINE DIATOMS

MARCH 2015

TOMOYO KATAYAMA

SOKA UNIVERSITY

Author: Tomoyo Katayama

Title: Photoprotective acclimation of xanthophyll pigments to high light in marine diatoms

Department: Environmental Engineering for Symbiosis
Faculty: Engineering
Degree: Ph.D.
Convocation: March 2015

We certify that we have read this dissertation and that, in our opinion, it is satisfactory in scope and quality as a dissertation for the degree of Doctor of Philosophy in Engineering.

February 2015

DISSERTATION COMMITTEE

Dr. Satoru Taguchi

Dr. Norio Kurosawa

Dr. Koji Suzuki

CONTENTS

page

ACKNOWLEDGEMENTS i

ABSTRACT iii

NOTATION x

CHAPTER I GENERAL INTRODUCTION 1

1.1. Light variation in the habitat of diatoms 1

1.2. Photoprotection in diatoms 3

1.3. Aims and scope of this study 6

1.4. Structure of the thesis 6

Figures 8

CHAPTER II PHOTOPROTECTION TO HIGH LIGHT IN MARINE DIATOM SPECIES 10

2.1. Introduction 10

2.2. Materials and methods 12

2.3. Results 21

2.3.1. Dark-light transition experiments 21

2.3.2. High light exposure experiments 25

2.4. Discussion 29

2.4.1. Dark-light transition experiments on a timescale of days 29

2.4.2. High light exposure experiments on a short timescale of minutes to hours 33

2.4.3. Conclusions 38

Tables 40

Figures 51

CHAPTER III PHOTOPROTECTION TO HIGH LIGHT IN NATURAL ASSEMBLAGES OF ICE ALGAE 77

3.1. Introduction 77

3.2. Materials and methods 80

3.3. Results 87

3.3.1. Characteristics of sea ice 87

3.3.2. High light exposure experiments 87

3.3.3. Dark recovery experiments 90

3.3.4. Comparison of photoprotective responses between ice algal community and mesophilic diatoms 90

3.4. Discussion 93

3.4.1. High light exposure experiments 93

3.4.2. Dark recovery 97

3.4.3. Conclusions 98

Tables 99

Figures 108

CHAPTER IV GENERAL CONCLUSIONS 126

4.1. Thermal dissipation through xanthophyll cycle 126

4.2. Relaxation of photodamage 127

4.3. Conclusions 127

4.4. Implication 128

Figures 131

REFERENCES 132

ACKNOWLEDGMENTS

I am grateful to Professor Satoru Taguchi for his guidance, helpful support, and numerous suggestions and discussions throughout the course of this study. I would like to gratefully acknowledge Professor Norio Kurosawa and Associate Professor Koji Suzuki for their thorough discussion, valuable suggestions and review of this dissertation.

I express my sincere appreciation to Assistant Professor Ai Murata and Mitsuko Obata for their helpful guidance, suggestions and numerous supports. I offer my heartfelt thanks and gratitude to all members of the laboratory for their valuable discussions and inspiration, especially, Shozo Motokawa, Yumi Fuchinoue, Takako Gorai, Kayo Takimoto, and Yasuhiro Masuda.

I am indebted to Professor Hiroshi Hattori at Tokai University, Professor Yasushi Fukamachi at Hokkaido University for assisting me in the sampling of ice core at Saroma-Ko Lagoon, Hokkaido from 2012 to 2014. I would like to acknowledge Mr. Kimihiko Maekawa at Saroma-ko Aquaculture Research Center for providing the space for the experiments in Saroma-Ko Lagoon. I would like to thank Professor Tomohiko Kikuchi of Yokohama University for providing the research vessel *Tachibana* and assisting in the collecting of seawater.

I deeply thank my friends for their unlimited support, warmth, and friendship. I am most grateful to my family, Shuji Katayama, Tomoko Katayama, Takayo Katayama, Shinsuke Katayama, and Atsushi Katayama, for their encouragement, endless inspiration and supports throughout my life.

I am greatly indebted to the founder of Soka University: Dr. Daisaku Ikeda and Mrs. Kaneko Ikeda for their guidance, unlimited encouragement and numerous supports.

This work was partially supported by the Sasagawa Scientific Research Grant (25-706)

from Japan Science Society.

ABSTRACT

Diatoms are one of the major components of natural assemblages microalgae from polar to tropical marine ecosystem. They inhabit in the highly mixed surface water column in coastal waters. Diatoms are also dominant members of the sea ice algal community. Microalgal communities found in sea ice, known as ice algae, play also an important role in primary production in the sea ice ecosystem. Light intensity varies from extremely low or dark to relatively high in the ocean environment. For instance, ice algae, predominated by diatoms, might be exposed suddenly from extremely low light conditions at the bottom sea ice to high light conditions in surface water column. The similar situation in which diatoms have to survive in such sudden increase in irradiance can be also induced by anthropogenic causes such as releasing to surface water after transportation in ship's ballast.

Although light is an essential resource for the survival of diatoms, light can be also harmful and supra-optimal irradiance damages photosystem II (PSII) and reduce the maximum quantum efficiency of PSII (F_v/F_m). One mechanism of the most important protective acclimation against the high light intensity for diatoms is the thermal dissipation of excess energy by xanthophyll cycle pigments in their de-epoxidated state, diatoxanthin (DT). The DT absorbs the excitation energy from Chl *a* and plays a role in the thermal dissipation as a photoprotective pigment. Thermal dissipation of the excess energy absorbed in PSII can be quantified by estimating a non-photochemical quenching (NPQ) of Chl *a* fluorescence. The photoprotection through NPQ is known to be linearly dependent on the presence of DT for most marine diatoms. In the recent studies, the non-linear relationship between the molar ratio of DT to Chl *a* ($DT_{Chl\ a}$) and NPQ has been observed for a few species of mesophilic marine diatoms.

The non-linear relationship between $DT_{Chl\ a}$ and NPQ occurred mostly with the *de novo* synthesis of DT molecules. It is believed that the *de novo* synthesized DT molecules can be: 1) free in the lipid matrix, 2) free in the lipid matrix in the close vicinity to the PSII light-harvesting complexes antenna, and 3) bound to the light-harvesting complexes antenna system where they participate to NPQ. The *de novo* synthesized DT molecules, which is not bound to the light-harvesting complexes, may be not involved in the NPQ process. NPQ is induced by the DT synthesis through the xanthophyll cycle, which could lead to thermal dissipation, but also decreases in fluorescence yield due to damage of PSII reaction centers. Total NPQ refers to both the photoprotective processes and the damage to the reaction centers of PSII, which might result in the increase with quenching under high light conditions. However, most of previous studies reporting relationship between DT and NPQ after exposure to the high light have examined the total NPQ, not distinguished both the NPQ components: thermal dissipation (NPQ_{Fast}) and photoinhibitory (NPQ_{Slow}) components of NPQ.

Energy-dependent quenching and xanthophyll cycle are key mechanisms of photoprotective acclimation in the avoidance of high light stress in photosynthesis. The amount of xanthophyll cycling and NPQ protection can determine the ecological success of a species or group in a particular light climate, as well as can be an indicator for the species successions. Xanthophyll cycle of the photoprotective mechanism has been demonstrated in the laboratory, most often in monocultures but only a few studies have investigated its *in situ* development, on the natural microalgal community. There are a few studies of photoprotection on natural marine diatoms to natural irradiance based on the examination of NPQ in addition to xanthophyll cycle.

The present study investigated the photoprotective acclimation of marine diatoms to high light based on the xanthophyll cycle pigments and Chl *a* fluorescence of PSII in both controlled

laboratory experiments and natural environment studies. The objectives of the present study were (1) to examine the photoprotective responses to high light condition of mesophilic marine diatom species in the laboratory on a timescale of days, and (2) on a short timescale of minutes to hours in mesophilic marine diatom species in the laboratory and ice algal community in the natural environment. A further motivation of the present study was to provide the implication of high irradiance on the ecological success of a species or group in the coastal water.

When the dark-acclimated *Thalassiosira weissflogii* were transferred to light and dark cycle (L-D cycle), the cell density immediately increased to the maximum and was saturated after 2 days. The F_v/F_m reached its maximum value on either day 1 or day 2. Similar levels were observed on both days. The increases in cell density and F_v/F_m suggested that the ability to resume photosynthesis upon exposure to the high light is maintained regardless of the length of continuous darkness, and cells acclimate to high light condition within 2 days. NPQ reached the lowest level on day 1 following exposure to L:D cycle with increase in F_v/F_m. After reaching the low levels, NPQ increased and stayed at relatively constant levels on day 3 and 4. The $DT_{Chl\ a}$ decreased on either day 1 or day 2, which could be caused by rapid cell division at the beginning of the L-D cycle. Afterward $DT_{Chl\ a}$ increased until day 4. The longer exposure to the high light may enforce the cells going through photoprotection process, such as activation of xanthophyll cycle and non-photochemical quenching.

Prior to the exposure to high light on a short timescale of minutes to hours, the range of the ratio of DD and DT to Chl *a* ($[DD+DT]_{Chl\ a}$) in the mesophilic diatoms, *T. weissflogii*, *Chaetoceros muelleri*, and *T. pseudonana*, were similar to the range of ice algal communities. After the exposure to high light for 120 min, de-epoxidation of DD to DT occurred rapidly in both the mesophilic diatom species and ice algal communities. The range of initial rate constants (*k*) of

de-epoxidation of DD to DT for the first 10 minutes in the mesophilic diatom species were similar to the range of ice algal communities. The maximum values of the molar ratio of DT produced through xanthophyll cycle to Chl *a* ($DT^{XC}_{Chl\ a}$) after the light exposure in the mesophilic diatom species were higher than those in the ice algal communities. The results suggest that the xanthophyll cycle of DD to DT in the ice algal communities is less active than the mesophilic diatoms for long exposure time. Increase in $DT_{Chl\ a}$ with the increase in $(DD+DT)_{Chl\ a}$ in the mesophilic diatom species indicates the occurrence of the *de novo* DT synthesis. In contrast, the increase in $DT_{Chl\ a}$ without significant changes in the amount of $(DD+DT)_{Chl\ a}$ observed for the ice algal communities suggests that the lack of response of *de novo* DT synthesis to the light exposure. The occurrence of *de novo* DT synthesis in ice algal communities and mesophilic diatoms might be influenced by low temperature. To test this hypothesis, further studies are required to investigate the functional response of ice algal communities to various temperature.

Prior to the high light exposure, any NPQ was not identified in both mesophilic diatom species and ice algal communities. After the exposure to high light for 120 min, the range of NPQ in the mesophilic diatom species were similar to the range of ice algal communities. The NPQ saturated with the $DT_{Chl\ a}$ in the mesophilic diatom species, whereas significantly linear relationships between them was observed in the ice algal communities in the similar experimental durations. The saturated relationship might be influenced by *de novo* DT synthesis. When the contribution of the *de novo* synthesized $DT_{Chl\ a}$ to total $DT_{Chl\ a}$ is significantly sufficient, the relationship between $DT_{Chl\ a}$ and NPQ might become saturated. The linear relationship between $DT^{XC}_{Chl\ a}$ and NPQ for the mesophilic diatoms and ice algal communities suggests that NPQ is linearly dependent on the light-induced $DT^{XC}_{Chl\ a}$.

The slopes of the relationship between $DT_{Chl\ a}$ and NPQ, reflecting the quenching

efficiency of DT, were lower in the mesophilic diatom species than those in the ice algal communities. The larger proportions of NPQ_{Slow} in the total NPQ during the DT synthesis in the ice algal communities than those of the mesophilic diatom species suggest that some ice algal cells may be likely to overestimate the quenching efficiency of DT by the enhancement of NPQ_{Fast}.

The low F_v/F_m at 120 min could be indicative of the degree of photoinhibition. The significant relationship between the F_v/F_m and the ratio of E_k to PAR (E_k/PAR) suggests that the strong shade acclimated cells of ice algae are suffered from severe photoinhibition and consequently causes delay in the recovery of photosynthetic capacity in comparison to mesophilic diatom species. The F_v/F_m at the end of incubations was also significantly dependent upon the amounts of $DT_{Chl\ a}$, which suggest that the photoinhibition could be reduced by enhancement of $DT_{Chl\ a}$ due to the synthesis of $DT^{de\ novo}$ which might be bound to the light-harvesting complexes.

The significant negative linear relationships between the relative F_v/F_m and $DT^{XC}_{Chl\ a}$ in the ice algal communities, which were also observed in the mesophilic diatom species, indicates that the synthesis of DT^{XC} might assist to resist photodamage and the PSII reaction center could be damaged progressively during the light exposure even if some excess energy is dissipated through xanthophyll cycle. The steeper slopes of the relative F_v/F_m and $DT^{XC}_{Chl\ a}$ in the ice algal communities than those in the mesophilic diatom species suggest that the lower efficiency of thermal dissipation through $DT^{XC}_{Chl\ a}$ in the ice algal communities might contribute to increase in the energy arriving at the reaction center. The relationship between the relative F_v/F_m and $DT^{de\ novo}_{Chl\ a}$, which is observed only for mesophilic diatoms, suggests that the *de novo* synthesis of DT in the mesophilic diatom species might assist to resist photodamage. The gentler slope of the relative F_v/F_m and $DT^{XC}_{Chl\ a}$ than those of the relative F_v/F_m and $DT^{de\ novo}_{Chl\ a}$ in the mesophilic diatoms suggests that the photoprotective capacity to reduce the damage of PSII in the DT^{XC} is higher than

those in the $DT^{de\ novo}$. However, the logarithmical decrease in the relative F_v/F_m with $DT^{de\ novo}{}_{Chl\ a}$ could indicate that the accumulation of $DT^{de\ novo}$ prevents the further photodamage. The photoprotective acclimation in the ice algal cells are not appeared to enhance the antioxidant function through the *de novo* DT synthesis. Mesophilc diatoms might relax the photodamage with synthesis of $DT^{de\ novo}$ which are binded to the light-harvesting complexes.

Following 120 min exposure to the high light in the ice algal cells, the kinetics of the recovery in the F_v/F_m in darkness within 24 hrs are coincided with the epoxidation of DT to DD and the relaxation of NPQ. The recovery in the F_v/F_m is related to the F_v/F_m values at the end of light exposure experiments might suggest that the less photodamage of PSII under high light conditions, the more repair of the photodamaged PSII under dark condition.

In conclusions, photoprotective acclimations of low- or dark-acclimated mesophilic diatoms to the high light are appeared to enhance the thermal dissipation through the xanthophyll cycle after not only a period of days under L-D cycle but also within minutes to hours. The present study demonstrated that the activity of xanthophyll cycle at the beginning of the light exposure is regarded as similar regardless of difference in the ecological groups. However, the activity of xanthophyll cycle at the second half of the light exposure time could be lower in the ice algal communities than those in the mesophilic diatoms, resulting the smaller synthesis of DT^{XC} in the ice algal cells. Mesophilic diatoms could reduce the photodamage in PSII due to the excess light exposure through the *de novo* synthesis of DT as the antioxidant function in addition to the high photoprotective capacity of DT^{XC} as thermal dissipation of excess energy. The capability of photoprotective acclimation might be elevated by the synthesis of DT through the xanthophyll cycle and the *de novo* DT synthesis. In natural environments, the ice algal community are adapted to stable, low light conditions and then the transition to high light could damage severely when they

are released into surface water column in spring because they are lack of the *de novo* DT synthesis. Instead, ice algal cells have been evolved to aggregate and sink out of the surface layer rapidly. Therefore, in the shallow coastal waters or stratified waters under near- or complete darkness, the possibility in survive of the damaged ice algal cells could be predicted within the water column.

NOTATION

Term	Definition	Units
a_{vol}	Cellular light abosrption per unit volume	10^{-13} m^2 µm^{-3}
Chl *a*	Chlorophyll *a*	–
Chl a_{cell}	Cellular Chl *a* content	pg cell^{-1}
Chl a_{vol}	Cellular Chl *a* content per unit volume	fg µm^{-3}
Chl *c*	Chlorophyll *c*	–
DD	Diadinoxanthin	–
DD_{cell}	Cellular DD content	pg cell^{-1}
$DD_{Chl\ a}$	Molar ratio of DD to Chl *a*	mol (100 mol)$^{-1}$
DD+DT	Sum of DD and DT	–
$(DD+DT)_{Chl\ a}$	Molar ratio of DD+DT to Chl *a*	mol (100 mol)$^{-1}$
D:L-Exp	Dark-light transition experiment	–
DS-Exp	Dark storage experiment	–
DT	Diatoxanthin	–
DT_{cell}	Cellular DT content	pg cell^{-1}
$DT_{Chl\ a}$	Molar ratio of DT to Chl *a*	mol (100 mol)$^{-1}$
$DT^{de\ novo}$	DT molecules that are produced through *de novo* synthesis	–
$DT^{de\ novo}{}_{Chl\ a}$	Molar ratio of $DT^{de\ novo}$ to Chl *a*	mol (100 mol)$^{-1}$
DT^{XC}	DT molecules that are produced through xanthophyll cycle	–
$DT^{XC}{}_{Chl\ a}$	Molar ratio of DT^{XC} to Chl *a*	mol (100 mol)$^{-1}$
ETR_{max}	Light-saturated rate of RLC	µmol e$^-$ (mg Chl *a*)$^{-1}$ s^{-1}
E_k	Light-saturation index	µmol photons m^{-2} s^{-1}
E_k/PAR	Ratio of E_k to PAR	Dimensionless
ETR	Electron transport rate	µmol e$^-$ (mg Chl *a*)$^{-1}$ s^{-1}
F	Minimum fluorescence under light condition	Instrument units

NOTATION

Term	Definition	Units
F_0	Minimum fluorescence measured in darkness	Instrument units
F_m	Maximal fluorescence measured in darkness	Instrument units
F'_m	Maximal fluorescence under light condition	Instrument units
F_m^r	Maximal fluorescence measured after relaxation removing the actinic light in darkness	Instrument units
F_v/F_m	Maximum quantum efficiency defined by $(F_m-F_0)/F_m$	Dimensionless
HL-Exp	High light exposure experiment	−
k	Initial rate constant of de-epoxidation of DD to DT	min^{-1}
LHP	Light-harvesting pigments	−
LHP_{cell}	Cellular LHP content	pg $cell^{-1}$
$LHP_{Chl\ a}$	Molar ratio of LHP to Chl *a*	mol $(100\ mol)^{-1}$
NPQ	Non-photochemical quenching defined by $(F_m-F'_m)/F'_m$	Dimensionless
NPQ_{Fsst}	Fast relaxing NPQ defined by $(F_m/F'_m) - (F_m/F_m^r)$	Dimensionless
NPQ_{Slow}	Slowly relaxing NPQ defined by $(F_m-F_m^r)/F_m^r$	Dimensionless
PAR	Photosynthetically active radiation	μmol photons m^{-2} s^{-1}
PPFD	Photosynthetic photon flux density	μmol photons m^{-2} s^{-1}
PSI	Photosystem I	−
PSII	Photosystem II	−
rETR	Relative electron transport rate	μmol e^- s^{-1}
R-Exp	Recovery experiment	−
RLC	Rapid light curve that are measured by plotting the ETR or rETR against the actinic PPFD	−
$S^{de\ novo}$	Slope of relationship between relative F_v/F_m and $DT^{de\ novo}_{Chl\ a}$ that means photoprotective capacity of $DT^{de\ novo}$ through antioxidant function	Dimensionless
S^{XC}	Slope of relationship between relative F_v/F_m and $DT^{XC}_{Chl\ a}$ that means photoprotective capacity of DT^{XC} through thermal dissipation	Dimensionless

NOTATION

Term	Definition	Units
V	Cell volume	μm^3 $cell^{-1}$
α	Light-limited slope of RLC	m^2 (mg Chl *a*)$^{-1}$ µmol e^- (µmol photons)$^{-1}$
$\Delta F/F'_m$	PSII operating efficiency	Dimensionless
μ	Growth rate	d^{-1}

CHAPTER I

GENERAL INTRODUCTION

1.1. Light variation in the habitat of diatoms

Primary productivity in aquatic environments accounts for approximately 45% of global primary productivity (Falkowski 1994). However, the total biomass of aquatic photosynthetic producers is less than 1% of the total photosynthetic biomass on our planet (Field et al. 1998). Aquatic photosynthetic producers, such as the natural phytoplankton assemblages, are responsible for the largest fraction of net primary production of marine ecosystems (Duarte and Cebrián 1996). Diatoms are a major component of the natural phytoplankton assemblages from tropical to polar marine ecosystem and account for approximately 40% of marine primary producers (Nelson et al. 1995). Diatom blooms occur extensively in the spring along the coastal areas of middle to high latitudes in the Northern Hemisphere (Smayda 1980). Diatoms inhabit in highly vertically mixed surface water column in coastal waters that are subjected to large fluctuations in irradiance (Jerlov 1976, Cullen and Lewis 1988). In middle latitude ocean, the situation in which diatoms have to survive in such sudden increase in irradiance is less common in the natural environment, but can be induced by anthropogenic causes such as releasing to surface water after transportation in ship's ballast (Medcof 1975). In high latitude oceans, primary production of pelagic phytoplankton in the ice-free waters and in the under-ice water columns is a major partitioning of total production in the sea ice ecosystems (Kirst and Wiencke 1995), whereas ice algal communities found mainly in the bottom surface of sea ice play an important role in primary production in the sea ice ecosystem, forming the energy base of the marine food web in ice-covered waters (Bluhm et al. 2010). In spring ice algal communities predominated by diatoms are released from retreating sea ice into

surface water column. Some ice algal communities might be exposed suddenly from extremely low light conditions at the bottom sea ice, often <1% of the surface irradiance (Arrigo et al. 1993), to high light conditions in surface water column.

The availability of light is one of the major factors controlling the growth of diatoms because of use of light as an energy source via photosynthesis. However, natural assemblages of diatoms may need to endure prolonged periods of near- or complete darkness (McMinn and Martin 2013). Numerous species of diatoms are able to withstand the absence of light for weeks to months at a time (*e.g.*, Antia 1976). Several mechanisms for the survival of marine diatoms under dark conditions have been proposed, including the formation of resting cells (Anderson 1975, Sicko-Goad et al. 1989) and heterotrophic nutrition (Lewin and Lewin 1960, Palmisano and Sullivan 1982). However, for the ubiquitous diatoms *Asterionella japonica* (Smayda 1958) and *Thalassiosira weissflogii* (McQuoid and Hobson 1996), the formation of resting cells and heterotrophy do not appear necessary for survival in prolonged darkness although reduced respiratory activity could be occurred. Diatoms have been shown to sustain their capability for photosynthesis and growth via dark-adapted survival strategies (Peters 1996).

Although light is an essential resource for the survival of diatoms, light can also be harmful and supra-optimal irradiance can lead to a variety of harmful reactions, some of which produce reactive oxygen species (Melis 1999). This phenomenon has potential to damage photosystem II (PSII) by photo-oxidation and reduces the photosynthetic electron transport capacity (Adams et al. 2006). Photo-oxidative damage of PSII can lead to degradation of D1 protein of PSII reaction centers (Melis 1999, Domingues et al. 2012), which binds the primary electron donors and acceptors in PSII. Marine diatoms evolved to adapt to high light to reduce harmful damage as becoming predominant microalgae in coastal ecosystems (Depauw et al. 2012).

1.2. Photoprotection in diatoms

One of the most important protective mechanisms used by diatoms against the high light intensity is the thermal dissipation of excess energy absorbed in PSII. It takes place in the light-harvesting complex antennae (LHC) of PSII (Ruban et al. 2012). The thermal dissipation of the excess energy absorbed in PSII under high irradiance conditions can be quantified by estimating a non-photochemical quenching (NPQ) of Chl *a* fluorescence. NPQ consists of a high-energy-state quenching (qE: NPQ_{Fast}), a state-transition (qT) and a photoinhibitory component (qI: NPQ_{Slow}) (Li et al. 2009). In diatoms, however, quenching related to state-transition has not been found (Goss and Jakob 2010). Under most conditions, the major contributor to NPQ is NPQ_{Fast}. The process of NPQ_{Slow} is thought to dissipate excess absorbed light energy as heat (Maxwell and Johnson 2000) and be essential in protecting the PSII from light-induced damage. This process requires the presence of a low pH in the lumen of the thylakoid and involves the light-induced formation of xanthophyll cycle pigments in their de-epoxidated state. In addition, the induction of NPQ_{Fast} is essential for the presence of specific nucleus-encoded antenna proteins, called LHCX (Bailleul et al. 2010), which is enhanced by blue-light (Schellenberger Costa et al. 2013). NPQ_{Slow} refers to the damage of PSII reaction centers (Osmond 1994). In diatoms, NPQ seemed to be closely correlated to the presence of xanthophyll cycle pigments in their de-epoxidated state, diatoxanthin (DT) (Jakob et al. 1999; Lavaud et al. 2002; Goss et al. 2006). Xanthophyll cycle pigments in diatoms consist predominantly of diadinoxanthin (DD) and DT (Fig. 1-1) (Demers et al. 1991, Moisan et al. 1998). In general, DD in the light-harvesting antenna transfers the excitation energy to chlorophyll *a* (Chl *a*) and plays a role in the acquisition of light energy as a photosynthetic light-harvesting pigment, whereas DT in the light-harvesting antenna absorbs the excitation energy from Chl *a* and plays a role in the thermal dissipation as a photoprotective pigment (Fig. 1-2) (Young et al. 1997, Harris et

al. 2009). The DD de-epoxidation began rapidly after the onset of high light and then some of DT, which is independent of DD de-epoxidation, was synthesized in mesophilic diatoms (Olaizola et al. 1994, Lavaud et al. 2004), which is regarded as *de novo* DT synthesis. Although the many previous studies observed that the relationship between the molar ratio of DT to Chl *a* and NPQ is linear in laboratory-cultivated marine diatoms (Jakob et al. 1999; Lavaud et al. 2002; Goss et al. 2006), a non-linear relationship for the marine diatom *Thalassiosira weissflogii* was reported by Lavaud et al. (2004). In the recent studies, the non-linear relationship has been also observed for a few species of marine diatoms (Lavaud et al. 2012, Lavaud and Lepetit 2013), which had been previously thought to have a linear relationship.

The non-linear relationship between DT and NPQ occurs mostly when the *de novo* synthesis of DT molecules is involved (Lavaud et al. 2004). The DT molecules that are produced through *de novo* synthesis are distributed among several pools which show a spatial and functional heterogeneity (Fig. 1-2) (Lepetit et al. 2010). It is believed that the *de novo* synthesized DT can be: 1) free in the lipid matrix of the thylakoid membranes, 2) free in the lipid matrix of the thylakoid membranes in the close vicinity to the PSII light-harvesting complexes antenna, and 3) bound to the light-harvesting complexes antenna system where they participate to NPQ. The *de novo* synthesized DT molecules, which is not bound to the light-harvesting complexes, may be not involved in the NPQ process (Schumann et al. 2007). It is important to note that total NPQ includes the photoprotective processes through thermal dissipation of excess energy (NPQ_{Fast}) and to the damage of PSII reaction centers (NPQ_{Slow}). The enhancement of NPQ_{Slow} might result in the increase with quenching under high light conditions. However, most of previous studies regarding relationship between DT and NPQ after exposure to the high light have examined the total NPQ, not distinguished both the NPQ components, including NPQ_{Fast} and NPQ_{Slow}.

Energy-dependent quenching and xanthophyll cycle are key mechanisms of photoprotective acclimation in the avoidance of high light stress in photosynthesis. The photoprotection through NPQ and xanthophyll cycling can determine the ecological success of a species or group in a particular light climate (Meyer et al. 2000, Dimier et al. 2007, Lavaud et al. 2007, Dimier et al. 2009, Kropuenske et al. 2010, van de Poll et al. 2011). Xanthophyll cycle in the photoprotective mechanism has been demonstrated in the laboratory, most often in monocultures (*e.g.*, Lavaud et al. 2002, 2003, 2004) but only a few studies have investigated its *in situ* development, on the natural microalgal community (Griffith et al. 2009, Chevalier et al. 2010). There are a few studies of photoprotection on natural marine diatoms to natural irradiance based on the examination of NPQ in addition to xanthophyll cycle (van de Poll et al. 2011). We understand little about the rapid photoprotective response of ice algae to high light condition in water column partly because of limitation on logistics in ice fields where people and transportation have to be supported (Kudoh et al. 2003, Petrou et al. 2011). Thus without solid evidence, the concept of 'seeding' of spring bloom in surface water column by ice algae released from the melting sea ice has been discussed for decades by various researchers (*e.g.*, Ackley et al. 1979, Smith and Nelson 1986). Whether or not these sea ice algae function as a seed population depends on various factors, including the viability of the cells once released from the sea ice, the sinking speed at which the cells settle through the water column, and the presence of herbivores in the water column (Takahashi et al. 2015). Under conditions where algae released from the sea ice remain in suspension in the upper water column and are not grazed, the possibility of seeding still exists. Cells that are suspended in the surface water column are exposed to high light, which usually cause photoinhibition. If ice algae that are released from the ice could reduce the high light stress in photosynthesis through photoprotective mechanisms, cells could quickly recover photosynthetic

capacity (Petrou et al. 2010) and there might be a high possibility of the ice algae in the seeding of spring bloom.

1.3. Aims and scopes of this study

The present study investigated the photoprotection of marine diatoms based on the xanthophyll cycle pigments and Chl *a* fluorescence of PSII in both controlled laboratory experiments and natural environment studies. A further motivation of the present study was to provide the implications of the ecological success of a species or group in the coastal water.

The objectives of the present study were to examine the photoprotective responses of marine planktonic diatom species to high light condition controlled in the laboratory and natural ice algal community to natural sunlight. I used three diatoms of coastal species, such as *Thalassiosira weissflogii*, *Chaetoceros muelleri*, and *T. pseudonana*, and the natural assemblages of ice algae. The biomass of ice algal community, measured as Chl *a*, is extremely large (Arrigo et al. 1993) and they are dominated by diatoms. The well-established ice algal community can be considered as the most representative community for the measurement of Chl *a* fluorescence in a field, which is otherwise usually undetectable due to lower Chl *a* concentrations in the sea. Although it would be premature to suggest the validity of the implication on the basis of this data alone, it is certain that this data will at least provide us with the basis for further research on the photoprotection of natural assemblages of microalgae.

1.4. Structure of the thesis

For the sake of simplicity, this thesis including this general introduction and review has been divided into four chapters. In this chapter, the reviews of the photoprotection of diatoms have

been presented and the aims of the present study have been explained. In the second chapter, studies on the response of the protection to high light levels in marine diatom species of laboratory monocultures have been presented. In the third chapter, studies on the protection to high light levels in diatom dominated ice algal community in the field have been presented. Finally, in the fourth chapter, a summary of the overall photoprotection of marine diatoms has been presented by elucidating the protection to high light conditions, and the discussion of the phoprotection in marine diatoms based on the present study have been presented and requirements for future research are highlighted.

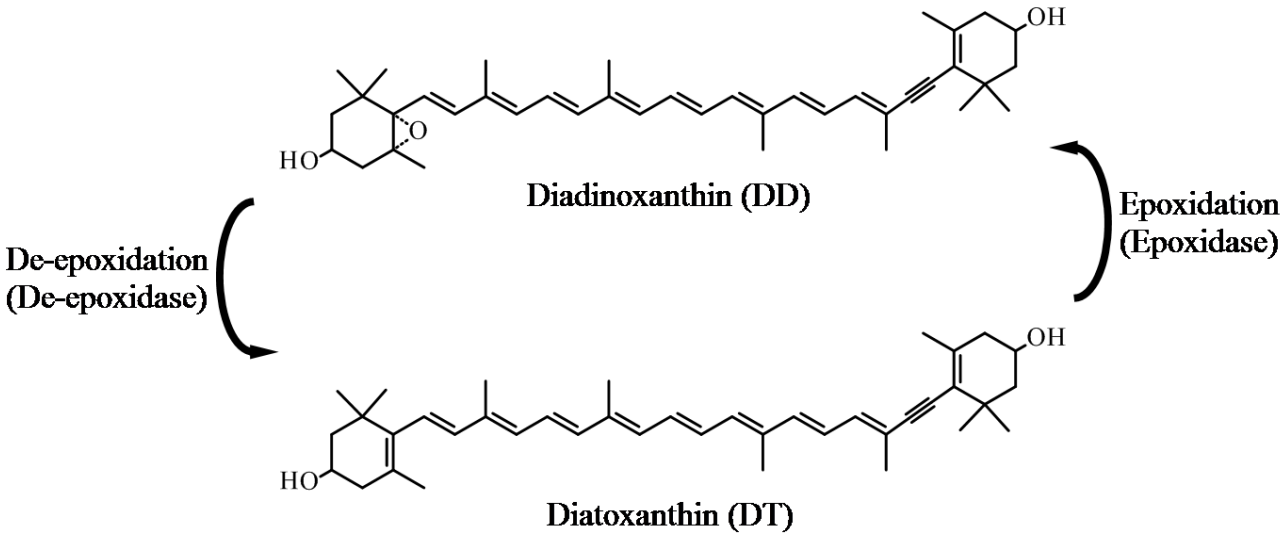

Figure 1-1. The xanthophyll cycle and their characteristics of diatoms (modified from Wilhelm et al. 2006). This figure also shows the enzymes catalyzing the de-epoxidation reaction (de-epoxidase) and the epoxidation reaction (epoxidase), which transform xanthophyll cycle pigments into either diadinoxanthin, DD or diatoxanthin, DT.

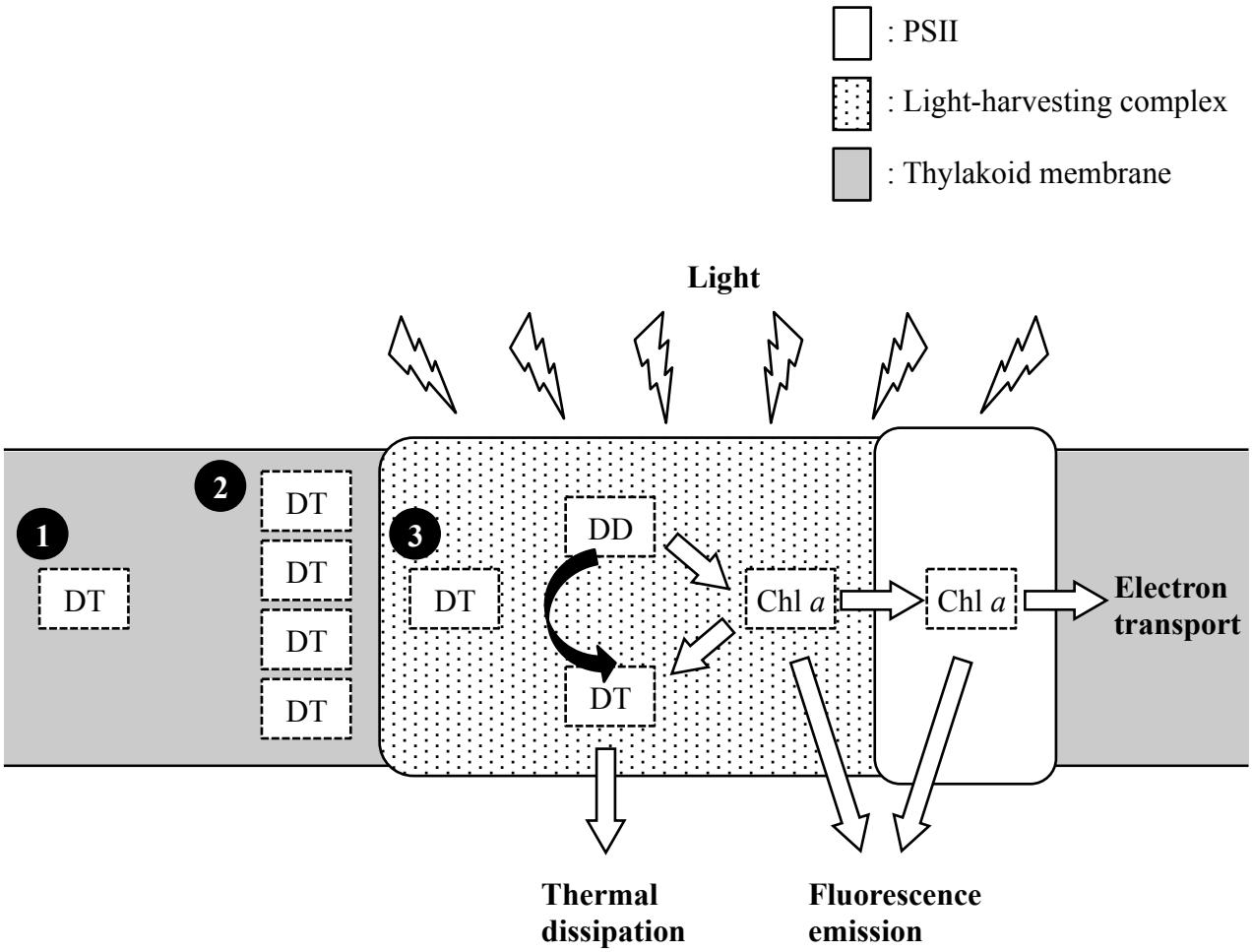

Figure 1-2. Allocation of absorbed light energy among fluorescence emission, electron transport, and thermal dissipation in PSII and the distribution of $DT^{de\ novo}$ molecules. It is believed that the $DT^{de\ novo}$ can be: 1) free in the lipid matrix of the thylakoid membrane, 2) free in the lipid matrix of the thylakoid membrane in the close vicinity to the PSII light-harvesting complexes antenna, and 3) bound to the light-harvesting complexes antenna system.

Chapter II

PHOTOPROTECTION TO HIGH LIGHT IN MARINE DIATOM SPECIES

2.1. Introduction

Marine diatoms could dissipate excess heat through xanthophyll cycle as photoprotective mechanisms to reduce the photoinhibition, which cause the decrease in the maximum quantum efficiency of PSII (F_v/F_m). Photoprotective responses to high light conditions have been studied on several marine diatom species with conflicting results. For example, in a number of planktonic diatoms, such as *Phaeodactylum tricornutum*, *Skeletonema costatum*, *Cylindrotheca fusiformis*, and *Ditylum brightwellii*, a linear relations between the molar ratio of DT to Chl *a* and NPQ have been reported in laboratory-controlled light conditions (Lavaud et al. 2002, Lavaud et al. 2004, Goss et al. 2006), whereas *Thalassiosira weissflogii* has a non-linear relationship (Lavaud et al. 2004). Several recent studies demonstrated that a non-linear relationship has been also observed for mesophilic diatoms *P. tricornutum* (Lavaud et al. 2012) and *S. costatum* (Lavaud and Lepetit 2013), which had been previously reported to have linear relationship. The relationship between the light-induced DT and NPQ might be species dependent.

The NPQ is composed of two different components in diatoms (Maxwell and Johnson 2000). The first component (NPQ_{Fast}) is induced by the DT synthesis through xanthophyll cycle, which could lead to heat dissipation. The second NPQ component (NPQ_{Slow}) can decrease the fluorescence yield due to damage of PSII reaction centers. Thus, the total NPQ involves with the photoprotective processes and the photoinhibition (Osmond 1994). However, most of previous studies have examined total NPQ, but not distinguished the NPQ components. To understand the contribution of each NPQ components to the total NPQ, the present study examined the dynamics

of each NPQ divided between photoprotective processes and photoinhibition under high light condition and compared the changes in the NPQ components with DT production.

There is a succession of species during spring bloom which progress from large diatom species to small diatom species (Smayda 1980). The amount of DT synthesis through xanthophyll cycle and NPQ can determine the ecological success of a species or group in a particular light climate (Lavaud et al. 2007, Dimier et al. 2009, Kropuenske et al. 2010, van de Poll et al. 2011), as well as can be an indicator for the species successions (Meyer et al. 2000, Dimier et al. 2007). Dimier et al. (2007) showed that there is a clear dependence of the maximum value of NPQ in three diatoms species not only on their habitats, but also on their seasonal distribution. They observed that the blooming diatom species in low light conditions during the late winter season in coastal waters responded to high light exposure with the low NPQ values, whereas the spring-blooming diatom species in highly dynamic light conditions in coastal water showed the low NPQ values. Cell size should be also one of the most important factors to understand phoroprotective responses. Cell size might have a potentially influence on the phoroprotective responses with the amount of xanthophyll cycle and NPQ. However, the possibility for a correlation of photoprotective responses and cell size has not yet been explored. In the present study, I investigated whether the amplitude and regulation of phoroprotective responses for marine diatoms are related to cell size.

In order to investigate the photoprotective responses of marine diatoms to high light conditions, the responses of xanthophyll pigments and NPQ of three coastal species in the laboratory were determined. I used *T. weissflogii*, which previously observed a non-linear relationship between the molar ratio of DT to Chl *a* and NPQ, and *Chaetoceros muelleri* and *T. pseudonana* of which the linearity of relationships were not known, as different cell sizes.

2.2. Materials and methods

2.2.1. Dark-light transition experiments

Bacillariophyceae *Thalassiosira weissflogii* [Grunow] G. Fryxell & Hasle (CCMP1336) was obtained from the National Center for Marine Algae and Microbiota, USA. Cells were maintained at 20˚C at a salinity of 35 in filter-sterilized, aged seawater enriched with f/2 medium (Guillard and Ryther 1962) and illuminated with a 12-h light and 12-h cycle (L-D cycle) at a photosynthetic photon flux density of 300 μmol photons m^{-2} s^{-1} provided by cool fluorescent tube. Irradiance was measured with a 4π sensor (Biospherical Instruments, QSL-100, USA). Our experimental designs were consisted of the following consecutive four incubations; the precondition to L-D cycle at 300 μmol photons m^{-2} s^{-1}, the dark condition, the short exposure to the L-D cycle, and subsequent exposure to the same L-D cycle. The cell division in those periods corresponded to dividing cells, no-dividing cells, dividing cells, and light-saturated no-dividing cells. Cells were preconditioned in a batch culture at least three times by transferring half of the initial culture during the exponential growth phase into new media every 2 days. Cells acclimated to a L-D cycle for 6 days were inoculated into eighteen dark bottles in filter-sterilized, aged seawater enriched with new f/2 medium for the dark storage experiment (DS-Exp). The initial cell density was adjusted to 7-8 × 10^3 cells ml^{-1}. Cells were incubated in the dark at 20˚C for 14 days in sterilized screw-top polycarbonate dark bottles; the cultures were slowly stirred, and the lids of bottles were unscrewed to capture air daily. Special attention was paid to maintaining complete darkness during the entire experimental period. On days 1, 5, and 11, a set of three dark bottles was randomly selected from the DS-Exp. On days 3, 8, and 14, a set of three dark bottles was randomly selected and used in the recovery experiments (R-Exp) after samples were taken for dark storage measurements. The dark duration was employed to allow the cells to recover from some stress caused by the irradiance of

300 μmol photons m^{-2} s^{-1} that was provided during the pre-incubation. The R-Exp was initiated by exposing the dark-acclimated cells in the three dark bottles to a L-D cycle of 300 μmol photons m^{-2} s^{-1} at 20˚C on days 3, 8, and 14. The bottles were inoculated with silicate in concentrations of 0, 10, or 130 μM, respectively. The total numbers of the R-Exp were nine. The stock solution of silicate was prepared by dissolving 0.284 g $Na_2SiO_3 \cdot 9H_2O$ into 100 ml distilled water. Subsequently, 0.74 ml and 9.6 ml of the stock solution were added to provide the addition of 10 and 130 μM of silicate. Changes in pH were minimal in the addition of stock solution. These experiments were named the +10 μM-Exp and +130 μM-Exp, respectively. All equipment and media were carefully autoclaved prior to the experiments.

On days 1, 3, 5, 8, 11, and 14 in the DS-Exp, triplicate subsamples were taken from each set of three dark bottles. These subsamples were used for measurements of nutrients, cell density, pigments, and variable Chl *a* fluorescence. On days 0, 1, 2, 3, and 4 in the R-Exp initiated on days 3, 8, and 14 of the DS-Exp, triplicate subsamples were taken from each set of three light bottles for the same measurements as in the DS-Exp.

2.2.2. High light exposure experiments

Bacillariophyceae *Thalassiosira weissflogii* [Grunow] G. Fryxell & Hasle (CCMP1336) was obtained from the National Center for Marine Algae and Microbiota, USA while *Chaetoceros muelleri* Lemmermann (CS-176) and *T. pseudonana* [Hustedt] Hasle et Heimdal (CS-173) were obtained from the CSIRO Algal Culture Collection, Australia. Cells were maintained at 20˚C at a salinity of 32 in filter-sterilized, aged seawater enriched with f/2 medium (Guillard and Ryther 1962) and illuminated with a 12-h light and 12-h cycle (L-D cycle) at a photosynthetic photon flux density of 40 μmol photons m^{-2} s^{-1} provided by cool fluorescent tube. Irradiance was measured

with a 4π sensor (Biospherical Instruments, QSL-100, USA). Prior to experiments, cells were preconditioned in a batch culture by transferring the initial culture during the exponential growth phase into new media, at least three times.

Cells acclimatized to low light condition (40 μmol photons m^{-2} s^{-1}) were inoculated into a polycarbonate bottle in filter-sterilized, aged seawater enriched with new f/2 medium for the high light exposure experiment (HL-Exp). The HL-Exp was started by exposing on the cells in exponential growth to 900 μmol photons $^{-2}$ s^{-1} and conducted at three times for each species. Subsamples were collected at 1, 3, 5, 10, 15, 30, 60, 90, and 120 min to measure pigments and variable Chl fluorescence. Prior to the high light exposure, subsamples were taken for measurements of cell abundance and volumes, and light absorption. Subsamples for cell volume were collected from a different bottle from those of HL-Exp.

2.2.3. Nutrients analysis

Subsamples for the analysis of nitrate, phosphate, and silicate were filtered through GF/F glass fiber filters (Whatman, USA) and the filtrates were stored in the dark at −20°C until further analysis. Concentrations of nitrate, phosphate, and silicate were determined using an auto-analyzer (SWAAT, BL-TEC, Japan) following the methods of Parsons et al. (1984).

2.2.4. Measurement of cell abundance and volume

Subsamples for cell densities were fixed with buffered 4% formaldehyde solution and stored in the dark at 4°C until further analysis (Iwasawa et al. 2009). Cell abundances of three species were determined under an inverted microscope (IMT-2, Olympus, Japan) (Hasle 1978). Growth rate (μ, day^{-1}) after the dark-light transition experiments (D:L-Exp) was estimated using the

following exponential growth equation (Guillard and Siercki 2005):

$$\mu = \ln(N_1/N_0)/(t_1 - t_0) \quad (2.1)$$

where N_0 and N_t are cell density at the beginning of (t_0) and 48 h after (t_1) the exposure to a L-D cycle, respectively.

Cell sizes of the three species in the HL-Exp were measured at a magnification of x1000. Because of varying cell shapes for the three species studied, cell volume (V) was determined by assuming the appropriate shape for each species (Hillebrand et al. 1999).

2.2.5. Pigment analysis

After light exposure for various periods in the HL-Exp, subsamples for pigment analysis were filtered through GF/F glass fiber filters (Whatman, USA) with the addition of 300 μmol L^{-1} DTT (final concentration), which was prepared from a 300 mmol L^{-1} stock solution and used to inhibit DD de-epoxidation during sample preparation (Olaizola et al. 1994, Kashino and Kudoh 2003). The filtration was conducted within 5 min of sampling. Filtered samples were immediately frozen in liquid nitrogen and stored at −80°C until further analysis. To check the possible epoxidation of xanthophyll pigments during the filtration, I compared the following treatments: firstly subsamples of suspension cells were immediately frozen in liquid nitrogen and secondly the subsamples were stored at −80°C followed by the filtration of thawed subsamples onto the filter. Because no significant differences in the concentrations of DD and DT, and the ratios of DD and DT to Chl *a* were observed between the treatments, I considered that no epoxidation was occurred during the filtration in the present study. Cells collected on filters were soaked in N, N-dimethylformamide, sonicated to break the cell walls, and extracted for 24 h at −20°C in the dark (Suzuki and Ishimaru 1990). The cell extracts were filtered through a 0.20-μm filter apparatus

(Millex-LG, Merck Millipore, Milford, MA, USA) to remove cellular debris and glass fibers. All extraction procedures were conducted under subdued light to prevent photodegradation of pigments. The extracts were evaluated by high-performance liquid chromatography (HPLC, 168 Diode Array Detector, C18 reversed-phase ultra-sphere 3 μm column; Beckman Coulter, Fullerton, CA, USA) using a solvent gradient system, with solvent A (80% methanol and 20% 0.5 M [v/v] ammonium acetate) and solvent B (70% methanol and 30% ethyl acetate) as described by Head and Horne (1993). A linear gradient from 0% to 100% B was provided over 25 min, followed by an isocratic hold at 100% B for 9 min. The flow rate was held constant at 1.0 mL min^{-1}. Peaks were quantified using standards for Chl *a*, Chl *c*, fucoxanthin (Fuco), DD, DT, and β-carotene (β-caro) obtained from the Danish Hydraulic Institute (Hørsholm, Denmark).

In the HL-Exp, initial rate constants (k) of temporal changes in the ratio of DT to Chl *a* were calculated for de-epoxidation of DD to DT in light conditions by fitting to a first-order kinetic model (Olaizola and Yamamoto 1994):

$$-k\mathrm{t} = \mathrm{Ln}[(DT_t - DT_\infty)/(DT_0 - DT_\infty)] \quad (2.2)$$

where DT_0 is the initial relative amount of DT, and DT_t is the relative amount of DT at time t after light exposure. The value for DT_∞ was assumed to be the value measured at 15 min after light exposure because DT levels were close to constant at this time. The temporal change in the ratio of sum of DD and DT (DD+DT) to Chl *a* from 0 to 120 min was fitted by a linear function (Olaizola et al. 1994):

$$Y = a + b\,X \quad (2.3)$$

where X is the time of light exposure and Y is the ratio of DD+DT to Chl *a*. The constants a and b represent Y-intercept and rate of *de novo* DT synthesis, respectively. The molar ratio of DT produced through *de novo* synthesis ($DT^{de\ novo}_{Chl\ a}$) to Chl *a* was estimated from the rate of *de novo*

DT synthesis. The molar ratio of DT produced through xanthophyll cycle to Chl *a* ($DT^{XC}_{Chl\ a}$) was subtracted from the molar ratio of DT identified by HPLC to Chl *a* ($DT_{Chl\ a}$) to $DT^{de\ novo}_{Chl\ a}$ as follows:

$$DT_{Chl\ a} = DT^{XC}_{Chl\ a} + DT^{de\ novo}_{Chl\ a} \quad (2.4).$$

2.2.6. Fluorescence analysis

Variations in Chl fluorescence were measured with a pulse-amplitude modulated chlorophyll fluorometer (Water-PAM, Walz, Germany). Subsamples for fluorescence analysis were placed in a 15-mm diameter quartz cuvette, which was illuminated by a circular array of 14 red light-emitting diodes with a peak illumination at 655 nm.

The minimum (F_0) and maximum (F_m) fluorescence were determined on dark-adapted cells for 30 min at given time. The maximum quantum efficiency of PSII (F_v/F_m) was calculated by the following equation (Schreiber et al. 1986):

$$F_v/F_m = (F_m–F_0)/F_m \quad (2.5).$$

The minimum (F) and maximum (F'_m) fluorescence in the light-acclimated state were measured with a saturation pulse. A saturation pulse of 3500 μmol photons m^{-2} s^{-1} was applied for 0.8 s to determine maximal fluorescence for F_m and F'_m. The PSII operating efficiency ($\Delta F/F'_m$) was calculated by the equation of Genty et al. (1989):

$$\Delta F/F'_m = (F'_m–F)/F'_m \quad (2.6).$$

The $\Delta F/F'_m$ was measured by illuminating the subsamples in a stepwise manner, increasing actinic light to 419 μmol photons m^{-2} s^{-1} in the D:L-Exp and 559–597 μmol photons m^{-2} s^{-1} in the HL-Exp with 30-s illumination periods at each step (Parkins et al. 2006). The electron transport rate (ETR) by PSII was obtained using the following equation:

$$ETR = PPFD \times 0.5 \times a^*_{PSII} \times \Delta F/F'_m \quad (2.7)$$

where PPFD is the photosynthetic photon flux density, and 0.5 is a factor accounting for equal photons falling on PSI and PSII (Hartig et al. 1998; Gilbert et al. 2000). The a^*_{PSII} was calculated from the Chl *a* concentration and the *in vivo* absorption by PSII at 655 nm. Absorption was measured as below. The rapid light curves (RLCs) were measured by plotting the ETR against the actinic PPFD. The light-limited slope (α) and the light-saturated rate (ETR_{max}) of the RLC were calculated according to Webb et al. (1974):

$$ETR = ETR_{max}(1-\exp[-\alpha \times PPFD/ETR_{max}]) \quad (2.8).$$

The light-saturation index (E_k), based on the observation of the ETR, was calculated using the following equation:

$$E_k = ETR_{max}/\alpha \quad (2.9).$$

The NPQ in the D:L-Exp was calculated using the equation of Krause and Weis (1991):

$$NPQ = (F_m - F'_m)/F'_m \quad (2.10)$$

where F_m and F'_m were measured as described above. The F'_m for calculating NPQ in the D:L-Exp was used in the value at an actinic light of 296 μmol photons m^{-2} s^{-1}, which was close to the irradiance in the R-Exp.

Measurement of NPQ in the HL-Exp was conducted by exposing samples to actinic light at 800-900 μmol photons m^{-2} s^{-1} for 30-s. The intensity of actinic light was determined based on the incubated light intensity of 900 μmol photons m^{-2} s^{-1} during the HL-Exp. NPQ was calculated by using of Eq. (2.10). The F_m for calculating NPQ in the HL-Exp is the maximal PSII fluorescence level of dark-acclimated cells for 30 min before the exposure to high light. Total NPQ is distinguished on the basis of their relaxing quenching kinetics: fast (NPQ_{Fast}) and slow (NPQ_{Slow}) relaxing NPQ components (Walters and Horton 1991). NPQ_{Fast} and NPQ_{Slow} were calculated

according to Maxwell and Johnson (2000):

$$NPQ_{Fast} = (F_m/F_m')-(F_m/F_m^r) \quad (2.11)$$

and

$$NPQ_{Slow} = (F_m-F_m^r)/F_m^r \quad (2.12)$$

where F_m^r is the maximal PSII fluorescence measured after relaxation removing the actinic light in darkness for 30 min. Total NPQ was equal to sum of NPQ_{Fast} and NPQ_{Slow}. Definitions of relative yields of fluorescence were summarized in Fig. 2-1.

2.2.7. Light absorption analysis

The total particulate absorption spectra of cells on GF/F glass fiber filters (Whatman, USA) were measured with a dual beam UV-visible spectrophotometer equipped with an integrating sphere (UV-2450, Shimadzu, Japan) following the quantitative filter technique (QFT) method of Mitchell and Kiefer (1988). Spectral absorptions were scanned from 400 to 760 nm. Optical density spectra of particulates $OD_f(\lambda)$ on filters were measured and corrected by subtracting the average optical density between 730 and 760 nm, $OD_f(730\text{-}760)$ (Babin and Stramski 2002). Corrected $OD_f(\lambda)$ was converted to the optical density of particle in suspension $OD_s(\lambda)$ (Cleveland and Weidemann 1993);

$$OD_s(\lambda) = 0.378\ OD_f(\lambda) + 0.523\ OD_f(\lambda)^2 \quad (2.13).$$

The equation was constructed with five taxonomic groups, which indicated 4 orders difference in cell volume. Centric diatoms such as *T. weissflogii* and *C. gracilis* were also included in the calculation. The range of cell volume was almost 10 folds, which was similar to the range in the present study. The equation was considered to be applicable to the mesophilic diatoms in the present study. The absorption coefficients $a_p(\lambda)$ were calculated by the following equation;

$$a_p(\lambda) = 2.303\ OD_s(\lambda)/X \quad (2.14)$$

where 2.303 is the conversion factor for $\log_e$ from $\log_{10}$ and X is the ratio of the filtered volume to the filtered clearance area of the filter. Following the measurement of $OD_f(\lambda)$, filters were immersed in 100% methanol for overnight pigment extraction according to the method of Kishino et al. (1985). The absorption coefficients for non-pigmented particles $a_d(\lambda)$ were calculated in the same manner as the total particulates using Eq. (2.13) and Eq. (2.14). The difference between $a_p(\lambda)$ and $a_d(\lambda)$ absorption coefficients was considered to be the light absorption coefficient $a_{ph}(\lambda)$ due to solely to phytoplankton. Finally, $a_{ph}(\lambda)$ was converted to Chl *a* specific absorption coefficient, $a^*_{ph}(\lambda)$, by dividing it by the Chl *a* concentration obtained from HPLC measurements.

2.2.8. Statistical analysis

The mean ± one standard deviation of all parameters that were obtained in the present chapter was always calculated and is reported throughout the present chapter. In the D:L-Exp, two-way analysis of variance (ANOVA) was conducted to assess the effects of three dark duration and three silicate enrichments on the parameters. The Student's *t*-test was used to detect differences between the two groups. Statistical significance between more than two groups was analyzed using Dunnett's or Turkey's multiple comparison test. *P* values less than 0.05 were considered to be significant.

2.3. Results

2.3.1. Dark-light transition experiments

2.3.1.1. Nutrient concentrations

Concentrations of silicate remained relatively constant in the DS-Exp. Temporal changes in nitrate and phosphate were similar to the silicate changes. The means concentration and one standard deviation were 76±5.9 μM for silicate, 750±47 μM for nitrate, and 36±2.2 μM for phosphate in the DS-Exp (Table 2-1). When the cells were returned to the normal L-D cycle conditions in the R-Exp, silicate concentrations decreased to about 0.94 μM in the +0 μM-Exp, whereas they also decreased and remained at 4.8 μM in the +10 μM-Exp and 101 μM in the +130 μM-Exp (Table 2-2). Concentrations of nitrate and phosphate at the end of the R-Exp were 600±29 μM and 22±1.3 μM, respectively. Neither nitrate nor phosphate was utilized at concentrations that limited cell growth.

2.3.1.2. Cell abundance

All cells were vegetative, and no empty frustules, damaged cells, or spore formation of *Thalassiosira weissflogii* were observed through out the DS-Exp. Initial cell densities on day 0 were $7.1\pm0.5\times10^3$ cells ml^{-1} in the DS-Exp. Cell densities increased by 35% in 11 days, and then decreased by 5% on day 14 in the DS-Exp. When the dark-acclimated cells were exposed to the normal L-D cycle, the cell density immediately increased to the maximum and was saturated within 2 days. A significant reduction in the growth rate was observed with an increasing length of dark incubation from 3 to 14 days ($p < 0.05$; Table 2-3) regardless of silicate availability (Table 2-4). The cell yields were the lowest at $67\pm2\times10^3$ cells ml^{-1} in the +0 μM-Exp, whereas they were $79\pm3\times10^3$ cells ml^{-1} in the +10 μM-Exp and $79\pm2\times10^3$ cells ml^{-1} in the +130 μM-Exp. The value in

the +0 μM-Exp was significantly lower than those in other experiments due to lack of silicate supply ($p < 0.01$).

2.3.1.3. Light-harvesting and photoprotective pigments

During the DS-Exp, the cellular Chl *a* contents (Chl a_{cell}) significantly decreased from 11 to 3.6 pg Chl *a* cell^{-1} with increasing darkness exposure ($p < 0.05$; Fig. 2-2A). The cellular contents of light-harvesting pigments (LHP_{cell}), including Chl *a*, Chl *c*, and fucoxanthin, also decreased from 17 to 6.6 pg LHP cell^{-1} (Fig. 2-2A). Once cells were transferred to the normal L-D cycle, the Chl a_{cell} significantly decreased within a range of 1.9 and 3.6 pg Chl *a* cell^{-1} on day 1 ($p < 0.01$; Fig. 2-3). Afterword the Chl a_{cell} increased to 4.9±0.90 pg Chl *a* cell^{-1} to by the end of the R-Exp. The significant decrease in the LHP_{cell} were observed on day 1 within a range of 3.1 and 5.5 pg cell^{-1} ($p < 0.01$, Fig. 2-4). Then, the LHP_{cell} increased 1.6 folds on day 4 compared with day 1. During the DS-Exp, the cellular DD contents (DD_{cell}) increased by 32%, from 1.2 to 1.6 pg DD cell^{-1}, on day 3 and then decreased by 49% until day 14 compared with day 3 (Fig. 2-2B). The cellular DT contents (DT_{cell}) decreased by 76%, from 1.4 to 0.33 pg DT cell^{-1}, on day 8 and then did not significantly change again until day 14. The cellular contents of sum of DD and DT ($[DD+DT]_{cell}$) decreased by 54% during a whole continuous dark duration. When the cells were transferred to the normal L-D cycle, the DD_{cell} significantly decreased within a range of 0.27 and 0.40 pg DD cell^{-1} on day 1 ($p < 0.01$; Fig. 2-5). Afterword the DD_{cell} increased to 0.65±0.10 pg DD cell^{-1} to by the end of the R-Exp. The DT_{cell} decreased to less than 0.1 pg DT cell^{-1} on day 1 and then increased to 0.60±0.14 pg DT cell^{-1} to by the end of the R-Exp (Fig. 2-6). The $(DD+DT)_{cell}$ decreased by 75% within one day (Fig. 2-7). Then the $(DD+DT)_{cell}$ increased 3.3 folds on day 4 compared with day 1. The cellular pigments contents were related with the dark storage length and the silicate availability significantly

until day 4 except DD_{cell} (Table 2-5).

During the DS-Exp, the molar ratios of the xanthophyll pigments DD ($DD_{Chl\ a}$) and DT ($DT_{Chl\ a}$) to Chl *a* distinctly changed over time (Fig. 2-2C) with the significant decrease in the Chl a_{cell}. The $DD_{Chl\ a}$ increased from 17 to 36 mol DD (100 mol Chl *a*)$^{-1}$ on day 11 and then did not significantly change again until day 14. The $DT_{Chl\ a}$ decreased by 61%, from 19 to 7.5 mol DT (100 mol Chl *a*)$^{-1}$, on day 8 and then increased by 90% on day 14 compared with day 8. The pool size of xanthophyll pigments ($[DD+DT]_{Chl\ a}$) increased 1.3 folds during a whole continuous dark duration. When the cells were transferred to the normal L-D cycle, the $DD_{Chl\ a}$ decreased by almost half on day 1 in the +0 μM- and +10 μM-Exp, whereas it stayed at similar levels to those on day 0 in the +130 μM-Exp (Fig. 2-8). All $DD_{Chl\ a}$ converged to approximately 20 mol DD (mol Chl *a*)$^{-1}$ until day 4. The $DT_{Chl\ a}$ decreased to less than 5 mol DT (mol Chl *a*)$^{-1}$ on day 1 (Fig. 2-9). Afterword the $DT_{Chl\ a}$ increased to 20±2.2 mol DT (mol Chl *a*)$^{-1}$ by the end of the R-Exp. The $DT_{Chl\ a}$ was related with the dark storage length and the silicate availability significantly until day 2, whereas $DD_{Chl\ a}$ was influenced on day 3 and day 4 (Table 2-5). This indicated the reduction in a pool size of xanthophyll pigments by 50% within one day (Fig. 2-10). Then the $(DD+DT)_{Chl\ a}$ increased 2.0 fold on day 4 compared with day 1.

2.3.1.4. Variable Chl fluorescence

The F_v/F_m increased by 41% on day 5, from 0.33 to 0.52, and then did not significantly change again until day 14 during the DS-Exp (Fig. 2-2D). When the dark-acclimated cells were exposed to the normal L-D cycle in the R-Exp, the F_v/F_m increased and reached its maximum value on either day 1 or day 2 (Fig. 2-11). Similar levels were observed on both days, with a mean and standard deviation of 0.62±0.024, regardless of the dark storage length but the silicate availability

(Table 2-6). After reaching these maximum levels, the F_v/F_m began to decrease to similar levels of 0.47±0.059 on day 3 and 0.36±0.044 on day 4 to those on day 0. On day 3 the F_v/F_m was influenced by both the length of dark storage and silicate availability. On day 4 both the effects of dark storage and silicate availability on F_v/F_m were diminished.

During the DS-Exp, the α increased by 56% on day 5 and then did not significantly change again until day 14 (Fig. 2-2E). The ETR_{max} increased by 37% on day 5 and then decreased by 26% on day 14 compared to day 5 (Fig. 2-2E). When the dark-acclimated cells were exposed to the normal L-D cycle in the R-Exp, the increase in the α on day 1 or day 2 were influenced by the length of dark storage and the silicate availability (Table 2-6, Fig. 2-12). The maximum α was reached on day 1 and fell within a range of 0.0011 to 0.0016 m^2 (mg Chl *a*)$^{-1}$ μmol e^{-1} (μmol photons)$^{-1}$. The decrease in the α on day 2 and day 3 were controlled by both the length of dark storage and silicate availability although the effect of both factors was disappeared on day 4 (Table 2-6) when the cells reached the saturated levels. The ETR_{max} increased by approximately 2.0 times on day 1 in regardless of silicate availability (Table 2-6, Fig. 2-13). The maximum ETR_{max} was reached on day 1 and fell within a range of 0.17 to 0.24 μmol e^- (mg Chl *a*)$^{-1}$ s^{-1}. The decrease in the ETR_{max} on day 2 and day 3 were controlled by both the length of dark storage and silicate availability although the effect of both factors was disappeared on day 4 (Table 2-6) when the cells reached the saturated levels.

During the DS-Exp, the E_k decreased from 169±14 on day 1 to 111±6.7 μmol photons m^{-2} s^{-1} on day 14 (Fig. 2-2E). During the R-Exp, the E_k decreased from 138±25 to 92±16 μmol photons m^{-2} s^{-1} with time (Fig. 2-14). The decreases in the E_k on day 1 and day 2 were controlled by both the length of dark storage and silicate availability although the effect of both factors was disappeared on day 3 and day 4 (Table 2-6) when the cells reached the saturated levels.

The NPQ reached the lowest level on day 1 following exposure to the normal L-D cycle (Fig. 2-15). These levels fell within a range of 0.21 to 0.48 for day 1, although the NPQ was influenced by the effects of dark storage and silicate availability (Table 2-6). After reaching the low levels, the NPQ increased and stayed at relatively small range at 0.65±0.12 on day 3 and day 4. On both days the NPQ was not influenced by the dark storage and silicate availability (Table 2-6).

2.3.2. High light exposure experiments

2.3.2.1. Cell conditions before the exposure to high light

For the three species grown at the low irradiance of 40 μmol photons m^{-2} s^{-1}, cell volume was about 5400 μm^3 $cell^{-1}$ for *T. weissflogii*, 370 μm^3 $cell^{-1}$ for *C. muelleri*, and 110 μm^3 $cell^{-1}$ for *T. pseudonana*, respectively (Table 2-7). Cellular Chl *a* per unit volume (Chl a_{vol}) and cellular light absorption per unit volume (a_{vol}) was smaller in the order of cell volume as follows; *T. weissflogii*, *C. muelleri*, and *T. pseudonana* (Turkey-test, $p < 0.01$; Table 2-7). The amounts of fucoxanthin, Chl *c* and β-carotene of light-harvesting pigments, which were normalized to Chl *a*, were larger in *C. muelleri* than those in either *T. weissflogii* or *T. pseudonana* (Table 2-8). Light-saturation index (E_k) was significantly lower in *T. pseudonana* than those in the other two species ($p < 0.05$; Table 2-9). Ratio of E_k to PAR (E_k/PAR) prior to the high light exposure was higher in *C. muelleri* than those in either *T. weissflogii* or *T. pseudonana* (Table 2-9). The maximum quantum efficiency of PSII (F_v/F_m) prior to the high light exposure was significantly lower in *T. pseudonana* than those in the other two species ($p < 0.05$; Table. 2-9).

2.3.2.2. Xanthophyll pigments in high light exposure experiments

After the cells of each species were exposed to high light, concentrations of Chl *a*, Chl *c*,

fucoxanthin, and β-carotene in the all three species showed no significant change during light exposure for 120 min, although the initial concentrations were only summarized in Table 2-8. The molar ratios of pigments to Chl *a* in the all three species showed no significant change except for DD and DT xanthophyll pigments during light exposure. The de-epoxidation of DD to DT by the xanthophyll cycle occurred after the exposure to high light. The molar ratio of DD to Chl *a* ($DD_{Chl\ a}$) decreased, whereas the molar ratio of DT to Chl *a* ($DT_{Chl\ a}$) increased over the 120 min (Fig. 2-16). During the light exposure experiments, the $DD_{Chl\ a}$ decreased by 27% in *T. weissflogii*, 11% in *C. muelleri*, and 56% in *T. pseudonana*. The initial rate constants (k) of temporal changes in the $DT_{Chl\ a}$ in the first 10 min of light exposure ranged from 0.15 min^{-1} for *C. muelleri* to 0.23 min^{-1} for *T. weissflogii* and *T. pseudonana* (Table 2-10). The maximum $DT_{Chl\ a}$ ranged from 11 mol DT (100 mol Chl $a)^{-1}$ for *C. muelleri* to 20 mol DT (100 mol Chl $a)^{-1}$ for *T. weissflogii* (Table 2-10). The molar ratios of DD+DT to Chl *a* ($[DD+DT]_{Chl\ a}$, pool size of xanthophyll pigments) for the all three species increased linearly during light exposure for 120 min ($p < 0.01$). The rates of *de novo* DT synthesis were significantly higher in the order of cell volume, and verse vice in the Chl a_{vol} ($p < 0.05$; Fig. 2-17). The molar ratios of DT produced through *de novo* synthesis to Chl *a* ($DT^{de\ novo}{}_{Chl\ a}$) from the rate of *de novo* DT synthesis and maximum $DT^{de\ novo}{}_{Chl\ a}$ were also significantly higher in the order of cell volume ($p < 0.05$; Fig. 2-18B). The maximum molar ratio of DT produced through xanthophyll cycle to Chl *a* ($DT^{XC}{}_{Chl\ a}$), obtained from the difference between $DT_{Chl\ a}$ and $DT^{de\ novo}{}_{Chl\ a}$ were significantly higher in *T. pseudonana* than those in the other two species ($p < 0.01$; Fig. 2-18A).

2.3.2.3. Variable Chl fluorescence in high light exposure experiments

Prior to the high light exposure, any non-photochemical quenching (NPQ) was not

identified in the all three species. After the exposure to high light, the NPQ showed an exponential increase (Fig. 2-19). The values of NPQ within first 10 min were highest in *T. weissflogii* and lowest in *T. pseudonana*. This order of species for NPQ values was not correlated with the order of species in the initial rate constants of de-epoxidation of DD to DT (*k*). At the end of light exposure experiments, the NPQ values were highest in *T. pseudonana* and lowest in *T. weissflogii*. The values of fast relaxing NPQ (NPQ_{Fast}) in *T. weissflogii* and *T. pseudonana* showed fast increase for the first 1 minutes followed by a not significant change, whereas in *C. muelleri* increased with time for 120 min (Fig. 2-19). At 120 min exposure time, the NPQ_{Fast} was highest in *C. muelleri* among the three species. The relative proportion of NPQ_{Fast} in the total NPQ in *C. muelleri* did not significantly change of 83±2.5% until 120 min but in *T. weissflogii* and in *T. pseudonana* decreased to 35% and 17%, respectively, after 120 min (Fig. 2-20).

The F_v/F_m in *T. weissflogii* and *C. muelleri* decreased until 60 min and 30 min, respectively. The values did not significantly change again until 120 min (Fig. 2-21). The F_v/F_m in *T. pseudonana* decreased with time for 120 min. At the end of experiments, the values of F_v/F_m ranged 31% in *T. weissflogii*, 20% in *C. muelleri*, and 62% in *T. pseudonana* compared to the initial values (Table 2-10, Fig. 2-22A). The relative F_v/F_m at 120 min of the exposure was significantly dependent upon the E_k/PAR ($p < 0.01$; Fig. 2-22B). The relationships between the relative F_v/F_m to the initial value and the $DT^{XC}_{Chl\ a}$ showed significant negative linear relationships in the all experiments ($p < 0.01$; Fig. 2-23A). The slope of the regression line (S^{XC}) was not significantly different between the all species (Table 2-11). The relationship between the relative F_v/F_m and the $DT^{de\ novo}_{Chl\ a}$ showed significant exponential decay ($p < 0.01$; Fig. 2-23B). The slopes ($S^{de\ novo}$) of the exponentially-decaying function in the all three species were much steeper than S^{XC} ($p < 0.01$). The $S^{de\ novo}$ was three times steeper in *T. pseudonana* than those in the other two species ($p < 0.05$),

whereas there were no difference of slope between *T. weissflogii* and *C. muelleri* (Table 2-11). The minimum value of the relative F_v/F_m in the function was 69.0% in *T. weissflogii*, 80.5% in *C. muelleri*, and 38.8% in *T. pseudonana*, respectively (Fig. 2-23B).

2.3.2.4. Relationship between DT and NPQ

The relationships between $DT_{Chl\ a}$ and NPQ were different between species. The NPQ saturated with the $DT_{Chl\ a}$ in *T. weissflogii* and *C. muelleri* (Fig. 2-24) and the initial slopes of the relationship between $DT_{Chl\ a}$ and NPQ were 0.63 (100 mol Chl *a* [mol DT]$^{-1}$) in *T. weissflogii* and 0.61 (100 mol Chl *a* [mol DT]$^{-1}$) in *C. muelleri*, respectively (Table 2-11). The relationship observed in *T. pseudonana* was linear with a slope of 0.16 (100 mol Chl *a* [mol DT]$^{-1}$), which was significantly lower than those in the other two species ($p < 0.01$). The relative proportions of NPQ_{Fast} in the total NPQ in the mesophilic diatoms dropped below 50% when the amounts of $DT_{Chl\ a}$ were 7.0 in *T. weissflogii* and 4.2 mol DT (100 mol Chl *a*)$^{-1}$ in *T. pseudonana*, whereas the relative proportion of NPQ_{Fast} in *C. muelleri* was never below 50% with DT synthesis (Fig. 2-25). In the all three species the ratio of DT produced through xanthophyll cycle to Chl *a* ($DT^{XC}_{Chl\ a}$) was linearly correlated to NPQ ($p < 0.01$, Fig. 2-26).

2.4. Discussion

2.4.1. Dark-light transition experiments on a timescale of days

2.4.1.1. Dark-acclimation and recovery of photosynthesis

The flexible response of F_v/F_m to either a continuous dark or normal L-D cycle indicates that the F_v/F_m can be a useful tool for the study of potential photosynthetic performance. Changes in the F_v/F_m are believed to reflect the photosynthetic performance of cells and to be most commonly interpreted in terms of photoacclimation to changing irradiance (e.g., Franklin et al. 2003). The steady increase in the F_v/F_m during dark storage is concordant with previous observations of *Thalassiosira weissflogii* (Van de Poll et al. 2006) and *Aureococcus anophagefferens* (Pelagophyte) (Popels et al. 2007). The low F_v/F_m values at the beginning of dark storage in this chapter suggest that the cells have been stressed during the pre-incubation normal L-D cycle of 300 μmol photons m^{-2} s^{-1} (prior to the DS-Exp), as suggested by Popels et al. (2007). The stress could be caused by damage of PSII because the irradiance employed for the pre-incubation is higher than that of the optimal growth reported for *T. weissflogii* (Armbrust et al. 1990). Therefore, the first 5 day-dark storage period may have been a recovery period for the repair of the reaction centers, as suggested by Popels et al. (2007).

Prolonged exposure to darkness prevents photosynthetic carbon metabolism. A significant decrease in the cellular pigment contents, including the light-harvesting pigments and the photoprotective xanthophyll pigments, during the dark storage may suggest that the cells could utilize pigments after metabolizing carbohydrates or lipids to survive in darkness, because no energy is provided through photosynthesis. Diatoms have been known to survive for extended periods in darkness, slowly consuming their reserves (Falkowski and Raven 2007). Such a strategy as adopted by diatoms facilitates outbursts of rapid growth when the environmental conditions

become favorable, such as releasing from ballast water, and this could be a similar situation to that of the spring bloom.

The higher values of the F_v/F_m following the normal L-D cycle in the R-Exp than those in the DS-Exp may contribute to new aspects of photoacclimation by PSII. At the exposure to high irradiance, the F_v/F_m reached immediately the maximum of 0.62±0.024 regardless of the different length of dark storage in the DS-Exp (Table 2-6). These values fell within the range of the F_v/F_m of the active growing *T. weissflogii*, which were approximately 0.6 to 0.7 (Lippemeier et al. 2001). Therefore, *T. weissflogii* could recover to the photosynthetically active state and restore growth even after 14 day-long storage in dark conditions state under the abundant supply of the macronutrients. The immediate cell divisions without any lag phase upon exposure to the L-D cycle confirm the previous finding that growth is possible as long as the length of dark storage is less than 14 days (Peters 1996). The significant reduction of growth rate during 14 days of darkness (Table 2-4) was controlled by the length of dark storage in regardless of the silicate availability.

In the R-Exp, the decrease in the F_v/F_m after the maximum might be associated with the light-saturated growth under the L-D cycle of high irradiance at 300 μmol photons m^{-2} s^{-1}. The changes in the F_v/F_m seem depending upon the silicate availability (Table 2-6) as suggested by Geider et al. (1993) and Lippemeier et al. (1999). However, the responses of F_v/F_m to the silicate availability disappear when the duration of the light-saturated cell growth became longer than 3 days (Table 2-6).

2.4.1.2. Acclimation of photoprotective xanthophyll pigments

Under dark conditions, the dominant form of xanthophyll pigments is the epoxidized DD form. The interconversion of DD and DT during dark storage is most effectively illustrated using

the ratios of DD to Chl *a* and/or DT to Chl *a* because Chl *a* is an essential pigment that transfers excitation energy to the reaction center of the photosystem (Scheer 2003). The increase in $DT_{Chl\ a}$ after the 8 days of dark storage may be due to chlororespiration, where the cells use the thylakoid membrane for respiration to generate ATP. Chlororespiratory electron flow generates a trans-thylakoid proton gradient strong enough to activate the DD de-epoxidation of the xanthophyll cycle in the dark (Jakob et al. 1999). Thus, the proton gradient generated by chlororespiration in prolonged dark storage could induce the de-epoxidation of DD.

After the cells were transferred to the L-D cycle, the initial decrease in cellular pigment contents and the ratio of xanthophyll pigments to Chl *a* could be caused by rapid cell division. The balance in the partition between light-harvesting pigments and photoprotective xanthophyll pigments seemed to be change with the more increase in the $(DD+DT)_{cell}$ than those in the LHP_{cell} when the cell growth was saturated after 2 days. The light saturation index for the growth of *T. weissflogii* has been reported to be approximately 100 μmol photons m^{-2} s^{-1} (Falkowski and Raven 2007) and 133 μmol photons m^{-2} s^{-1} is the optimal growth irradiance (Costello and Chisholm 1981). The much enhancement of cellular photoprotective xanthophyll pigments than cellular light-harvesting pigments might suggest that the irradiance of 300 μmol photons m^{-2} s^{-1} was saturating for growth, and that cells were beginning to protect themselves from the excess light. The increase in $DT_{Chl\ a}$ in the second half of L-D cycle may enhance the thermal dissipation of excess energy and photoprotection through non-photochemical quenching as suggested by Lavaud et al. (2004). The observed values of $DT_{Chl\ a}$ (20 mol DT [mol Chl *a*]$^{-1}$) at the end of the R-Exp were within the ranges of previously reported studies of diatoms (3.3–28 mol DT [100 mol Chl *a*]$^{-1}$; Olaizola et al. 1994, Olaizola and Yamamoto 1994, Lohr and Wilhelm 1999, Kashino and Kudoh 2003, Lavaud et al. 2004, Goss et al. 2006, Wu et al. 2012, Lavaud and Lepetit 2013) after the

exposure to high light from low-light conditions. The energy dissipation capacity of the xanthophyll cycle in diatoms is more active than in green algae or more complex plants (Ruban et al. 2004, Goss et al. 2006). Thus, marine diatom *T. weissflogii* can tolerate sudden light fluctuations, such as the exposure of cells that were dark-acclimated for even 14 days to light in the present chapter.

2.4.1.3. Variable Chl fluorescence

The initial increases in the α and the ETR_{max} resulted in a decrease in the E_k during the first half of the DS-Exp, suggesting that cells initiate to acclimate to dark conditions. The unchanged α during the second half of dark storage in this chapter was similar to previous reports in shade-acclimated plants (Ihnken et al. 2010). The decrease in the ETR_{max} observed during the second half of dark storage was concomitant with a decrease in the cellular content of light-harvesting pigments. Previous studies have reported the decrease in the light-saturated photosynthetic rate during near-darkness or complete darkness using the ^{14}C (Palmisano and Sullivan 1982) and Chl fluorescence methods (White and Critchley 1999, Lüder et al. 2002, Lazzara et al. 2007, Wulff et al. 2008) as well as a positive linear relationship between the Chl *a* content and the ETR_{max} of macroalgae in the darkness (Lüder et al. 2002). The cells may reduce the energy transfer from the light-harvesting antennae to the reaction centers of PSII by decreasing light-harvesting pigment content.

The increase in the ETR_{max} to maximum levels that was caused by exposing the cells to light immediately after dark storage was confirmed in terrestrial plants based on the Chl fluorescence method (White and Critchley 1999). Previous studies have reported the increase in both the light-saturated photosynthetic rate (P_m^B) and the light-limited slope (α^B) based on the ^{14}C method in marine phytoplankton during light exposure following dark conditions (Harding et al.

1981, Erga and Skjoldal 1990). The increases in the α in the first day of the normal L-D cycle were more influenced by both the length of darkness and silicate availability than those in the ETR_{max} (Table 2-6). Photosynthesis could be immediately activated by the availability of light energy after returning to normal L-D cycle conditions.

The decrease in both α and ETR_{max} after day 2 following exposure to the normal L-D cycle may be indicative of a photoprotective mechanism to regulate the energy flow required for photosynthesis regardless of the length of darkness and silicate availability (Table 2-6). The decrease are accompanied by a dissipation of excess energy in cellular photophysiological states as the non-photochemical quenching state. The E_k estimated in this chapter, which is analogous to a similar index employed for the traditional *P* versus *I* curve based on the end product of photosynthesis, indicates the domination of photochemical or non-photochemical quenching under light conditions as follows: photochemical quenching dominates below the irradiance at E_k, whereas non-photochemical quenching dominates the fluorescence quenching above the irradiance at E_k (Henley 1993). Therefore, after exposure to the second half of normal L-D cycle, *T. weissflogii* may engage in more non-photochemical quenching by photoprotection through xanthophyll cycle activity than photochemical quenching regardless of the length of dark storage and silicate availability (Table 2-6). Therefore, the E_k as obtained in this chapter can be a good index to follow the photoacclimation during the transition between dark to light regime.

2.4.2. High light exposure experiments on a short timescale of minutes to hours

2.4.2.1. Dynamics of xanthophyll pigments

The *k* values observed in the three species (0.15–0.23 min^{-1}) were within the range of previously reported studies of mesophilic diatoms (0.089–2.2 min^{-1}; Olaizola et al. 1994, Olaizola

and Yamamoto 1994, Lohr and Wilhelm 1999, Kashino and Kudoh 2003, Lavaud et al. 2004). The range of observed maximum values of $DT_{Chl\ a}$ (11–20 mol DT [100 mol Chl *a*]$^{-1}$) after high light exposure in *Thalassiosira weissflogii*, *Chaetoceros muelleri*, and *T. pseudonana* were similar to the range of previously reported studies of mesophilic diatoms (3.3–28 mol DT [100 mol Chl *a*]$^{-1}$; Olaizola et al. 1994, Olaizola and Yamamoto 1994, Lohr and Wilhelm 1999, Kashino and Kudoh 2003, Lavaud et al. 2004, Goss et al. 2006, Wu et al. 2012, Lavaud and Lepetit 2013).

The maximum values of $DT^{XC}_{Chl\ a}$ (2.2–7.6 mol DT [100 mol Chl *a*]$^{-1}$, Fig. 2-18A) after the light exposure in the all three species was located at the lower end of the range of previously reported studies of mesophilic diatoms (2.6–25 mol DT [100 mol Chl *a*]$^{-1}$; Olaizola et al. 1994, Olaizola and Yamamoto 1994, Lohr and Wilhelm 1999, Kashino and Kudoh 2003, Lavaud et al. 2004, Goss et al. 2006, Wu et al. 2012, Lavaud and Lepetit 2013).

The increases in the molar ratios of DD+DT to Chl *a* (pool size of xanthophyll pigments) for the all three species during light exposure suggest that DT synthesis includes *de novo* DT synthesis (Olaizola et al. 1994). The light-exposure induced DT synthesis occurs not only through the xanthophyll cycle but also through *de novo* formation. The *de novo* synthesis of xanthophyll pigments under excess light conditions is commonly observed in diatoms and plants (Olaizola et al. 1994, Schindler and Lichtenthaler 1994). The range of rates of *de novo* DT synthesis (0.051–0.15 mol DD+DT [100 mol Chl *a*]$^{-1}$ min^{-1}) and maximum values of $DT^{de\ novo}_{Chl\ a}$ (6.1–18 mol DT [100 mol Chl *a*]$^{-1}$) in the all three species are similar to the range of previously reported studies of mesophilic diatoms from 0.024 to 0.14 mol DD+DT (100 mol Chl *a*)$^{-1}$ min^{-1} (Olaizola et al. 1994, Olaizola and Yamamoto 1994, Lohr and Wilhelm 1999, Lavaud et al. 2004) and from 1.2 to 14 mol DT (100 mol Chl *a*)$^{-1}$) (Olaizola et al. 1994, Olaizola and Yamamoto 1994, Lohr and Wilhelm 1999, Lavaud et al. 2004, Wu et al. 2012), respectively. Previous studies found that the rate of $DT^{de\ novo}$

was dependent on the light intensity (Olaizola et al. 1994; Giovagnetti et al. 2014) and the prolonged exposure time (Giovagnetti et al. 2014). Although the biosynthetic sequence of xanthophyll pigments in diatoms has been hypothesized from β-caro via violaxanthin to DD and DT (Lohr and Wilhelm 2001, Wilhelm et al. 2006), the present study observed no change in the amounts of β-caro when the pool size of xanthophyll pigments increased. Lohr and Wilhelm (1999) proposed that the additional pool of xanthophyll pigments under conditions of excess light serves as a precursor for the synthesis of the light-harvesting pigments, such as Fuco, in subsequent low light conditions with almost no additional metabolic costs. It is speculated that, because the larger cells of *T. weissflogii* have the most *de novo* DT synthesis (Fig. 2-18B), larger diatom species might be more capable for acclimating to light limited conditions.

2.4.2.2. Characteristics of Chl fluorescence

Photoinhibition might cause the induction of NPQ. NPQ is induced by DT synthesis through the xanthophyll cycle, which could lead to heat dissipation and photoprotection. However, there is also quenching due to damage of PSII reaction centers (Maxwell and Johnson 2000). The damage to PSII reaction centers results in decrease in the fluorescence yield within the PSII reaction center. The total NPQ can be divided to thermal dissipation (NPQ_{Fast}) and photoinhibitory (NPQ_{Slow}) components (Osmond 1994). The small relative proportions of NPQ_{Slow} found in *C. muelleri* during light exposure experiments suggest a lower contribution of photoinhibition to the increase in total of NPQ and a higher contribution of the xanthophyll cycle in comparison with *T. weissflogii* and *T. pseudonana*. In *T. weissflogii* and *T. pseudonana*, the steady increase in the total NPQ without the increase in NPQ_{Fast} after the initial rise of NPQ during first minute could be due to the damage of PSII reaction centers and is unrelated to thermal dissipation through xanthophyll

cycle.

The F_v/F_m values in the all three species fell within the range of the F_v/F_m of active growing phytoplankton (Büchel and Wilhelm 1993, Lippemeier et al. 2001). During light exposure for 120 min the decreases in F_v/F_m in comparison with the initial values were larger in *T. pseudonana* and smaller in *C. muelleri*, suggesting that the photoinhibition caused by high light can be the most substantial in *T. pseudonana* and the smallest in *C. muelleri* (Fig. 2-21A). The photoinhibition in the all three species might be associated with the lower ratio of E_k to PAR (E_k/PAR) prior to the light exposure experiments. The higher values of E_k/PAR in *C. muelleri* suggest weaker acclimation to shade among the three species. Therefore, the significant relationship between the F_v/F_m and E_k/PAR suggests that the weak-shade acclimated cells have the advantage which is associated with relaxation of photoinhibition caused by the high light exposure and consequently might advance the recovery of photosynthetic capacity (Petrou et al. 2010) among the mesophilic diatom species.

2.4.2.3. Photoprotective ability

The significant relationship between the $DT^{XC}_{Chl\ a}$ or $DT^{de\ novo}_{Chl\ a}$ and the relative F_v/F_m to the initial values in the all three species (Fig. 2-23) indicates that the accumulation of DT^{XC} and $DT^{de\ novo}$ might assist to reduce the photodamage. The gentler slope (S^{XC}) of relationship between the relative F_v/F_m and $DT^{XC}_{Chl\ a}$ than those of the relative F_v/F_m and $DT^{de\ novo}_{Chl\ a}$ ($S^{de\ novo}$) (Table 2-11) suggests that the photoprotective capacity, which reduce the damage of PSII, in the DT^{XC} is higher than those in the $DT^{de\ novo}$. Therefore, the photoprotective capacity of thermal dissipation (S^{XC}) must be higher than those of the antioxidant function ($S^{de\ novo}$) (see Notation for details).

The negative linear relationships between the relative F_v/F_m and $DT^{XC}_{Chl\ a}$ indicate that

the PSII reaction center could be damaged progressively during the light exposure even if some excess energy is dissipated through xanthophyll cycle. No difference in the values of S^{XC} among the three species (Table 2-11) suggests that photoprotective capacity of DT^{XC} is similar between species. The species-specific values of $S^{de\ novo}$ (Table 2-11) might be dependent upon addressing of $DT^{de\ novo}$ to the several pools. The $DT^{de\ novo}$ molecules are distributed among three pools which show a spatial and functional heterogeneity (Lepetit et al. 2010). It is believed that $DT^{de\ novo}$ can be: 1) free in the lipid matrix, 2) free in the lipid matrix in the close vicinity to the PSII light-harvesting complexes antenna, and 3) bound to the light-harvesting complexes antenna system where they participate to NPQ. The $DT^{de\ novo}$, which is not bounded to the light-harvesting complexes, may be not directly related to NPQ (Schumann et al. 2007). The *de novo* synthesized DT molecules in the close vicinity to the PSII light-harvesting complexes in diatoms are assumed to have an antioxidant protective shield around the PSII by serving as another photoprotective mechanism (Lepetit et al. 2010), which is not related to thermal dissipation. The threefold higher values of $S^{de\ novo}$ in *T. pseudonana* indicate that there are threefold larger DT freely in the lipid matrix, which is not involved in NPQ and/or an antioxidant photoprotective function. In *T. weissflogii* and *C. muelleri*, the $DT^{de\ novo}$ appears to be a main part of the pool being bound to the light-harvesting complexes and/or located in the lipid matrix in the close vicinity to the PSII light-harvesting complexes.

When the logarithmic decreases in the F_v/F_m reach to the minimum (Fig. 2-23B), no further prevention of photodamage by the synthesis of $DT^{de\ novo}$ should be occurred. The differences in the values of $S^{de\ novo}$ between the species might be dependent upon the balance between the thermal dissipation and the antioxidant function of $DT^{de\ novo}$. The lowest values of $S^{de\ novo}$ which are observed in *T. pseudonana* suggest that the synthesis of $DT^{de\ novo}$ is involved mostly in the antioxidant function. The higher minimum values in *C. muelleri* than those in *T. weissflogii* with

similar values of $S^{de\ novo}$ might suggest that the synthesis of $DT^{de\ novo}$ in *C. muelleri* is involved in the thermal dissipation rather than the antioxidant function at the second half of exposure.

The significant difference in the $DT_{Chl\ a}$ and NPQ relationship in the all three species (Fig. 2-24) could be related to the *de novo* DT synthesis, which was confirmed by the linear relationship between the only $DT^{XC}_{Chl\ a}$ and NPQ (Fig. 2-26). When the contribution of $DT^{de\ novo}$, which is not bounded to the light-harvesting complexes, to the total DT is significant, the relationship between $DT_{Chl\ a}$ and NPQ might become saturated. In previous studies, the slope of the relationship between $DT_{Chl\ a}$ and NPQ was shown to reflect the quenching efficiency of DT (Goss and Jakob 2010) and to be comparable to different diatom species (Goss et al. 2006, Lavaud et al. 2004). The range of the observed slopes (0.16–0.63 [100 mol Chl *a* (mol DT)$^{-1}$]) in the all three species in the present chapter are not significantly different to the range of previously reported studies for mesophilic diatoms (0.49–1.0 [100 mol Chl *a* (mol DT)$^{-1}$]; Goss et al. 2006, Lavaud et al. 2004, Lavaud et al. 2012, Lavaud and Lepetit 2013). Although the quenching efficiency of DT might be influenced by the quenching not only due to thermal dissipation of DT production through the xanthophyll cycle but also photoinhibition, the initial increase in NPQ with DT synthesis could be enhanced almost by thermal dissipation (NPQ_{Fast}). It could be considered that the photoinhibitory NPQ component (NPQ_{Slow}) is unlikely to have a significant effect on the quenching efficiency of DT. The lowest quenching efficiency of DT in *T. pseudonana* than the other two species possibly indicates that the amount of $DT_{Chl\ a}$ in the light-harvesting complexes involved in NPQ is a smaller fraction of the total pool of xanthophyll pigments in *T. pseudonana*, as suggested by Lavaud et al. (2004)

2.4.3. Conclusions

By maintaining the ability to resume photosynthesis upon exposure to the L-D cycle,

Thalassiosira weissflogii could have the ability to initiate the growth even if the cells have been stored up to 14 days in the dark. The long exposure to the high light may enforce the cells going through photoprotection process such as activation of xanthophyll cycle and non-photochemical quenching after the cell growth is saturated. Under high light condition in a short timescale of minutes to hours, the significant difference in the $DT_{Chl\ a}$ and NPQ relationship is still observed in mesophilic diatom species, and the amounts of *de novo* synthesized DT could be related to cell volume which are variable between species. The gentler slopes of the relationship between the relative F_v/F_m and $DT^{XC}{}_{Chl\ a}$ than those between the relative F_v/F_m and $DT^{de\ novo}{}_{Chl\ a}$ suggest that the photoprotective capacity of DT^{XC} as thermal dissipation might be higher than those of $DT^{de\ novo}$ as an antioxidant function. Although the photoprotective capacities of DT^{XC} are similar between species, those of $DT^{de\ novo}$ are smallest in the smallest species of *T. pseudonana*. Therefore, the small mesophilic diatoms might be likely to have lower photoprotective capacity in comparison with large mesophilic diatoms.

Table 2-1. Nutrient concentrations on day 3, 8, and 14 during the dark storage experiments in *T. weissflogii*. Nutrient concentrations in μM. Mean ± one standard deviation.

Day	Nitrate	Phosphate	Silicate
3	739 ± 40	36 ± 2.6	74 ± 4.1
8	754 ± 34	36 ± 2.4	73 ± 4.6
14	754 ± 56	36 ± 2.2	75 ± 4.3

Table 2-2. The nutrient concentrations on day 0, 1, 2, and 4 during the recovery experiments (R-Exp) in *T. weissflogii* with the mean ± one standard deviation of three dark storage treatments.

		Nitrate		Phosphate		Silicate	
Experiment	Day	(μM)	(%)	(μM)	(%)	(μM)	(%)
+0 μM-Exp	0	737 ± 18	100	36 ± 0.65	100	71 ± 1.3	100
	1	703 ± 25	95	34 ± 1.2	95	50 ± 13	71
	2	650 ± 12	88	26 ± 1.8	74	1.1 ± 0.36	1.5
	4	622 ± 8.8	84	23 ± 0.52	63	0.94 ± 0.32	1.3
+10 μM-Exp	0	796 ± 20	100	34 ± 0.50	100	93 ± 1.9	100
	1	695 ± 42	87	32 ± 0.91	94	88 ± 6.6	95
	2	644 ± 25	81	26 ± 0.66	78	18 ± 9.9	20
	4	614 ± 7.1	77	20 ± 0.79	60	4.5 ± 2.0	4.8
+130 μM-Exp	0	713 ± 7.6	100	38 ± 0.21	100	203 ± 3.5	100
	1	657 ± 18	92	33 ± 0.99	86	186 ± 7.0	92
	2	603 ± 27	85	27 ± 1.6	70	128 ± 11	63
	4	564 ± 18	79	22 ± 0.33	58	101 ± 2.4	50

Table 2-3. Growth rates in the recovery experiments (R-Exp) in *T. weissflogii*. Mean ± one standard deviation of growth rates was observed on the cells exposed to the L-D cycles in the +0 μM-Exp, +10 μM-Exp, and +130 μM-Ex on day 3, day 8, and day 14 of the dark storage experiments. Growth rates in d^{-1}.

	Growth rate		
Experiment	Day 3	Day 8	Day 14
+0 μM-Exp	1.03 ± 0.030	0.952 ± 0.023	0.937 ± 0.031
+10 μM-Exp	1.10 ±0.055	0.977 ± 0.041	0.870 ± 0.042
+130 μM-Exp	0.979 ± 0.064	0.932 ± 0.025	0.914 ± 0.022

Table 2-4. Results of two-way analysis of variance in growth rate among the length of day in the dark incubation (DS-Exp) and silicate availability in the recovery experiment (R-Exp) in *T. weissflogii*. DF=degree of freedom, F=F value, *p*=probability.

Source of variation	DF	F	*p*
Dark incubation (A)	2	25.4	< 0.001
Silicate availability (B)	2	2.62	0.101
A×B	4	4.22	0.014
Residual	18		
Total	26		

Table 2-5. Results of two-way analysis of variance in Chl a_{cell}, LHP_{cell}, DD_{cell}, DT_{cell}, $DD_{Chl\ a}$, and $DT_{Chl\ a}$ among the length of day in the dark incubation (DS-Exp) and silicate availability in the recovery experiment (R-Exp) in *T. weissflogii*. DF=degree of freedom, F=F value, *p*=probability. Significant ($p < 0.05$) are indicated in bold.

	Day 1			Day 2			Day 3			Day 4		
Source of Variation	DF	F	*p*	DF	F	*p*	DF	F	*p*	DF	F	*p*
Chl a_{cell}	2	27.68	**<0.01**	2	15.94	**<0.01**	2	27.00	**<0.01**	2	39.23	**<0.01**
Dark incubation (A)	2	14.27	**<0.01**	2	38.91	**<0.01**	2	21.09	**<0.01**	2	41.69	**<0.01**
Silicate availability (B)	4	5.81	**<0.01**	4	6.75	**<0.01**	4	3.46	**<0.05**	4	12.99	**<0.01**
A×B												
LHP_{cell}												
Dark incubation (A)	2	26.97	**<0.01**	2	13.87	**<0.01**	2	17.71	**<0.01**	2	28.91	**<0.01**
Silicate availability (B)	2	9.05	**<0.01**	2	34.84	**<0.01**	2	22.03	**<0.01**	2	44.03	**<0.01**
A×B	4	4.77	**<0.01**	4	4.99	**<0.01**	4	2.29	0.099	4	8.65	**<0.01**
DD_{cell}												
Dark incubation (A)	2	2.64	0.099	2	38.92	**<0.01**	2	0.68	0.52	2	2.87	0.083
Silicate availability (B)	2	1.52	0.25	2	18.67	**<0.01**	2	24.73	**<0.01**	2	143.55	**<0.01**
A×B	4	2.02	0.14	4	0.95	0.46	4	0.88	0.49	4	3.37	**<0.05**
DT_{cell}												
Dark incubation (A)	2	13.65	**<0.01**	2	41.89	**<0.01**	2	28.79	**<0.01**	2	11.12	**<0.01**
Silicate availability (B)	2	29.76	**<0.01**	2	13.98	**<0.01**	2	36.23	**<0.01**	2	47.53	**<0.01**
A×B	4	3.34	**<0.05**	4	7.06	**<0.01**	4	1.78	0.18	4	1.75	0.18
$DD_{Chl\ a}$												
Dark incubation (A)	2	33.36	**<0.01**	2	28.63	**<0.01**	2	36.23	**<0.01**	2	42.26	**<0.01**
Silicate availability (B)	2	0.70	0.51	2	2.43	0.12	2	4.70	**<0.05**	2	8.94	**<0.01**
A×B	4	7.92	**<0.01**	4	0.76	0.56	4	8.60	**<0.01**	4	13.24	**<0.01**
$DT_{Chl\ a}$												
Dark incubation (A)	2	13.61	**<0.01**	2	29.97	**<0.01**	2	9.19	**<0.01**	2	0.39	0.68
Silicate availability (B)	2	11.99	**<0.01**	2	9.11	**<0.01**	2	0.071	0.93	2	5.91	**<0.05**
A×B	4	0.94	0.46	4	3.29	**<0.05**	4	13.02	**<0.01**	4	3.10	**<0.05**

Table 2-6. Results of two-way analysis of variance in the fluorescence parameters among the length of day in the dark incubation (DS-Exp) and silicate availability in the recovery experiment (R-Exp) in *T. weissflogii*. DF=degree of freedom, F=F value, *p*=probability. Significant ($p < 0.05$) are indicated in bold.

	Day 1			Day 2			Day 3			Day 4		
Source of Variation	DF	F	*p*	DF	F	*p*	DF	F	*p*	DF	F	*p*
F_v/F_m												
Dark incubation (A)	2	1.86	0.19	2	1.91	0.18	2	9.20	**<0.01**	2	0.46	0.64
Silicate availability (B)	2	9.00	**<0.01**	2	9.97	**<0.01**	2	9.89	**<0.01**	2	2.39	0.12
A×B	4	3.60	**<0.05**	4	3.89	**<0.05**	4	3.08	**<0.05**	4	2.27	0.10
α												
Dark incubation (A)	2	8.40	**<0.01**	2	4.00	**<0.05**	2	14.81	**<0.01**	2	0.69	0.51
Silicate availability (B)	2	8.12	**<0.01**	2	39.95	**<0.01**	2	34.48	**<0.01**	2	3.17	0.066
A×B	4	2.71	0.063	4	6.33	**<0.01**	4	16.96	**<0.01**	4	1.85	0.16
ETR_{max}												
Dark incubation (A)	2	13.78	**<0.01**	2	33.60	**<0.01**	2	11.01	**<0.01**	2	1.59	0.23
Silicate availability (B)	2	1.38	0.28	2	8.59	**<0.01**	2	4.34	**<0.05**	2	2.46	0.11
A×B	4	1.93	0.15	4	5.85	**<0.01**	4	4.36	**<0.05**	4	2.03	0.13
E_k												
Dark incubation (A)	2	25.94	**<0.01**	2	19.96	**<0.01**	2	1.55	0.24	2	0.22	0.81
Silicate availability (B)	2	7.69	**<0.01**	2	3.35	0.058	2	1.96	0.17	2	2.29	0.13
A×B	4	3.17	**<0.05**	4	4.03	**<0.05**	4	2.82	0.056	4	1.14	0.37
NPQ												
Dark incubation (A)	2	3.77	**<0.05**	2	37.79	**<0.01**	2	0.62	0.55	2	0.78	0.48
Silicate availability (B)	2	24.47	**<0.01**	2	33.52	**<0.01**	2	2.78	0.089	2	0.03	0.97
A×B	4	0.26	0.90	4	0.17	0.95	4	2.39	0.089	4	4.12	**<0.05**

Table 2-7. Cell volume (V), cellular Chl *a* content per unit volume (Chl a_{vol}), and cellular light absorption per unit volume (a_{vol}) before high light exposure experiments in three diatom species. V in μm^3 $cell^{-1}$, Chl a_{vol} in fg μm^{-3}, and a_{vol} in 10^{-13} m^2 μm^{-3}. Mean ± one standard deviation.

	V	Chl a_{vol}	a_{vol}
T. weissflogii	5391 ± 385	1.08 ± 0.19	0.0709 ± 0.0064
C. muelleri	371 ± 49	2.27 ± 0.13	0.187 ± 0.015
T. pseudonana	112 ± 13	7.88 ± 1.1	1.12 ± 0.11

Table 2-8. Molar ratio of pigment to Chl *a* (mol [100 mol Chl *a*]$^{-1}$) before high light exposure experiments in three diatom species. Mean ± one standard deviation.

	Fucoxanthin	Chl *c*	DD	DT	β-carotene
T. weissflogii	56 ± 2	24 ± 2	9.5 ± 0.3	0.25 ± 0.4	5.8 ± 1
C. muelleri	74 ± 1	43 ± 0.3	9.1 ± 0.2	0.00 ± 0.00	6.9 ± 0.2
T. pseudonana	60 ± 2	25 ± 1	12 ± 0.6	1.0 ± 0.07	5.8 ± 0.4

Table 2-9. Light-saturation index (E_k), ratio of E_k to PAR, and maximum quantum efficiency (F_v/F_m) before high light exposure experiments in three diatom species. E_k in μmol photons m^{-2} s^{-1}, and E_k/PAR and F_v/F_m in relative unit. Mean ± one standard deviation.

	E_k	E_k/PAR	F_v/F_m
T. weissflogii	494 ± 113	10.1 ± 2.3	0.717 ± 0.0012
C. muelleri	631 ± 67	13.1 ± 1.4	0.723 ± 0.0054
T. pseudonana	267 ± 53	6.85 ± 1.4	0.674 ± 0.011

Table 2-10. Initial rate constant (k) of de-epoxidation of DD to DT, maximum $DT_{Chl\ a}$, rate of *de novo* DT synthesis, and decrease in F_v/F_m in comparison with the initial value during light exposure experiments in three diatom species. k in min^{-1}, $DT_{Chl\ a}$ in mol DT (100 mol Chl a)$^{-1}$, rate of *de novo* DT synthesis in mol DT (100 mol Chl a)$^{-1}$ min^{-1}, and decrease in F_v/F_m in %. Mean ± one standard deviation.

	k	$DT^{Chl\ a}$	Rate of *de novo* DT synthesis	Decrease in F_v/F_m
T. weissflogii	0.232 ± 0.046	20.2 ± 0.64	0.148 ± 0.0063	30.5 ± 1.6
C. muelleri	0.151 ± 0.018	10.7 ± 0.99	0.0836 ± 0.0091	19.9 ± 3.4
T. pseudonana	0.234 ± 0.038	13.7 ± 0.55	0.0509 ± 0.013	61.6 ± 1.6

Table 2-11. Slope between $DT^{XC}_{Chl\ a}$ and relative F_v/F_m to the initial value (S^{XC} in relative unit), slope between $DT^{de\ novo}_{Chl\ a}$ and relative F_v/F_m to the initial value ($S^{de\ novo}$ in relative unit), and slope between $DT_{Chl\ a}$ and NPQ (100 mol Chl *a* [mol DT]$^{-1}$) during light exposure experiments in three diatom species. Mean ± one standard deviation.

	S^{XC}	$S^{de\ novo}$	$DT_{Chl\ a}$ and NPQ
T. weissflogii	−10.7 ± 1.0	−17.9 ± 2.3	0.634 ± 0.068
C. muelleri	−8.62 ± 3.3	−14.4 ± 0.61	0.609 ± 0.084
T. pseudonana	−10.3 ± 1.3	−53.8 ± 16	0.155 ± 0.012

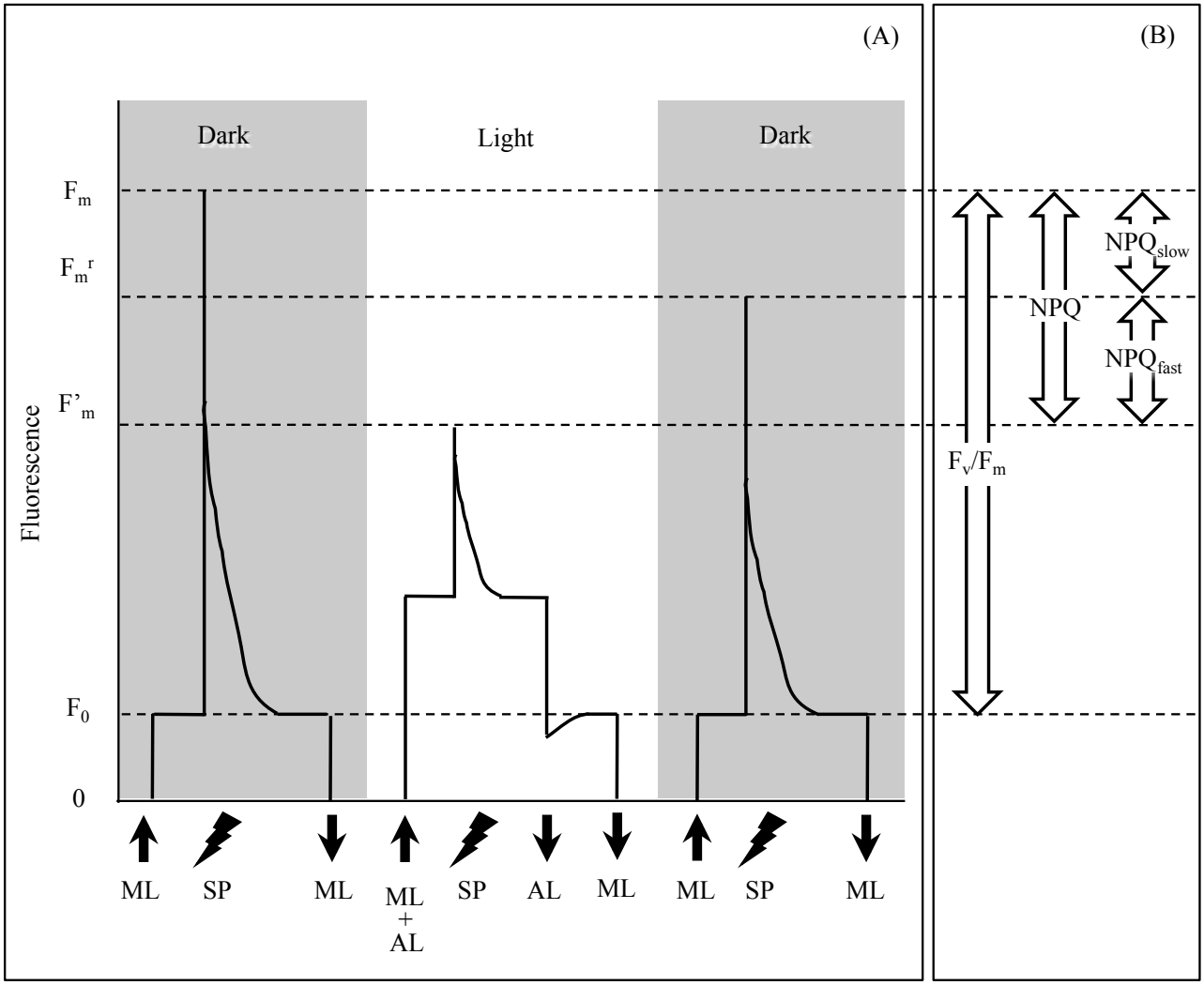

Figure 2-1. Sequence of a typical fluorescence trace (A) and definition of the relative yields of fluorescence (B).

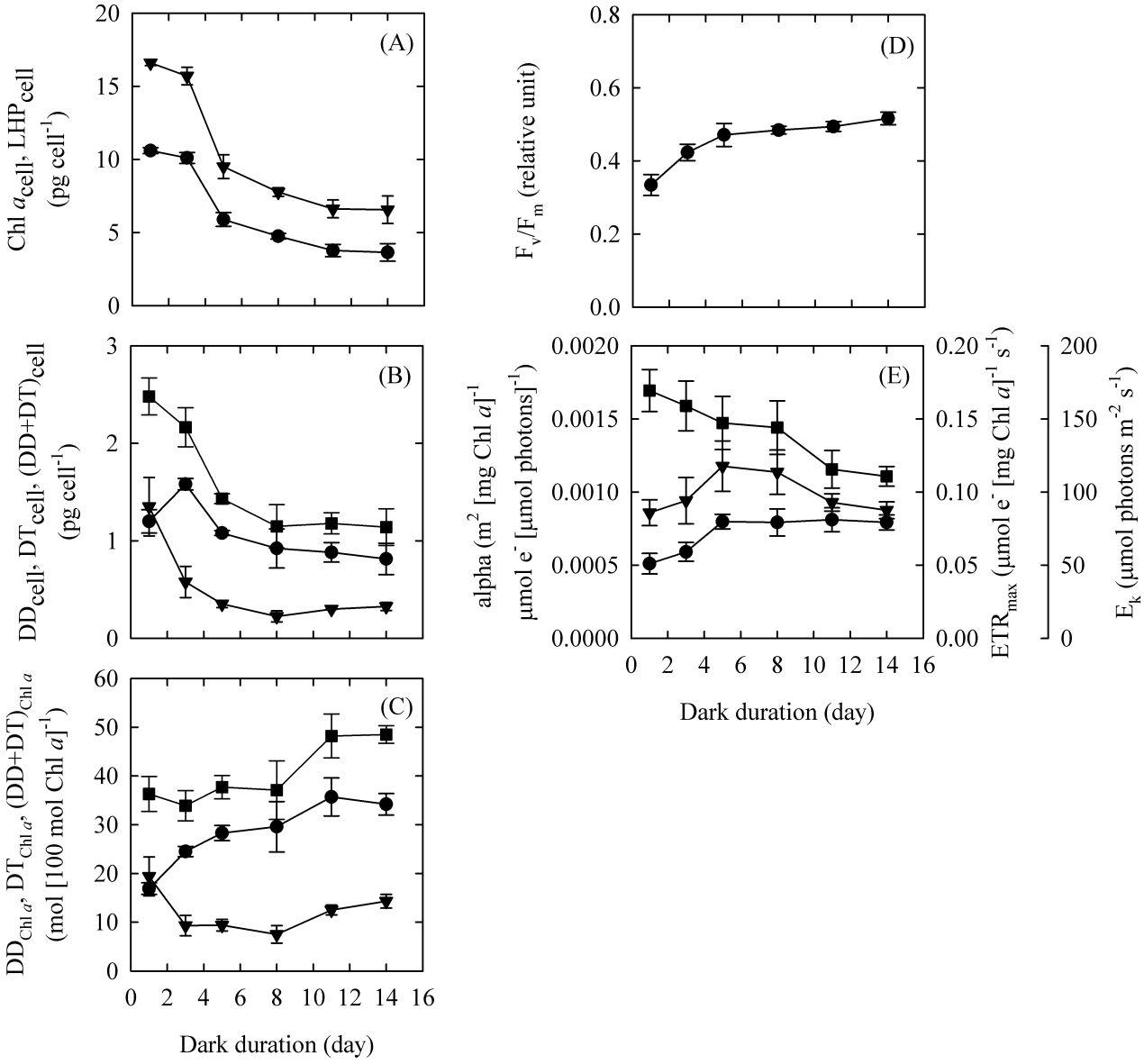

Figure 2-2. Temporal changes in Chl a_{cell} (circle) and LHP_{cell} (reversed triangle) (A), DD_{cell} (circle), DT_{cell} (reversed triangle), and $(DD+DT)_{cell}$ (square) (B), $DD_{Chl\,a}$ (circle), $DT_{Chl\,a}$ (reversed triangle), and $(DD+DT)_{Chl\,a}$ (square) (C), F_v/F_m (D) and α (circle), ETR_{max} (reversed triangle), and E_k (square) (E) in the DS-Exp in *T. weissflogii*. Error bars indicate one standard deviation of the mean.

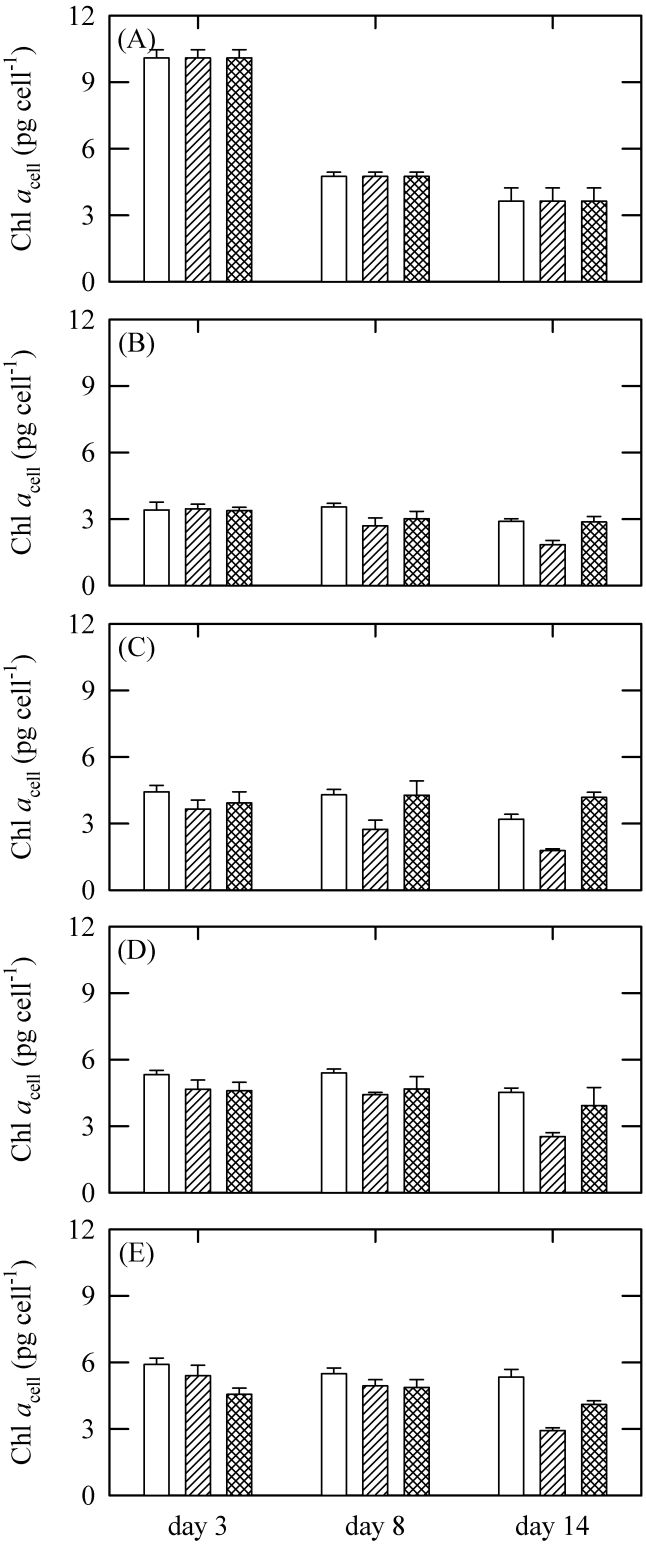

Figure 2-3. Temporal changes in Chl a_{cell} in the +0 μM-Exp (white bar), +10 μM-Exp (hatched bar), and +130 μM-Exp (cross-hatched bar) on day 0 (A), day 1 (B), day2 (C), day3 (D), and day 4 (E) in the R-Exp in *T*. *weissflogii*. Incubation was started on days 3, 8, and 14 of DS-Exp. Error bars indicate one standard deviation of the mean.

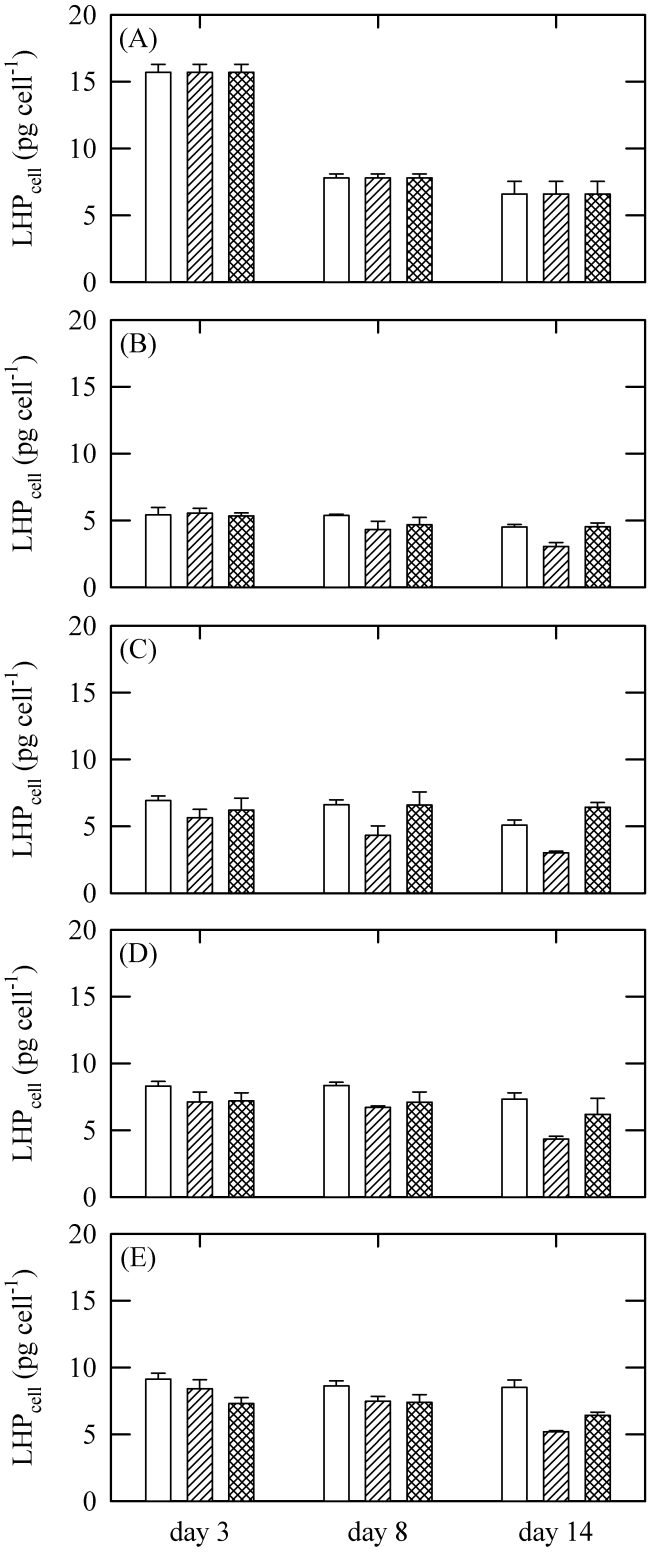

Figure 2-4. Temporal changes in LHP_{cell} in the +0 μM-Exp (white bar), +10 μM-Exp (hatched bar), and +130 μM-Exp (cross-hatched bar) in the R-Exp in *T. weissflogii*. See Fig. 2-3 for the panel numbers, error bars, and the legends for x-axis.

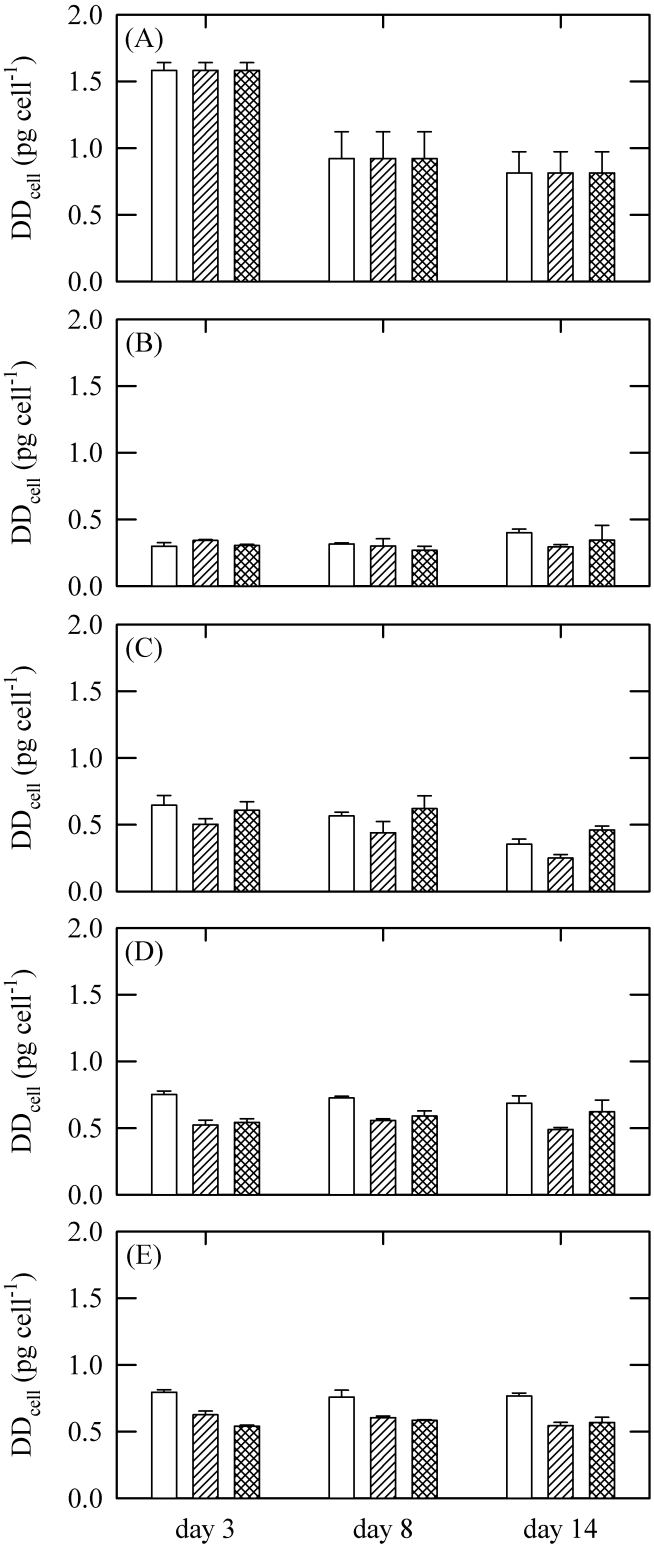

Figure 2-5. Temporal changes in DD_{cell} in the +0 μM-Exp (white bar), +10 μM-Exp (hatched bar), and +130 μM-Exp (cross-hatched bar) in the R-Exp in *T. weissflogii*. See Fig. 2-3 for the panel numbers, error bars, and the legends for x-axis.

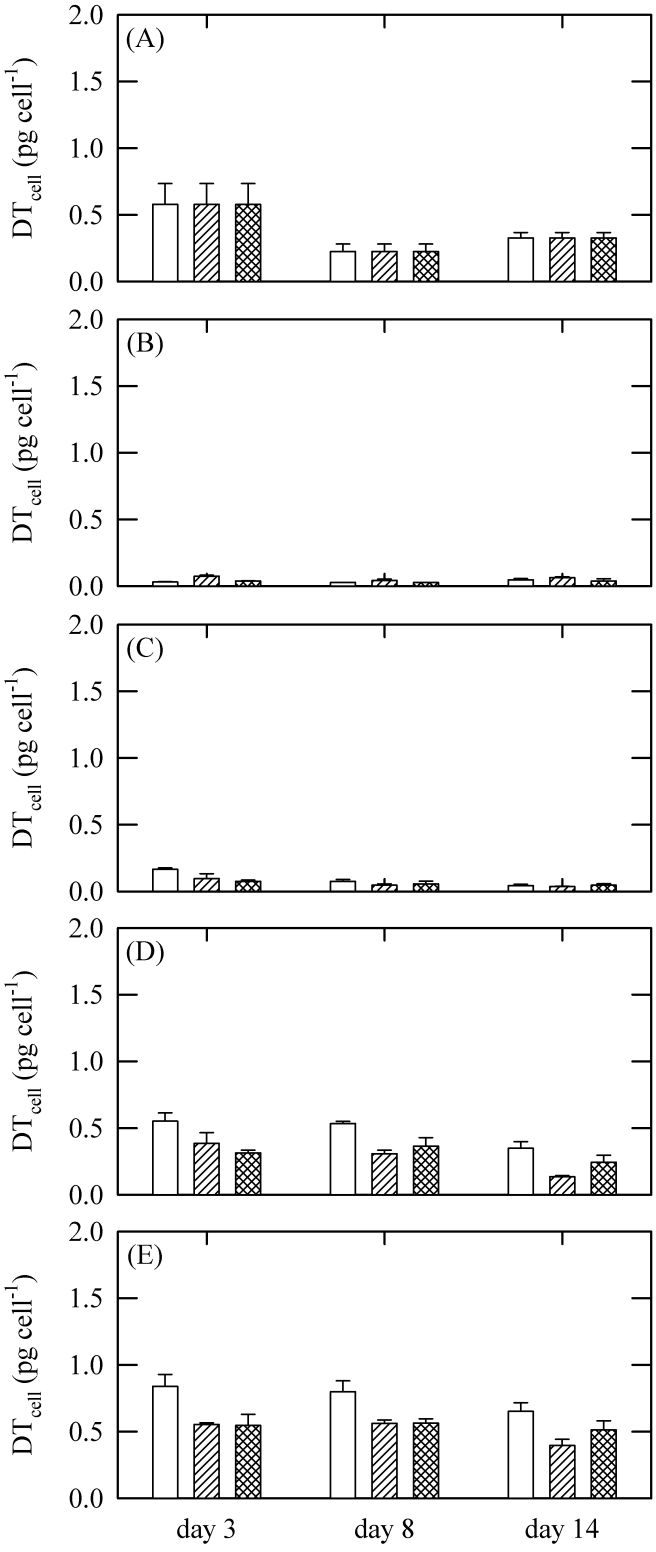

Figure 2-6. Temporal changes in DT_{cell} in the +0 μM-Exp (white bar), +10 μM-Exp (hatched bar), and +130 μM-Exp (cross-hatched bar) in the R-Exp in *T. weissflogii*. See Fig. 2-3 for the panel numbers, error bars, and the legends for x-axis.

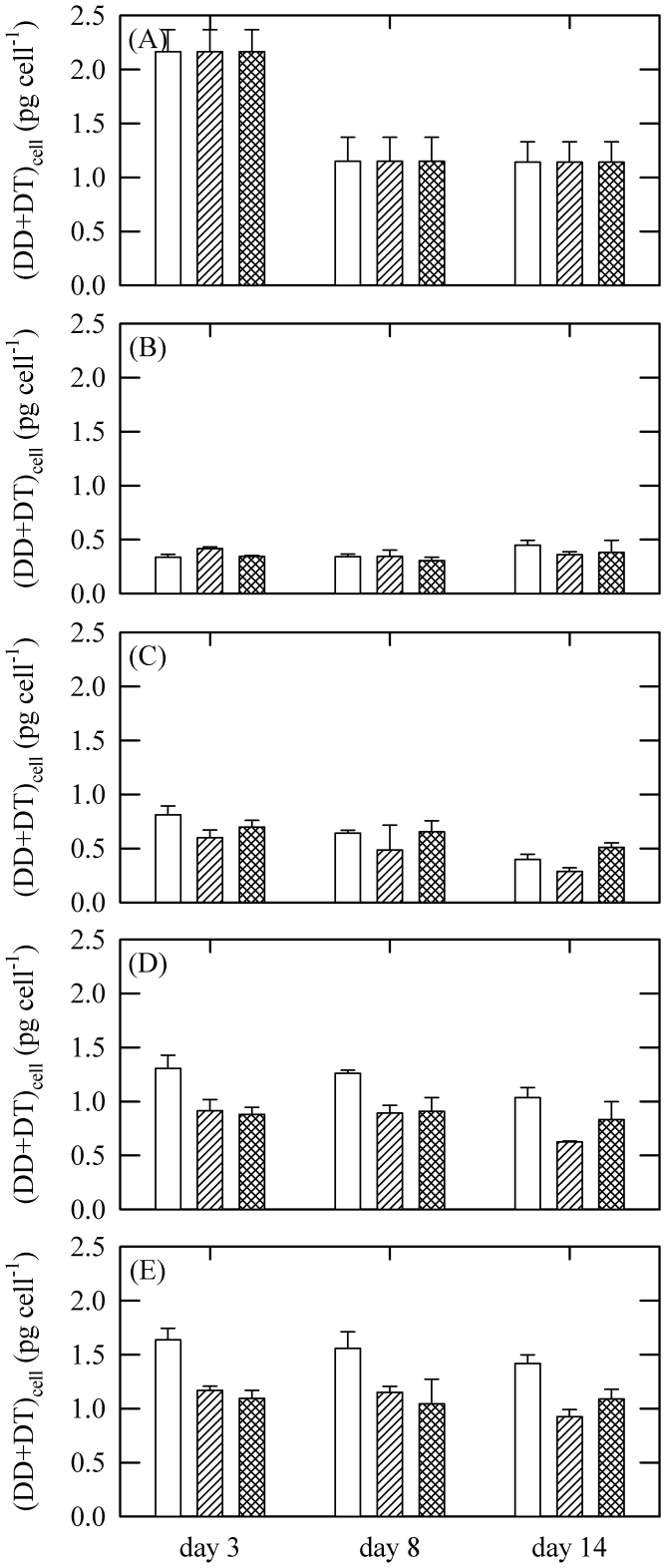

Figure 2-7. Temporal changes in $(DD+DT)_{cell}$ in the +0 μM-Exp (white bar), +10 μM-Exp (hatched bar), and +130 μM-Exp (cross-hatched bar) in the R-Exp in *T*. *weissflogii*. See Fig. 2-3 for the panel numbers, error bars, and the legends for x-axis.

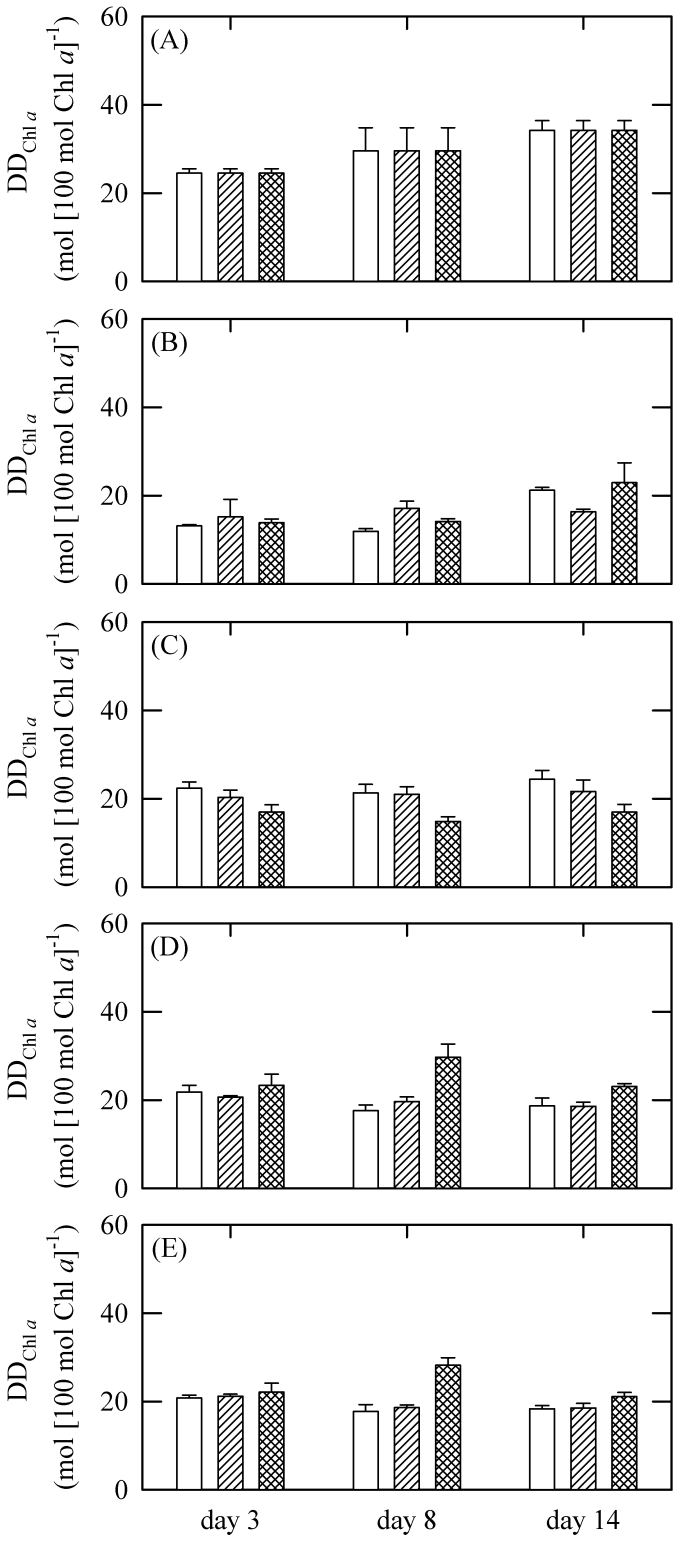

Figure 2-8. Temporal changes in $DD_{Chl\ a}$ in the +0 μM-Exp (white bar), +10 μM-Exp (hatched bar), and +130 μM-Exp (cross-hatched bar) in the R-Exp in *T. weissflogii*. See Fig. 2-3 for the panel numbers, error bars, and the legends for x-axis.

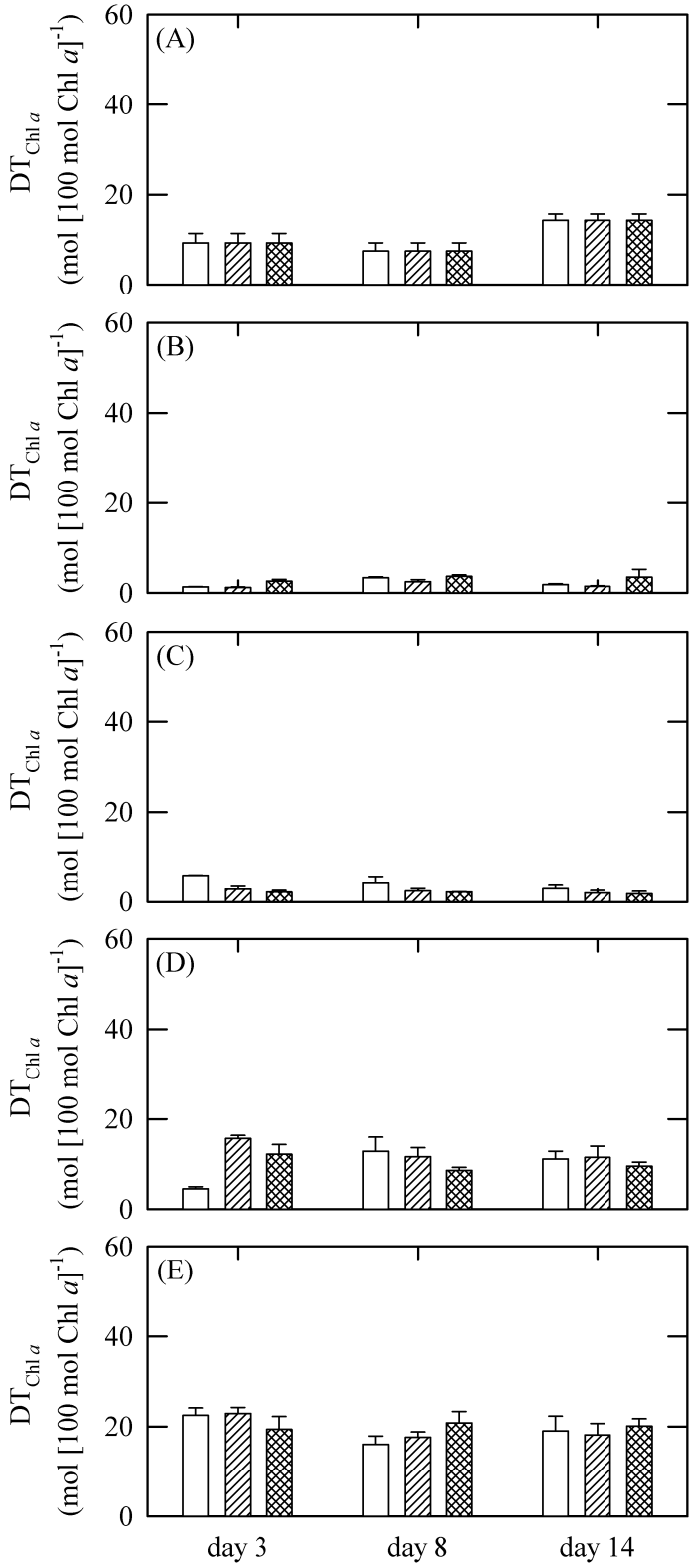

Figure 2-9. Temporal changes in $DT_{Chl\ a}$ in the +0 μM-Exp (white bar), +10 μM-Exp (hatched bar), and +130 μM-Exp (cross-hatched bar) in the R-Exp in *T. weissflogii*. See Fig. 2-3 for the panel numbers, error bars, and the legends for x-axis.

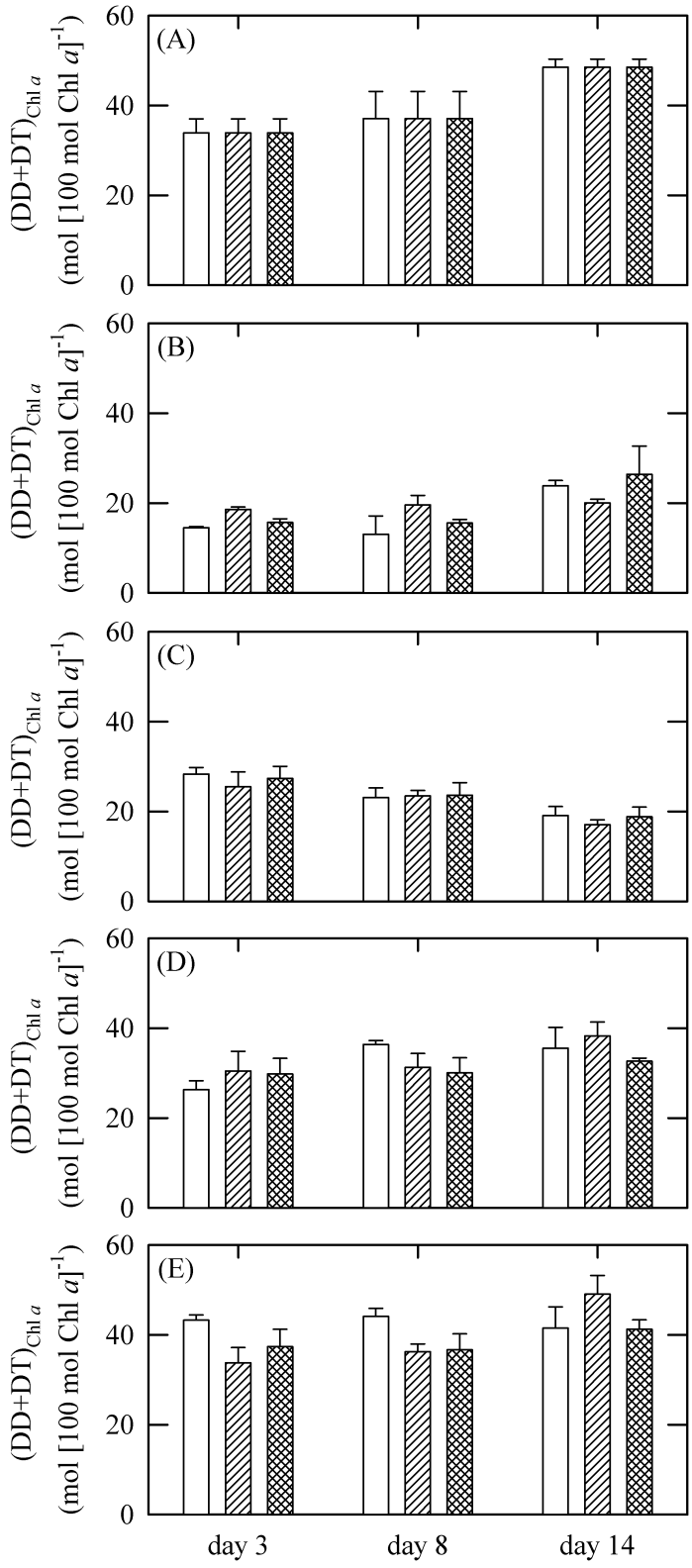

Figure 2-10. Temporal changes in $(DD+DT)_{Chl\ a}$ in the +0 μM-Exp (white bar), +10 μM-Exp (hatched bar), and +130 μM-Exp (cross-hatched bar) in the R-Exp in *T*. *weissflogii*. See Fig. 2-3 for the panel numbers, error bars, and the legends for x-axis.

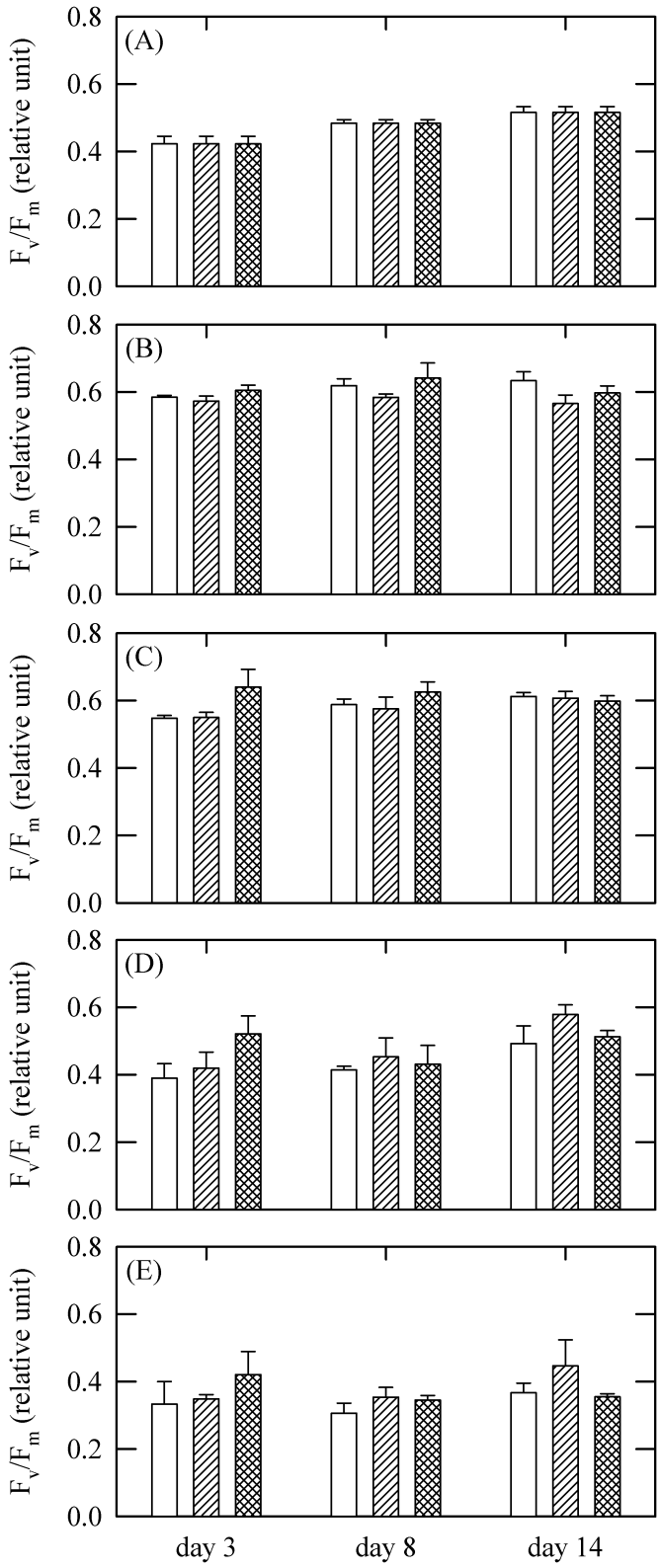

Figure 2-11. Temporal changes in F_v/F_m in the +0 μM-Exp (white bar), +10 μM-Exp (hatched bar), and +130 μM-Exp (cross-hatched bar) in the R-Exp in *T. weissflogii*. See Fig. 2-3 for the panel numbers, error bars, and the legends for x-axis.

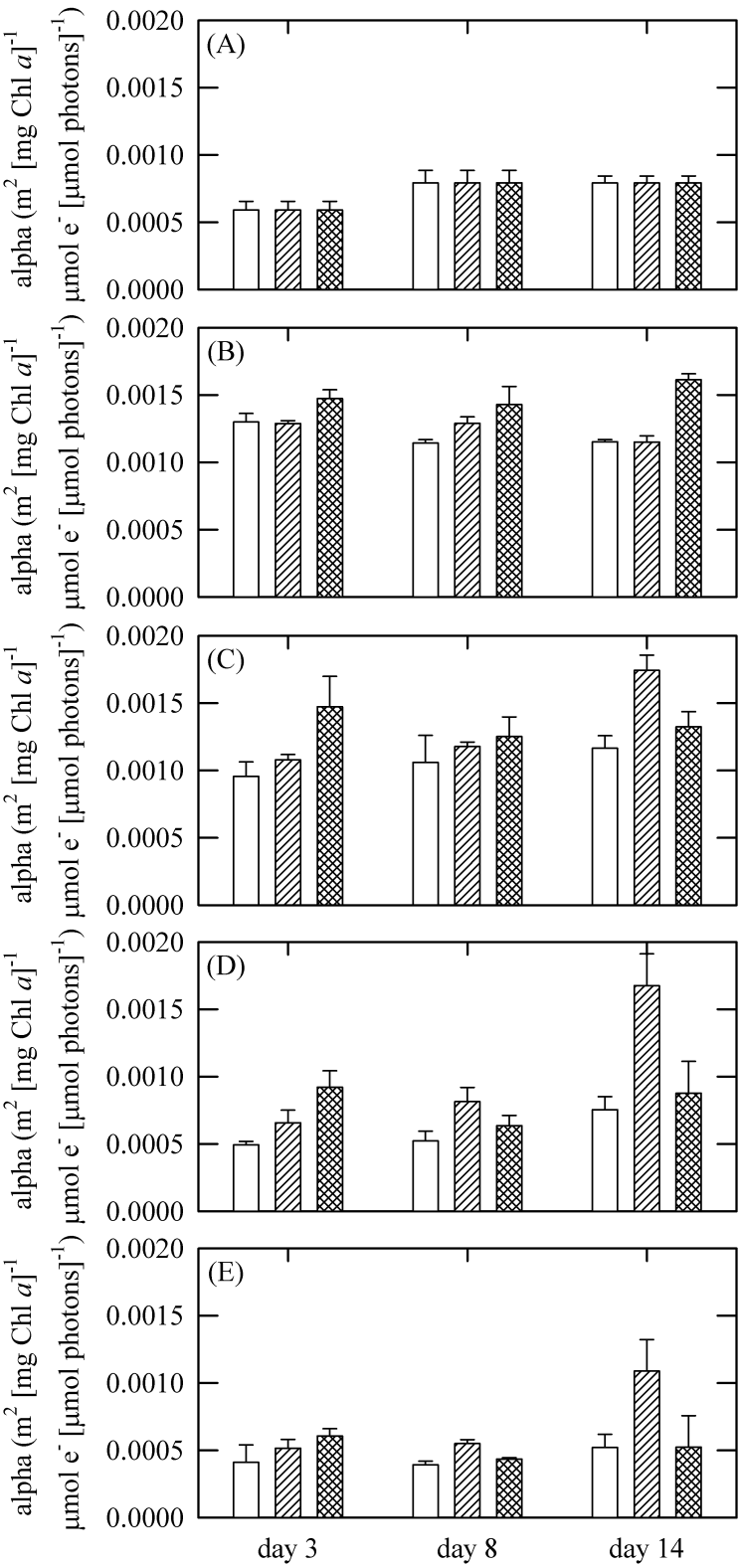

Figure 2-12. Temporal changes in α in the +0 µM-Exp (white bar), +10 µM-Exp (hatched bar), and +130 µM-Exp (cross-hatched bar) in the R-Exp in *T. weissflogii*. See Fig. 2-3 for the panel numbers, error bars, and the legends for x-axis.

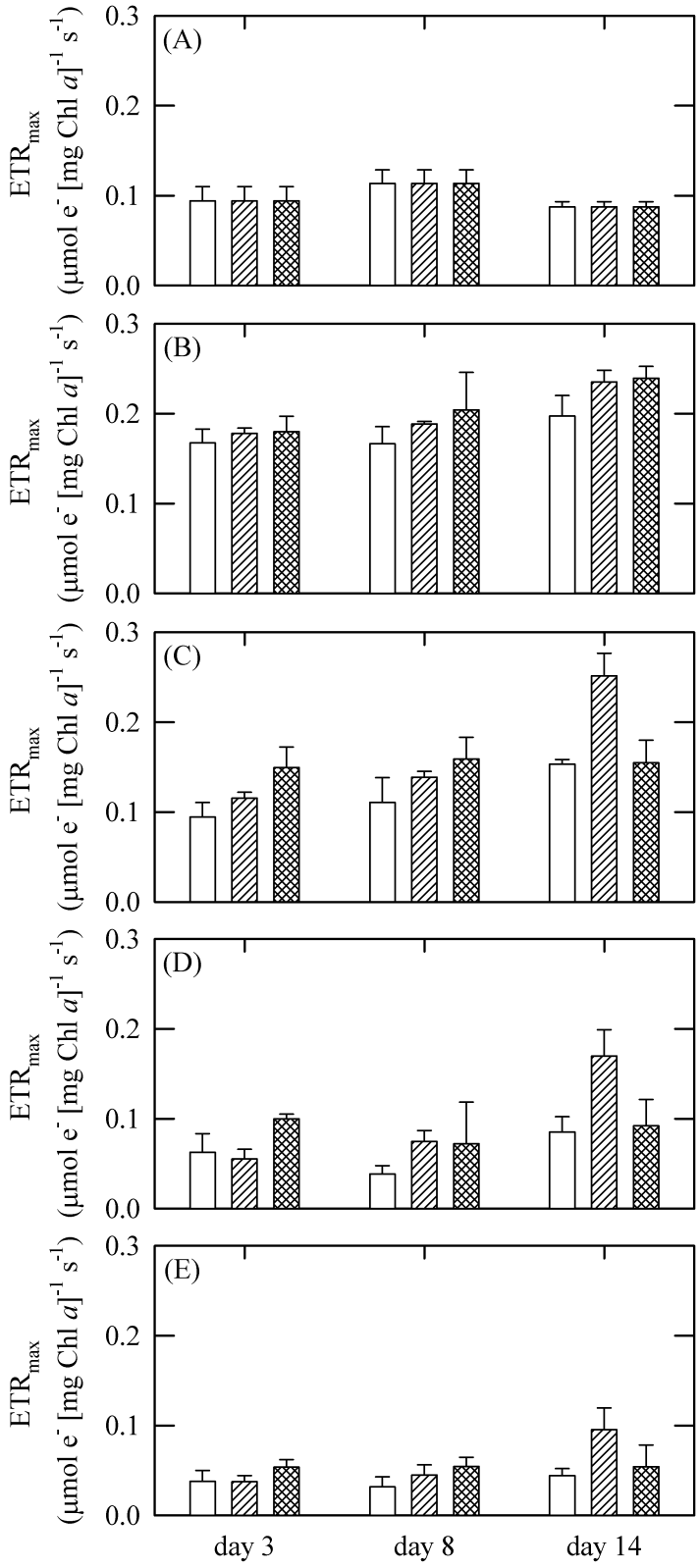

Figure 2-13. Temporal changes in ETR_{max} in the +0 μM-Exp (white bar), +10 μM-Exp (hatched bar), and +130 μM-Exp (cross-hatched bar) in the R-Exp in *T. weissflogii*. See Fig. 2-3 for the panel numbers, error bars, and the legends for x-axis.

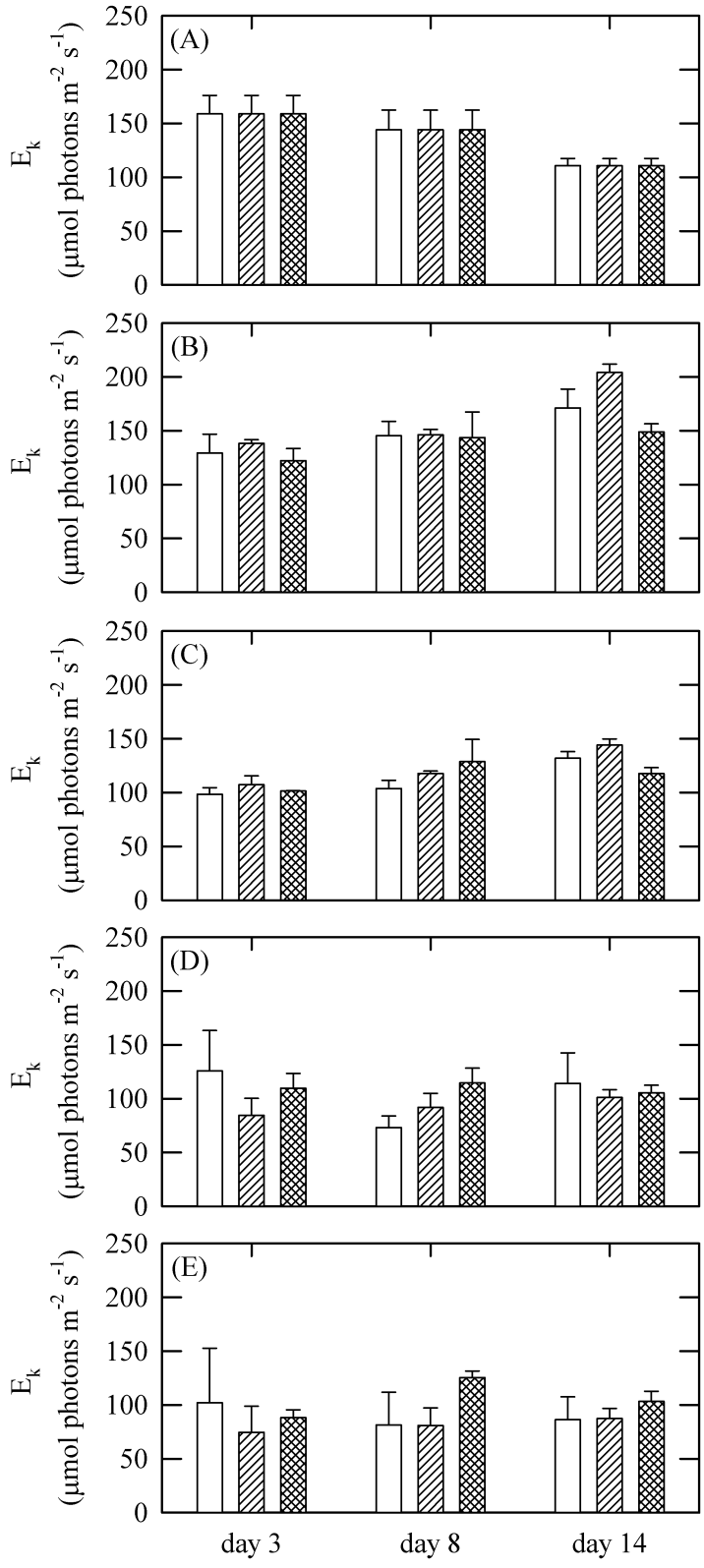

Figure 2-14. Temporal changes in E_k in the +0 μM-Exp (white bar), +10 μM-Exp (hatched bar), and +130 μM-Exp (cross-hatched bar) in the R-Exp in *T. weissflogii*. See Fig. 2-3 for the panel numbers, error bars, and the legends for x-axis.

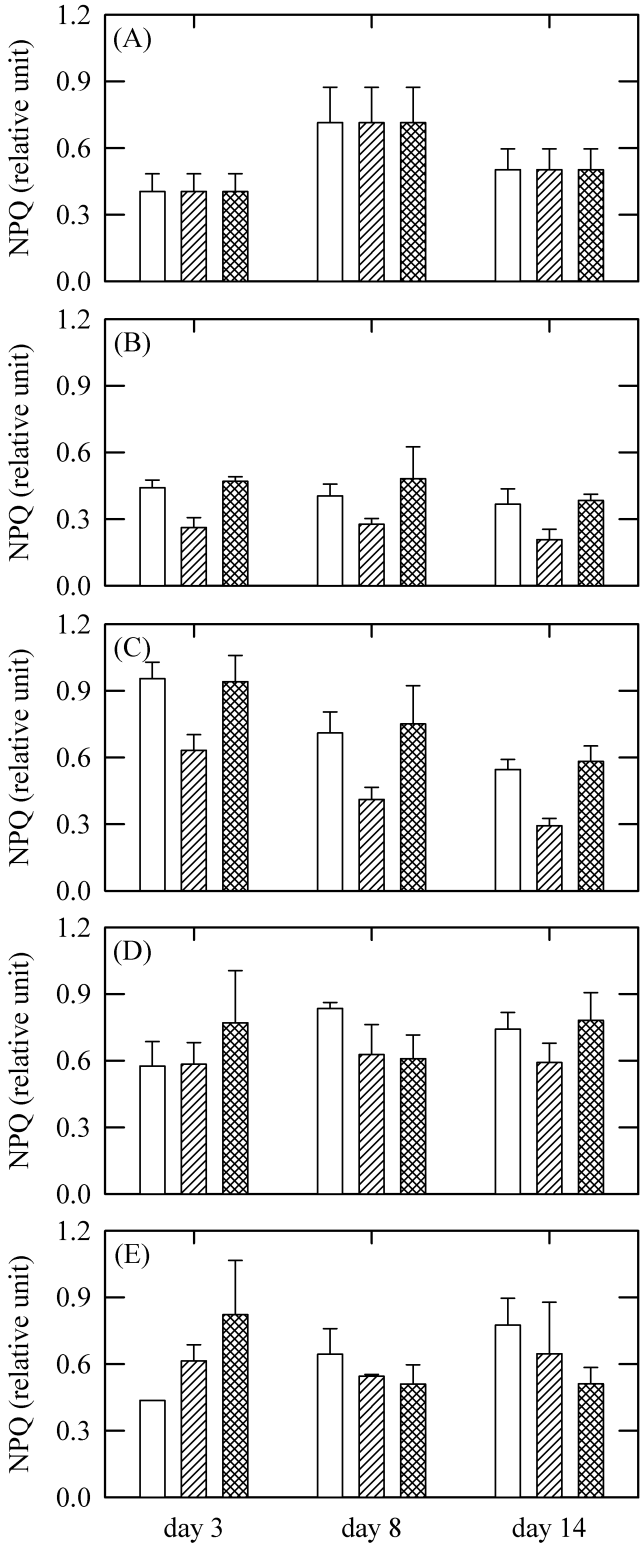

Figure 2-15. Temporal changes in NPQ in the +0 μM-Exp (white bar), +10 μM-Exp (hatched bar), and +130 μM-Exp (cross-hatched bar) in the R-Exp in *T. weissflogii*. See Fig. 2-3 for the panel numbers, error bars, and the legends for x-axis.

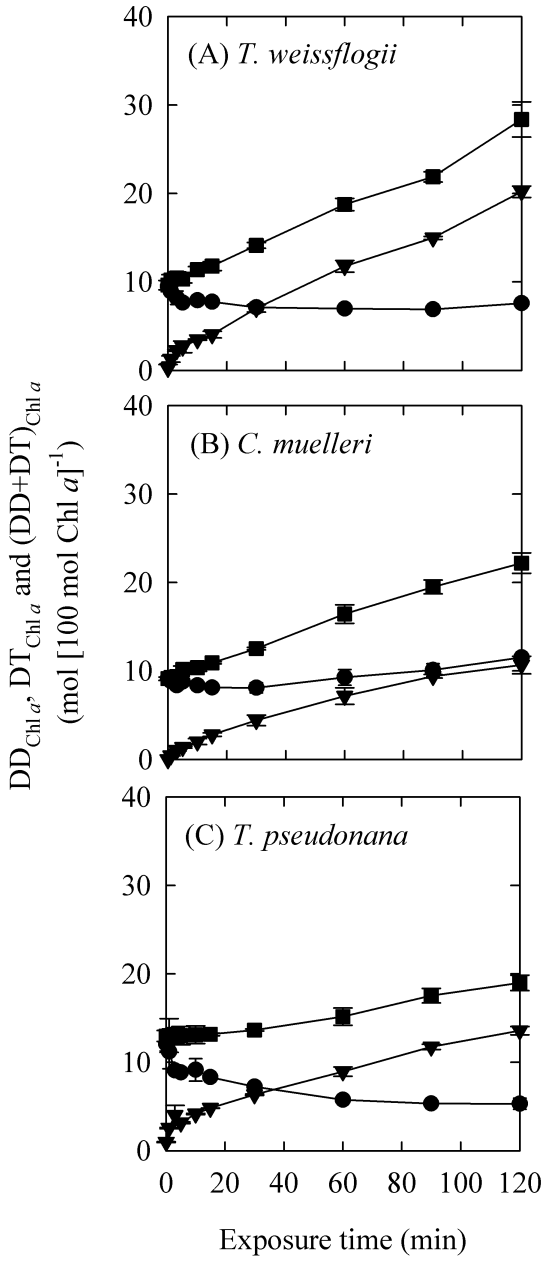

Figure 2-16. Temporal changes in molar ratios of DD (circle), DT (reversed triangle), and DD+DT (square) to Chl *a* in *T. weissflogii* (A), *C. muelleri* (B), and *T. pseudonana* (C) after exposure to high light. Error bars indicate one standard deviation of the mean.

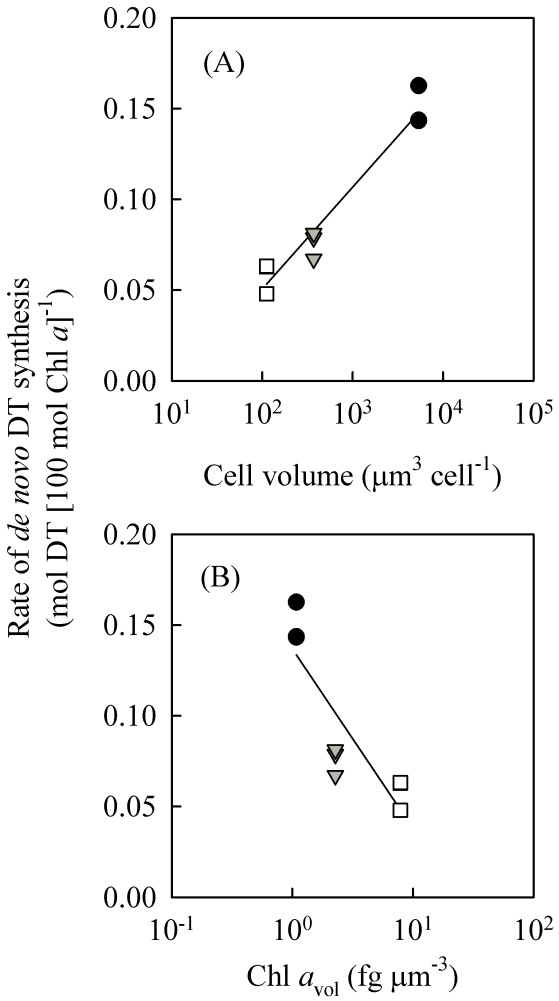

Figure 2-17. The relationship between rate of *de novo* DT synthesis and cell volume (A) and between rate of *de novo* DT synthesis and Chl a_{vol} (B) in *T. weissflogii* (circle), *C. muelleri* (reversed triangle), and *T. pseudonana* (square) after exposure to high light. [Rate of $DT^{de\ novo}$ synthesis] = 0.056 [Cell volume] – 0.062, r = 0.95; [Rate of $DT^{de\ novo}$ synthesis] = –0.099 + 0.14, r = 0.87.

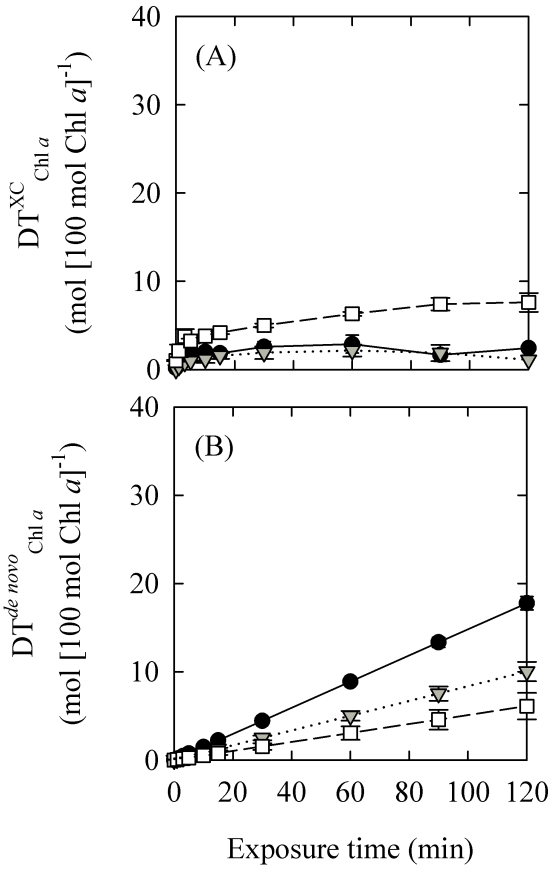

Figure 2-18. Temporal changes in molar ratios of DT^{XC} (A) and $DT^{de\ novo}$ (B) to Chl *a* in *T. weissflogii* (circle), *C. muelleri* (reversed triangle), and *T. pseudonana* (square) after exposure to high light. Error bars indicate one standard deviation of the mean.

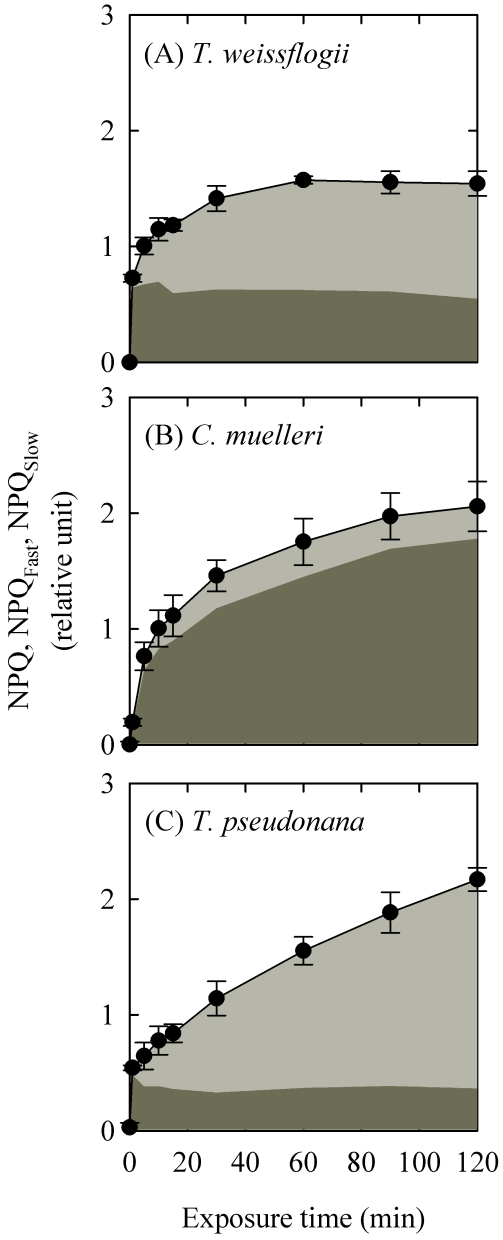

Figure 2-19. Temporal changes in NPQ (circle) in *T. weissflogii* (A), *C. muelleri* (B), and *T. pseudonana* (C) after exposure to high light. Areas of dark gray and light gray indicate NPQ_{Fast} and NPQ_{Slow}, respectively. Error bars indicate one standard deviation of the mean.

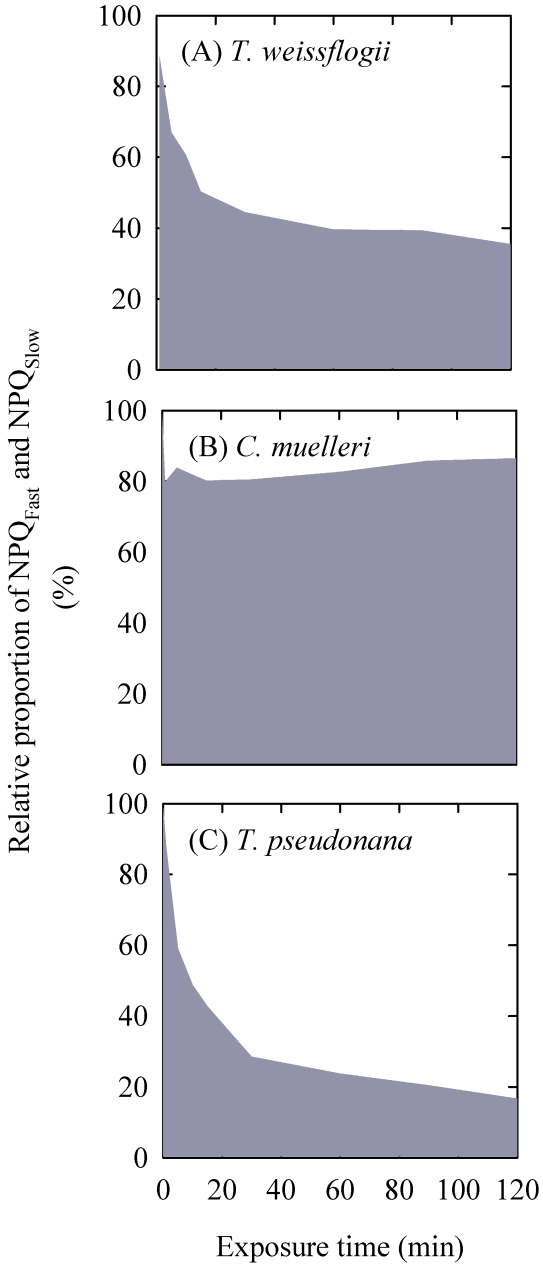

Figure 2-20. Temporal changes in relative proportion of NPQ_{Fast} (gray) and NPQ_{Slow} (white) in *T. weissflogii* (A), *C. muelleri* (B), and *T. pseudonana* (C) after exposure to high light.

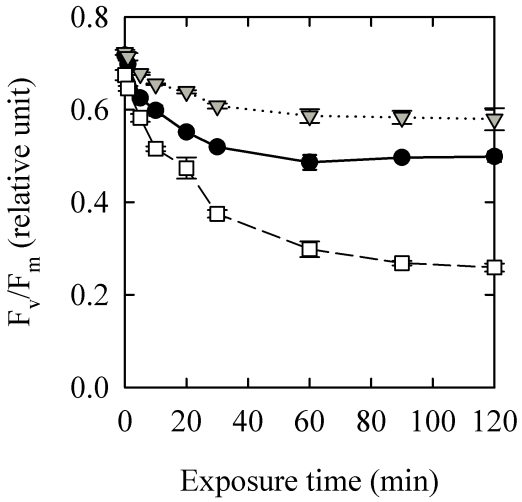

Figure 2-21. Temporal changes in F_v/F_m in *T. weissflogii* (circle), *C. muelleri* (reversed triangle), and *T. pseudonana* (square) after exposure to high light. Error bars indicate one standard deviation of the mean.

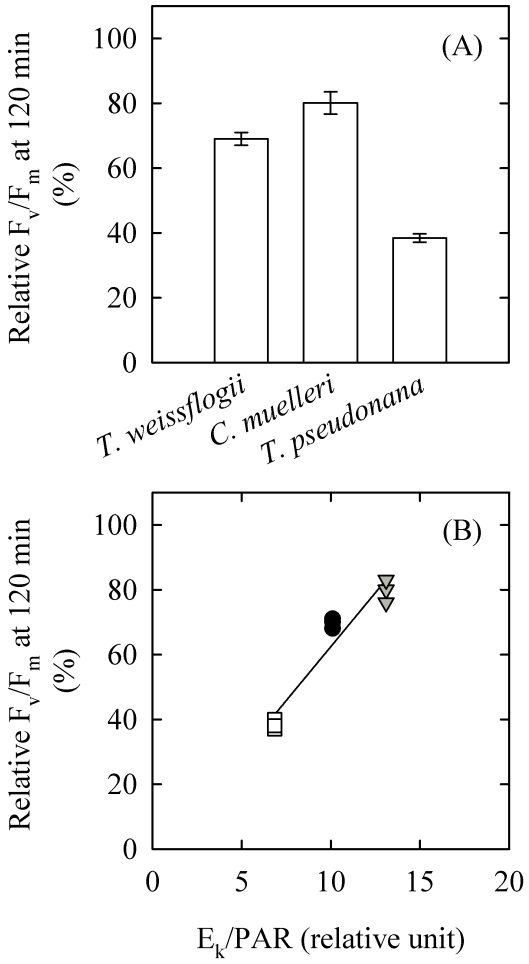

Figure 2-22. Relative F_v/F_m at 120 min exposure to the initial value (A) and relationship between E_k/PAR and relative F_v/F_m to the initial value in *T. weissflogii* (circle), *C. muelleri* (reversed triangle), and *T. pseudonana* (square) (B) after exposure to high light. Error bars indicate one standard deviation of the mean. $F_v/F_m = 6.7\ E_k/PAR - 4.1$, $r = 0.96$.

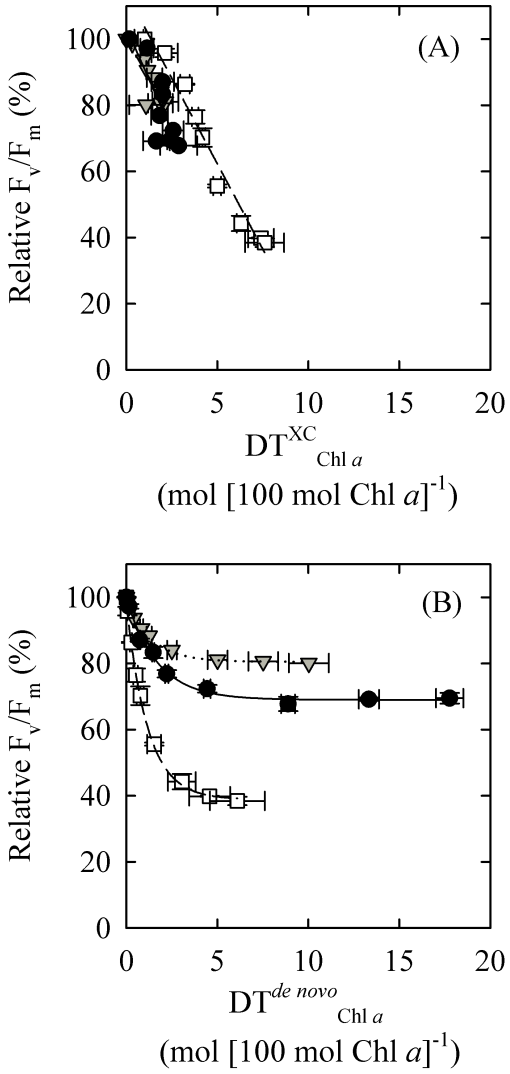

Figure 2-23. Relationship between $DT^{XC}_{Chl\ a}$ and relative F_v/F_m to the initial value (A) and between $DT^{de\ novo}_{Chl\ a}$ and relative F_v/F_m to the initial value (B) in *T. weissflogii* (circle), *C. muelleri* (reversed triangle), and *T. pseudonana* (square) after exposure to high light. Error bars indicate one standard deviation of the mean. $F_v/F_m = -11\ DT^{XC}_{Chl\ a} + 100$, $r = 0.83$; $F_v/F_m = 69 + 31\ (\exp\ [-18\ \{DT^{de\ novo}_{Chl\ a}/31\}])$, $r = 0.99$, in *T. weissflogii*, $F_v/F_m = -8.6\ DT^{XC}_{Chl\ a} + 99$, $r = 0.86$; $F_v/F_m = 80 + 19\ (\exp\ [-14\ \{DT^{de\ novo}_{Chl\ a}/19\}])$, $r = 0.99$, in *C. muelleri*, $F_v/F_m = -10\ DT^{XC}_{Chl\ a} + 114$, $r = 0.98$; $F_v/F_m = 39 + 60\ (\exp\ [-54\ \{DT^{de\ novo}_{Chl\ a}/60\}])$, $r = 0.99$, in *T. pseudonana*.

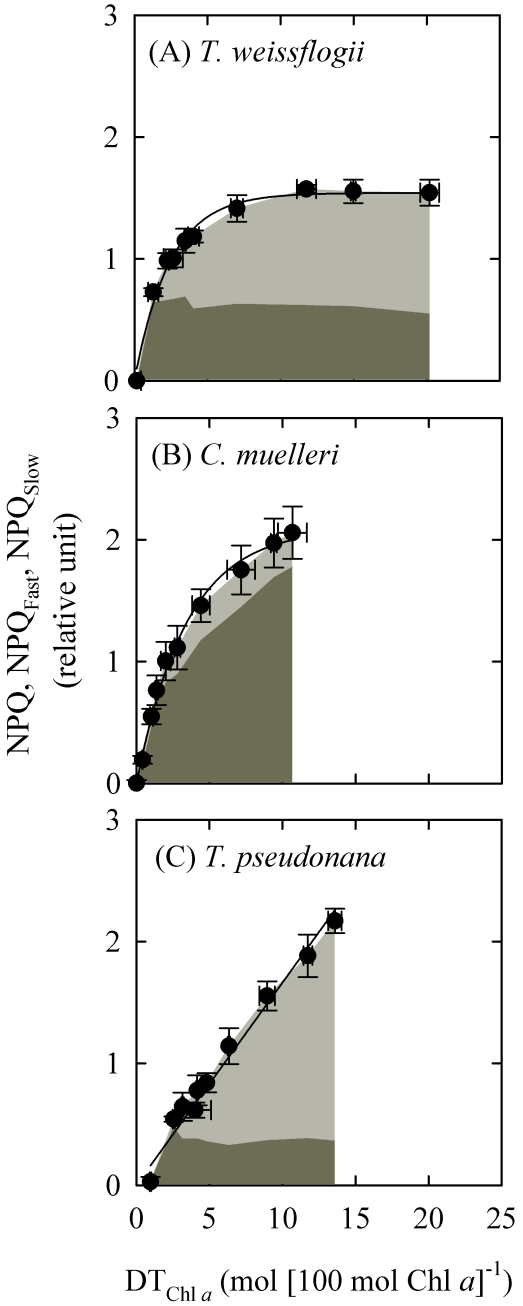

Figure 2-24. Relationship between $DT_{Chl\ a}$ and NPQ (circle) in *T. weissflogii* (A), *C. muelleri* (B), and *T. pseudonana* (C) after exposure to high light. Areas of dark gray and light gray indicate NPQ_{Fast} and NPQ_{Slow}, respectively. Error bars indicate one standard deviation of the mean. NPQ = 1.5 (1 – exp [–0.63 $\{DT_{Chl\ a}/1.5\}$]), r = 0.99, in *T. weissflogii*, NPQ = 2.1 (1 – exp [–0.61 $\{DT_{Chl\ a}/2.1\}$]), r = 0.99, in *C. muelleri*, NPQ = 0.16 $DT_{Chl\ a}$ + 0.058, r = 0.99, in *T. pseudonana*.

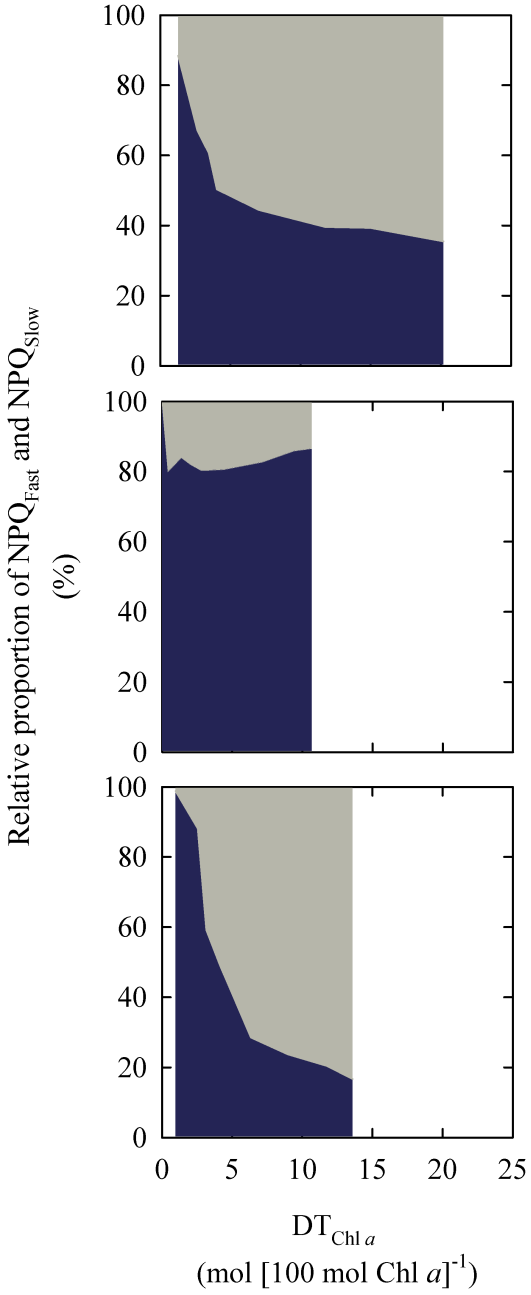

Figure 2-25. Relationship between $DT^{XC}_{Chl\ a}$ and relative proportion of NPQ_{Fast} (dark gray) and NPQ_{Slow} (gray) in *T. weissflogii* (A), *C. muelleri* (B), and *T. pseudonana* (C) after exposure to high light.

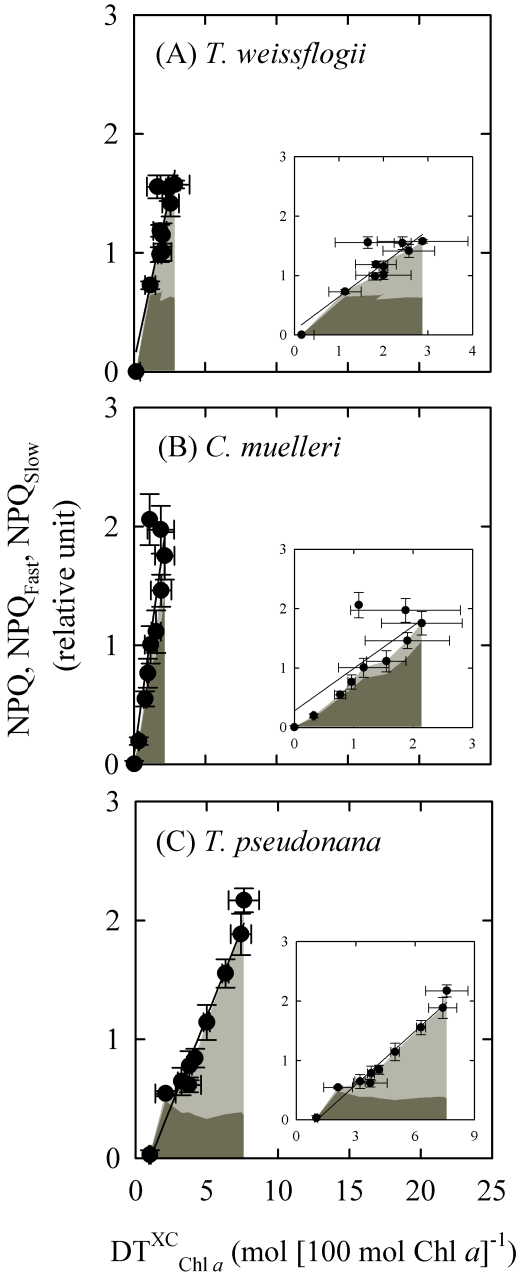

Figure 2-26. Relationship between $DT^{XC}_{Chl\ a}$ and NPQ (circle) in *T. weissflogii* (A), *C. muelleri* (B), and *T. pseudonana* (C) after exposure to high light, shown enlarged in the insets. Areas of dark gray and gray indicate NPQ_{Fast} and NPQ_{Slow}, respectively. Error bars indicate one standard deviation of the mean. NPQ = 0.49 $DT_{Chl\ a}$ + 0.080, r = 0.89, in *T. weissflogii*, NPQ = 0.78 $DT_{Chl\ a}$ + 0.28, r = 0.71, in *C. muelleri*, NPQ = 0.30 $DT_{Chl\ a}$ – 0.32, r = 0.98, in *T. pseudonana*.

Chapter III

PHOTOPROTECTION TO HIGH LIGHT IN NATURAL ASSEMBLAGES OF ICE ALGAE

3.1. Introduction

In polar and subpolar regions, diatoms bloom extensively in the spring, particularly in coastal waters (Smayda 1980). Diatoms predominantly inhabit the bottom surface of sea ice, and algal communities found in sea ice are known as ice algae. Although primary production by pelagic phytoplankton in the ice-free waters and in the under-ice water columns accounts for approximately 75% of primary production in the Arctic and Antarctica (Kirst and Wienchke 1995), ice algal communities play an important role in the succession of primary production in the sea ice ecosystem, forming the energy base of the marine food web in ice-covered waters (Bluhm et al. 2010). Snow cover and sea ice force ice algal communities to acclimate to extremely low light conditions, often <1% of the surface irradiance (Arrigo et al. 1993). Ice algae are able to survive extended periods of near- or complete darkness by using different strategies (McMinn and Martin 2013). When ice algae are released from retreating sea ice, some cells might be exposed suddenly to high light levels.

The concept of 'seeding' of spring bloom in surface water column by ice algae released from the melting sea ice has been discussed for decades by various researchers (*e.g.*, Ackley et al. 1979, Smith and Nelson 1986). There is the circumstantial evidence about co-occurrence of species in the sea ice and water column (Saito and Taniguchi 1978, Bianchi et al. 1992). Whether these sea ice algae function as a seed population or not depends on various factors, including the speed at which the cells settle through the water column, the viability of the cells once released from the sea

ice, and the presence of herbivores in the water column. If the sea ice algae settle rapidly (Riebesell et al. 1991) or are quickly grazed by pelagic zooplankton and incorporated into rapidly settling pellets (Scharek eta l. 1994, Mitchel et al. 1997), then the released algal cells never have the chance to serve as inoculum for an open water phytoplankton bloom. Under conditions where algae released from the sea ice remain in suspension in the upper water column and are not eaten immediately, the possibility of seeding still exists. Cells suspended in the surface water column are exposed to sudden high light, which cause photoinhibition. If ice algae suspended in the surface water column could reduce the damage of PSII, ice algal community could promptly recover photosynthetic capacity (Petrou et al. 2010) and there might be a high possibility of the ice algae as the seeding population of spring bloom.

Photoprotective mechanism of xanthophyll cycle to reduce photodamage has been demonstrated in the laboratory, most often in monocultures (*e.g.*, Lavaud et al. 2002, 2003, 2004) but only a few studies have investigated its *in situ* development, on the natural microalgal community (Griffith et al. 2009, Chevalier et al. 2010). There are a few studies of photoprotection on natural marine diatoms under natural irradiance based on the examination of NPQ with DT synthesis through xanthophyll cycle (van de Poll et al. 2011). We know little about the photoprotective response of ice algae to high light conditions partly because of limitation in logistics to field ice conditions that can support people and transportation. Shade-acclimated ice algae, which have been reported in accordance with light-saturation index E_k (Kirst and Wiencke 1995) in comparison with light acclimation of tropical phytoplankton, might be prone to photodamage by light stress due to sudden exposure to high light conditions when cells are released from retreating sea ice.

I investigated the photoprotective responses of an ice algal community to direct sunlight

by examining NPQ and xanthophyll pigments. To define the general features of photoprotection in ice algal communities when released from sea ice, I compared the effects of high light exposure on Saroma-Ko Lagoon ice algal communities with marine mesophilic diatoms studied in the Chapter II. The ice algal community was obtained from sea ice at Saroma-Ko Lagoon during the sea ice season, when fast ice cover reached approximately 0.5 m thick toward the end of ice season (Shirasawa et al. 2005). The ice algal communities have known to acclimate to irradiance at the undersurface of the sea ice (Kudoh et al. 1997) and have the large Chl *a* biomass of 200–400 mg m^{-3} (Satoh et al. 1989, Obata and Taguchi 2009). Irradiance at the undersurface of the sea ice is never sufficient to cause photoinhibition for the ice algal communities (McMinn and Hattori 2006).

3.2. Materials and methods

3.2.1. Ice-core sampling and experimental design

Sampling of ice algal communities were conducted at a station (44°N, 143°E) off the eastern shore of Saroma-Ko Lagoon, Hokkaido (Fig. 3-1). Ice-core samples were collected within a 2 m^2 surface area on March 5, 2012, February 27, 2013, and March 5, 2014, using a Cold Region Research and Engineering Laboratory (CRREL) ice-core sampler (Rand and Mellor 1985). The ice-core samples were immediately placed in a dark ice box and were transported to a land-based laboratory within 30 min. The bottom 3-cm portion of each ice core was sliced horizontally in a dark room and carefully crushed into filtered seawater in a 4 L opaque bottle (Garrison and Buck 1986). The filtered seawater was prepared by filtering seawater collected from a layer 1–4 m below the ice-water interface through GF/F glass fiber filters (Whatman, Maidstone, UK), and the salinity was 28±1.3. The samples were then allowed to melt completely at 0°C under dark conditions within 6 h. Exposure to ambient light was carefully avoided during the entire procedure.

The light exposure experiment was conducted at the Saroma Research Center of Aquaculture, Tokoro, Hokkaido, in a simulated *in situ* incubation (Fig. 3-1). Ice algal suspensions were transferred into a 4 L translucent bottle (Nalgene, USA) and the bottle was suspended in a water bath at 0°C. Ice algal samples were exposed to sunlight for 120 min at midday on March 7, 2012 (Exp. 1), February 28 (Exp. 2) and March 1, 2013 (Exp. 3), and March 7, 2014 (Exp. 4), respectively. The light-exposed ice algal samples except Exp. 1 were stored in the darkness within 24 hours. Subsamples for analysis of species and cell volume were collected prior to the exposure to the high light. Subsamples for analysis of pigments and variable Chl fluorescence were collected during the period of light exposure from 1 to 120 min and within 24 hours after the dark storage.

3.2.4. Photosynthetic available radiation

Photosynthetic available radiation (PAR) in the air and at the undersurface of the sea ice was simultaneously measured with a PAR air sensor (LI-190SA, Li-Cor, USA) and a PAR underwater sensor (LI-193A, Li-Cor, USA) on the day prior to the day of the light exposure experiments. Light transmission through snow cover was described using the Lambert-Beer law. To calculate PAR at the upper surface of the ice algal layer (>3 cm from the undersurface of the ice), I employed the extinction coefficient (K) for sea ice in the Saroma-Ko Lagoon (4.5 m^{-1}) reported by Kishino (1993). The PAR at the upper surface of the ice algal layer (E_z) was calculated using the following equation:

$$E_z = E_0 \times e^{-Kz} \quad (3.1)$$

where E_0 is PAR at the surface of the sea ice, and z is the depth of the sea ice. The monthly mean PAR in the air in February, 2012 and 2013 were obtained from Abashiri Local Meteorological Observatory, Hokkaido, Japan.

3.2.5. Water temperature and salinity

Water temperature of the ice algal samples for incubation was determined with a thermometer (DDR-140KD, Takagi, Japan). The salinity of the seawater used to melt the sea ice and the ice algal samples for incubation was determined with a conductivity analyzer (ES-51, Horiba, Japan).

3.2.6. Analysis of species and cell volume

Subsamples for species analysis were fixed with buffered 4% formaldehyde solution and stored in the dark at 4°C until further analysis (Iwasawa et al. 2009). The ice algal community was

identified and counted by using the counting chamber under an inverted microscope (Olympus, IMT-2, Japan) at ×200 magnification (Hasle 1978), in accordance with the taxonomy of Tomas (1997).

Cell sizes of each species were measured at a magnification of x1000. Cell volume (V) was determined by assuming the appropriate shape for each species (Hillebrand et al. 1999).

3.2.8. Pigment analysis

After light exposure for various periods, subsamples for pigment analysis were filtered through a GF/F glass fiber filter (Whatman, UK) with the addition of 100 or 300 μmol L^{-1} DTT (final concentration), which was prepared from a 100 or 300 mmol L^{-1} stock solution and used to inhibit DD de-epoxidation during sample preparation (Olaizola et al. 1994, Kashino and Kudoh 2003). The filtration in the laboratory was conducted within 5–10 min of sampling. Filtered samples were immediately frozen in liquid nitrogen and stored at −80°C until further analysis. Cells collected on filters were soaked in N, N-dimethylformamide, sonicated to break the cell walls, and extracted for 24 h at −20°C in the dark (Suzuki and Ishimaru 1990). The cell extracts were filtered through a 0.20-μm filter apparatus (Millex-LG, Merck Millipore, Milford, MA, USA) to remove cellular debris and glass fibers. All extraction procedures were conducted under subdued light to prevent photodegradation of pigments. The extracts were evaluated by high-performance liquid chromatography (HPLC, 168 Diode Array Detector, C18 reversed-phase ultra-sphere 3 μm column; Beckman Coulter, Fullerton, CA, USA) using a solvent gradient system, with solvent A (80% methanol and 20% 0.5 M [v/v] ammonium acetate) and solvent B (70% methanol and 30% ethyl acetate) as described by Head and Horne (1993). A linear gradient from 0% to 100% B was provided over 25 min, followed by an isocratic hold at 100% B for 9 min. The flow rate was held

constant at 1.0 mL min^{-1}. Peaks were quantified using standards for Chl *a*, Chl *c*, fucoxanthin (Fuco), DD, DT, and β-carotene (β-caro) obtained from the Danish Hydraulic Institute (Hørsholm, Denmark).

Initial rate constants (*k*) for temporal changes in the ratio of DT to Chl *a* were calculated for de-epoxidation of DD to DT in light conditions by fitting to a first-order kinetic model (Olaizola and Yamamoto 1994):

$$-kt = \mathrm{Ln}[(DT_t - DT_\infty)/(DT_0 - DT_\infty)] \quad (3.2)$$

where DT_0 is the initial relative amount of DT, and DT_t is the relative amount of DT at time *t* after light exposure. The value for DT_∞ was assumed to be the value measured at 20 min after light exposure because DT levels were close to constant at this time.

3.2.9. Fluorescence analysis

Variations in Chl fluorescence were measured with a pulse-amplitude modulated chlorophyll fluorometer (Water-PAM, Walz, Germany). Subsamples for fluorescence analysis were placed in a 15-mm diameter quartz cuvette, which was illuminated by a circular array of 14 red light-emitting diodes with a peak illumination at 655 nm.

Measurement of NPQ was conducted by exposing samples to actinic light at 1650 μmol m^{-2} s^{-1} for 30 s. The intensity of actinic light was determined based on the average of the observed maximum light intensity (1500 μmol m^{-2} s^{-1}) on the day prior to the day of the experiments. NPQ was calculated using the equation of Krause and Weis (1991):

$$NPQ = (F_m - F'_m)/F'_m \quad (3.3)$$

where F_m is the maximal PSII fluorescence level of dark-acclimated cells for 30 min before the light exposure experiment and F'_m is the maximal PSII fluorescence in light-saturated cells at a given

time. A saturation pulse of 3500 μmol photons m^{-2} s^{-1} was applied for 0.8 s to determine maximal fluorescence for F_m and F'_m. Total NPQ is distinguished on the basis of their relaxing quenching kinetics: fast (NPQ_{Fast}) and slow (NPQ_{Slow}) relaxing NPQ components (Walters and Horton 1991). NPQ_{Fast} and NPQ_{Slow} were calculated according to Maxwell and Johnson (2000):

$$NPQ_{Fast} = (F_m/F'_m)-(F_m/F_m^r) \quad (3.4)$$

and

$$NPQ_{Slow} = (F_m-F_m^r)/F_m^r \quad (3.5)$$

where F_m^r is the maximal PSII fluorescence measured after relaxation removing the actinic light in darkness for 30 min. Total NPQ was equal to sum of NPQ_{Fast} and NPQ_{Slow}. Definitions of relative yields of fluorescence were summarized in Fig. 2-1 in Chapter II (p. 49).

The minimum (F_0) and maximum (F_m) fluorescence were determined on dark-adapted cells for 30 min at given time. The maximum quantum efficiency of PSII (F_v/F_m) was calculated by the following equation (Schreiber et al. 1986):

$$F_v/F_m = (F_m-F_0)/F_m \quad (3.6).$$

The minimum (F) and maximum (F'_m) fluorescence in the light-acclimated state were measured with the saturation pulse. The PSII operating efficiency ($\Delta F/F'_m$) was calculated by the equation of Genty et al. (1989):

$$\Delta F/F'_m = (F'_m-F)/F'_m \quad (3.7).$$

The $\Delta F/F'_m$ was measured by illuminating the subsamples in a stepwise manner, increasing actinic light to 504 μmol photons m^{-2} s^{-1} in Exp.1, 478 μmol photons m^{-2} s^{-1} in Exp.2 and Exp. 3, and 556 μmol photons m^{-2} s^{-1} in Exp. 4 with 30-s illumination periods at each step (Parkins et al. 2006). The relative electron transport rate (rETR) by PSII was obtained using the following equation (Genty et al. 1989):

$$rETR = PPFD \times 0.5 \times \Delta F/F'_m \quad (3.8)$$

where PPFD is the photosynthetic photon flux density, and 0.5 is a factor accounting for equal photons falling on PSI and PSII (Hartig et al. 1998; Gilbert et al. 2000). The rapid light curves (RLCs) were measured by plotting the rETR against the actinic PPFD. The light-limited slope (α) and the light-saturated rate ($rETR_{max}$) of the RLC were calculated according to Webb et al. (1974):

$$rETR = rETR_{max}(1-\exp[-\alpha \times PPFD/rETR_{max}]) \quad (3.9).$$

The light-saturation index (E_k), based on the observation of the rETR, was calculated using the following equation:

$$E_k = rETR_{max}/\alpha \quad (3.10).$$

3.2.10. Light absorption analysis

The total particulate absorption spectra of cells on GF/F glass fiber filters (Whatman, USA) were measured with a dual beam UV-visible spectrophotometer equipped with an integrating sphere (UV-2450, Shimadzu, Japan) following the quantitative filter technique (QFT) method of Mitchell and Kiefer (1988). Spectral absorptions were scanned from 400 to 760 nm. Optical density spectra of particulates $OD_f(\lambda)$ on filters were measured and corrected by subtracting the average optical density between 730 and 760 nm, $OD_f(730\text{-}760)$ (Babin and Stramski 2002). Corrected $OD_f(\lambda)$ was converted to the optical density of particle in suspension $OD_s(\lambda)$ (Cleveland and Weidemann 1993);

$$OD_s(\lambda) = 0.378\ OD_f(\lambda) + 0.523\ OD_f(\lambda)^2 \quad (3.11).$$

The absorption coefficients $a_p(\lambda)$ were calculated by the equation;

$$a_p(\lambda) = 2.303\ OD_s(\lambda)/X \quad (3.12)$$

where 2.303 is the conversion factor for $\log_e$ from $\log_{10}$ and X is the ratio of the filtered volume to

the filtered clearance area of the filter. Following the measurement of $OD_f(\lambda)$, filters were immersed in 100% methanol for overnight pigment extraction according to the method of Kishino et al. (1985). The absorption coefficients for non-pigmented particles $a_d(\lambda)$ were calculated in the same manner as the total particulates using Eq. (3.11) and Eq. (3.12). The difference between $a_p(\lambda)$ and $a_d(\lambda)$ absorption coefficients was considered to be the light absorption coefficient $a_{ph}(\lambda)$ due to solely to phytoplankton. Finally, $a_{ph}(\lambda)$ was converted to Chl *a* specific absorption coefficient, $a^*_{ph}(\lambda)$, by dividing it by the Chl *a* concentration obtained from HPLC measurements.

3.2.11. Statistical analysis

The mean ± one standard deviation is reported throughout the present study. The Student's *t*-test was used to detect differences between the two groups. Statistical significance between more than two groups was analyzed using Dunnett's or Turkey's multiple comparison test. Analysis of covariance was carried out to compare the slopes of regression lines of the relationship between DT and F_v/F_m of initial value and the slopes of regression lines of the relationship between DT and NPQ. *P* values less than 0.05 were considered to be significant.

3.3. Results

3.3.1. Characteristics of sea ice

Freezing period of sea ice prior to sampling day for ice core was approximately 20 days longer in Exp. 2 and 3 than in Exp. 1 and 4 (Table 3-1). The ice was more than 40 cm thick with less than 10 cm snow cover in three years (Table 3-1). The extinction coefficient in ice algal layer was 47 m^{-1} in 2012, 40 m^{-1} in 2013, and 18 m^{-1} in 2014, respectively. The Chl *a* biomass at the bottom of the ice algal layer was highest in 765±47 mg Chl *a* m^{-2} in 2012 (Table 3-1).

The relative photosynthetic available radiation (PAR) at the undersurface of sea ice and at the upper surface of the ice algal layer to PAR in the air was lowest in 2013 (Table 3-1). The monthly mean PAR at the undersurface and upper-surface of the ice algal layer in February was 58 and 237 μmol photons m^{-2} s^{-1} in 2012, 28 and 93 μmol photons m^{-2} s^{-1} in 2013, 70 and 119 μmol photons m^{-2} s^{-1} in 2014, respectively.

3.3.2. High light exposure experiments

3.3.2.1. Cell conditions prior to the exposure to high light

Prior to the exposure experiments to high light, the ice algal communities were dominated by diatoms, representing about 98% in Exp. 1, 99% in Exp. 2, 100% in Exp. 3, and 98% in Exp. 4, respectively. In Exp. 1, the pennate *Pinnularia quadratarea* var. *constricta* and *Navicula transitans* var. *derasa* accounted for 52% and 30% of all cells, respectively (Table 3-2). More than 80% of the cells in Exp. 2, Exp. 3, and Exp. 4 were the centric *D. conefervacea*. The total cell volume of the ice algal communities was highest in 24×10^{-6} μm^3 ml^{-1} in Exp. 1 and lowest in Exp. 3 in 12×10^{-6} μm^3 ml^{-1} (Table 3-3). Cellular Chl *a* content per unit volume (Chl a_{vol}) in Exp. 4 was 3.9±0.17 fg μm^{-3} and significantly lower than in the other experiments (Turkey-test, $p < 0.01$; Table 3-4). Cellular

light absorption per unit volume (a_{vol}) in Exp. 1 was 0.38±0.023 m^2 μm^{-3} and significantly higher than those in the other experiments ($p < 0.01$; Table 3-4). The amounts of fucoxanthin and Chl *c* of light-harvesting pigments, which were normalized to Chl *a*, were larger in Exp. 1 than those in the other experiments, whereas the amounts of β-carotene were smaller in Exp. 1 (Table 3-5). Light-saturation index (E_k) was higher in Exp. 3 than those in either Exp. 2 or Exp. 4 (Table 3-6). Based on the monthly mean PAR at the undersurface of ice algal layer in February, the ratio of E_k to PAR (E_k/PAR) prior to the high light exposure was also higher in Exp. 3 than those in either Exp. 2 or Exp. 4 (Table 3-6). The maximum quantum efficiency of PSII (F_v/F_m) prior to the high light exposure ranged from 0.39 in Exp. 3 to 0.63 in Exp. 1, which was related to the values of E_k/PAR (Table 3-6).

The high light exposure experiments were conducted around the time of the day when the sunlight intensity was the highest (Fig. 3-2). The average PAR ranged from approximately 580 μmol photons m^{-2} s^{-1} in Exp. 3 to 1400 μmol photons m^{-2} s^{-1} in Exp. 2 (Table 3-7).

3.3.2.2. Xanthophyll pigments

After ice algal communities were exposed to sunlight, concentrations of Chl *a*, Chl *c*, fucoxanthin, and β-carotene in the all experiments showed no significant change during light exposure for 120 min, although the initial concentrations were only summarized in Table 3-5. The molar ratios of pigments to Chl *a* in the all experiments showed no significant change or less variation compared to those of DD and DT during light exposure. The de-epoxidation of DD to DT by xanthophyll cycle occurred after the exposure to sunlight. The molar ratio of DD to Chl *a* ($DD_{Chl\ a}$) decreased, whereas the molar ratio of DT to Chl *a* ($DT_{Chl\ a}$) increased over the 120 min (Fig. 3-3). During the light exposure experiments, the $DD_{Chl\ a}$ decreased by 42% in Exp. 1, 15% in Exp. 2,

32% in Exp. 3, and 21% in Exp. 4, respectively. The initial rate constant (k) of temporal changes in the $DT_{Chl\ a}$ in the first 10 minute of light exposure ranged from 0.17 min^{-1} in Exp. 1 to 0.30 min^{-1} in Exp. 3 (Table 3-8). Because the molar ratio of DD+DT to Chl *a* ($[DD+DT]_{Chl\ a}$, pool size of xanthophyll pigments) did not change significantly during light exposure for 120 min, the $DT_{Chl\ a}$ produced for ice algal communities could be synonymous with the molar ratio of DT produced through xanthophyll cycle to Chl *a* ($DT^{XC}_{Chl\ a}$). The maximum $DT^{XC}_{Chl\ a}$ ranged from 1.03 mol DT (100 mol Chl a)$^{-1}$ in Exp. 2 to 4.50 mol DT (100 mol Chl a)$^{-1}$ in Exp. 3 (Table 3-8).

3.3.2.3. Variable Chl fluorescence

Prior to the high light exposure, any non-photochemical quenching (NPQ) was not identified in the all experiments. After the exposure to high light, the NPQ showed an exponential increase (Fig. 3-4). At the end of light exposure experiments, the NPQ values were highest in Exp. 1 and lowest in Exp. 2. The values of fast relaxing NPQ (NPQ_{Fast}) showed fast increase for the first 30 minutes (Fig. 3-4). The relative proportion of NPQ_{Fast} in the total NPQ was less than those of slow relaxing NPQ (NPQ_{Slow}) after 30 min (Fig. 3-5). At 120 min exposure time, the relative proportion of NPQ_{Fast} in the total NPQ reached to 7.2% in Exp. 1, 18% in Exp. 2, 31% in Exp. 3, and 14% in Exp. 4, respectively (Fig. 3-5).

The F_v/F_m in the all experiments decreased with time during 120 min exposure (Fig. 3-6). At the end of experiments, the decrease in F_v/F_m compared to the initial values ranged from 75% in Exp. 3 to 97% in Exp. 2 (Table 3-8, Fig. 3-7A). The relationships between the relative F_v/F_m to the initial value and the $DT^{XC}_{Chl\ a}$ showed significant negative linear relationships in the all experiments ($p < 0.01$; Fig. 3-7B). The slope (S^{XC}) of the regression line was steepest in −97±12 in Exp. 2 and gentlest in −21±5.2 in Exp. 3 ($p < 0.01$; Table 3-9).

3.3.2.4. Relationship between DT and NPQ

The relationships between $DT_{Chl\ a}$ and NPQ were significantly linear in the all experiments ($p < 0.01$; Fig. 3-8). The slope of the regression line was gentlest in 0.42±0.16 (100 mol Chl *a* [mol DT]$^{-1}$) in Exp. 3 ($p < 0.01$, Table 3-9). The relative proportions of NPQ_{Fast} in the total NPQ in the ice algal communities dropped below 50% when the amounts of $DT_{Chl\ a}$ were 1.5 mol DT (100 mol Chl *a*)$^{-1}$ in Exp. 1, 0.22 mol DT (100 mol Chl *a*)$^{-1}$ in Exp. 2, 1.3 mol DT (100 mol Chl *a*)$^{-1}$ in Exp. 3, and 0.21 mol DT (100 mol Chl *a*)$^{-1}$ in Exp. 4, respectively (Fig. 3-9).

3.3.3. Dark recovery experiments

When the light-exposed cells in Exp. 2, Exp. 3, and Exp. 4 were stored in the darkness within 24 hrs, epoxidation of DT to DD occurred (Fig. 3-10) as well as the decrease in NPQ occurred (Fig. 3-11A). The pool size of xanthophyll pigments ($[DD+DT]_{Chl\ a}$) was relatively similar before and after the dark exposure except Exp. 4 (Fig. 3-10C). After the dark storage of 24 hrs, the F_v/F_m increased to 18% in Exp. 2, 85% in Exp. 3, and 74% in Exp. 4 in comparison with the light exposure (Fig. 3-11B). The relative F_v/F_m values at 24 hrs of dark storage in comparison with the initial values indicated a logarithmical relationship with the relative F_v/F_m at 120 min light exposure (Fig. 3-12).

3.3.4. Comparison of photoprotective responses between ice algal community and mesophilic diatoms

Prior to the high light exposure, cellular Chl *a* content per unit volume (Chl a_{vol}) (3.9–7.0 fg μm^{-3}) in the ice algal communities and cellular light absorption per unit volume (a_{vol}) (0.18–0.38

$\times 10^{-13}$ m^2 μm^{-1}) were within the range of mesophilic diatoms from 1.1 to 7.9 fg μm^{-3} and from 0.071 to 1.1 $\times 10^{-13}$ m^2 μm^{-3} in the Chapter II, respectively (Fig. 3-13A, B). The light saturation index (E_k) (59–144) and the ratios of E_k to PAR (1.4–5.1) in the ice algal communities were lower than those of the mesophilic diatoms (267–631 μmol photons m^{-2} s^{-1} and 6.9–13, respectively) (Fig. 3-13C, D).

After the exposure to high light, the initial rate constants (*k*) of de-epoxidation of DD to DT for ice algal communities (0.17–0.30 min^{-1}) were similar values to those of mesophilic diatom species cultured in the laboratory in the Chapter II (0.15–0.23 min^{-1}) (Fig. 3-14A). The maximum values of $DT_{Chl\ a}$ (1.0–4.5 mol DT [100 mol Chl *a*]$^{-1}$) at the end of light exposure experiments in the ice algal communities were lower than the range of mesophilic diatoms in the Chapter II (11–20 mol DT [100 mol Chl *a*]$^{-1}$) ($p < 0.01$, Fig. 3-15A). The $DT_{Chl\ a}$ in the ice algal communities increased without significant changes in xanthophyll pool size during the light exposure experiments (Fig. 3-3), whereas the increase in $DT_{Chl\ a}$ with significant changes in xanthophyll pool size was observed for the mesophilic diatoms (Fig. 2-16 in p. 64). In the present study, the $DT_{Chl\ a}$ which were synthesized in the ice algal communities could be synonymous with the molar ratio of DT produced through xanthophyll cycle to Chl *a* ($DT^{XC}_{Chl\ a}$). The range of the maximum $DT^{XC}_{Chl\ a}$ (1.0–4.5 mol DT [100 mol Chl *a*]$^{-1}$) in the ice algal communities overlapped the range of mesophilic diatoms (2.2–7.6 mol DT [100 mol Chl *a*]$^{-1}$) (Fig. 3-15B). The accumulation of $DT^{de\ novo}_{Chl\ a}$ (6.1–18 mol DT [100 mol Chl *a*]$^{-1}$) was observed only in the mesophilic diatoms in the Chapter II but not in the ice algal communities (Fig. 3-15C).

The range of NPQ values (1.6–2.9) at the end of light exposure experiments in the ice algal communities overlapped the range of mesophilic diatoms in the Chapter II (1.5–2.2) (Fig. 3-16A). The range of the decrease in F_v/F_m compared to the initial values (75–97%) during the light

exposure experiments in the ice algal communities were larger than the range of mesophilic diatoms (20–62%) (Fig. 3-16B). The relative F_v/F_m at 120 min of the exposure was significantly dependent upon the ratio of E_k to PAR (E_k/PAR) (Fig. 3-17A) and the amounts of $DT_{Chl\ a}$ (Fig. 3-17B). The significant negative linear relationships between the relative F_v/F_m and $DT^{XC}_{Chl\ a}$ were observed in both ice algal communities (Fig. 3-7) and mesophilic diatom species (Fig. 2-23A in p. 71). The slopes (S^{XC}) of the regression line was steeper in the ice algal communities (< −20) than in the mesophilic diatom species (> −11) ($p < 0.01$, Fig. 3-18A). The relationship between the relative F_v/F_m and $DT^{de\ novo}_{Chl\ a}$ were observed in only mesophilic diatom species but not in the ice algal communities (Fig. 3-18B).

Significantly linear relationships between $DT_{Chl\ a}$ and NPQ was observed in the ice algal communities ($p < 0.01$; Fig. 3-8), whereas the NPQ saturated with the $DT_{Chl\ a}$ in the mesophilic diatom species (Fig. 2-24 in p. 72). The initial slope of the relationship between $DT_{Chl\ a}$ and NPQ was lower than 2 in the ice algal communities, whereas for mesophilic diatom species, the maximum of the slope was less than was less than 1 (Fig. 3-18C). There were significant difference in the slopes between mesophilic diatom species and ice algal communities ($p < 0.01$). The relative proportions of NPQ_{Fast} in the total NPQ in the ice algal communities dropped below 50% when the amounts of $DT_{Chl\ a}$ were at least 0.2 in Exp. 4 but no more than 1.5 mol DT (100 mol Chl a)$^{-1}$ in Exp. 1 (Fig. 3-9), whereas for the mesophilic diatoms when the amounts of $DT_{Chl\ a}$ were at least 4.2 mol DT (100 mol Chl a)$^{-1}$ (Fig. 2-25 in p. 73).

3.4. Discussion

3.4.1. High light exposure experiments

3.4.1.1. Dynamics of xanthophyll pigments

The conversion of DD to DT in the ice algal communities at the exposure to high levels of light in the present chapter is confirmed also in previous studies for ice algal communities (*e.g.,* Griffith et al. 2009), Antarctic phytoplankton communities (van de Poll et al. 2011) and microphytobenthos where conditions are light-limited (Chevalier et al. 2010). Although the initial rate constants (k) for de-epoxidation of DD to DT in the cultured diatom species were obtained in the controlled laboratory experiments (Fig. 3-14A), a few k values have been estimated for ice algal communities which are predominately consisted by diatoms (Kudoh et al. 2003, Griffith et al. 2009). In the present study, the range of the rate constants (0.17–0.30 min^{-1}) were similar to the range of previously reported studies of ice algal communities (0.21–1.3 min^{-1}; Kudoh et al. 2003, Griffith et al. 2009) and mesophilic diatoms (0.089–2.2 min^{-1}; Olaizola et al. 1994, Olaizola and Yamamoto 1994, Lohr and Wilhelm 1999, Kashino and Kudoh 2003, Lavaud et al. 2004) even exclusion of outliers (Fig. 3-14A). Although Lavaud et al. (2004) found the k value for mesophilic diatoms was light dependent, other studies have noted that k values did not respond significantly to light (Olaizola et al. 1994; Kashino and Kudoh 2003). The initial conversion of DD to DT, which was mediated by the de-epoxidase enzyme to dissipate excess light energy, seemed to be triggered by instantaneous exposure to high light levels, regardless of the exposed light intensity (Kashino and Kudoh 2003).

The maximum $DT^{XC}_{Chl\ a}$ (1.0–4.5 mol DT [100 mol Chl a]$^{-1}$) after the light exposure in the ice algal communities observed in the present chapter was located within, but at the lower end of, the range (0.9–25 mol DT [100 mol Chl a]$^{-1}$), which were reported by the previous studies for

ice algal communities (Kudoh et al. 2003, Griffith et al. 2009, Mangoni et al. 2009). These values reported for ice algal communities were lower than those values in mesophilic diatoms observed in the Chapter II and the previous studies (2.6–25 mol DT [100 mol Chl *a*]$^{-1}$; Olaizola et al. 1994, Olaizola and Yamamoto 1994, Lohr and Wilhelm 1999, Kashino and Kudoh 2003, Lavaud et al. 2004, Goss et al. 2006, Wu et al. 2012, Lavaud and Lepetit 2013) even inclusion of outliers ($p < 0.01$; Fig. 3-15B). Although there were no differences in the initial rate of de-epoxidation observed between two habitats of polar and temperate seas, the maximum $DT^{XC}_{Chl\ a}$ showed difference between two habitats. The results suggest that the xanthophyll cycle of DD to DT in the ice algal communities is less active than the mesophilic diatoms for the long light exposure time.

The lack of response of *de novo* DT synthesis to the light exposure in the ice algal communities suggests that *de novo* DT synthesis might be minimal or under a detection limit at low temperatures, or under the present experimental conditions and/or methods. Previous studies have indicated an increase in DT without a change in xanthophyll pool size when the ice algal communities were exposed to high light levels for 60–120 min (Kudoh et al. 2003; Griffith et al. 2009). The $DT_{Chl\ a}$ accumulation without significant changes in the amount of $(DD+DT)_{Chl\ a}$ in the present study suggests that these dynamics in the ice algal communities are controlled by the xanthophyll cycle rather than by *de novo* synthesis of DT as suggested for other groups of algae by Olaizola et al. (1994) and Lavaud et al. (2004). In contrast, *de novo* synthesis of DT was observed during light exposure experiments involving mesophilic diatoms in the Chapter II and the previous studies (*e.g.,* Lavaud et al. 2004). The *de novo* DT synthesis, which are observed only in the mesophilic diatom species, might play a role in the photoprotection through thermal dissipation as indicated in the Chapter II and/or antioxidant function (Lepetit et al. 2010). Because there is an obvious difference in habitat temperatures between ice algal communities (–1°C) and mesophilic

diatoms (20°C), low temperatures could slow down metabolic processes (Morgan-Kiss et al. 2006). In addition to ice algal communities, Moisan et al. (1998) reported planktonic *Phaeocystis antarctica* (Prymnesiophyceae) grown at 3°C, which inhabit the polar sea, had no *de novo* synthesis of DT during the exposure to high light for 60 min. Therefore, the occurrence of *de novo* DT synthesis in ice algal communities and mesophilic diatoms might be influenced by low temperature. To test this hypothesis, further studies are required to investigate the functional response of ice algal communities to various temperatures.

3.4.1.2. Characteristics of Chl fluorescence

The decrease in F_v/F_m (74–93 %) at 120 min of light exposure in comparison with the initial F_v/F_m values in the ice algal communities (–1°C) observed in the present chapter were higher than those values in mesophilic diatoms (20°C) observed in both the Chapter II and the previous studies (7–81 %; Olaizola et al. 1994, Olaizola and Yamamoto 1994; Wu et al. 2012) except outlier ($p < 0.05$; Fig. 3-16B). For Antarctic planktonic diatom communities grown at –1°C under light-limited conditions, the decrease in F_v/F_m at 120 min of light exposure was 42±4.3 % (Katayama, personal communication), which fall within the range of mesophilic diatoms (Fig. 3-16B). This may suggest that the ice algal cells could be subjected to strong damage by high irradiances unlike the other ecological groups of marine diatoms. The F_v/F_m at 120 min, which was significantly dependent upon the ratio of E_k to PAR (E_k/PAR) (Fig. 3-17A), could be indicative of the degree of photoinhibition. The significantly lower E_k/PAR are observed in the ice algal communities than those in the mesophilic diatoms (Fig. 3-13D). The lower E_k/PAR, the more photoinhibition in the ice algal communities might be induced. The significant relationship between the F_v/F_m and E_k/PAR suggests that the strong shade acclimated cells of ice algae are suffered from

severe photoinhibition and consequently causes delay in the recovery of photosynthetic capacity (Petrou et al. 2010) in comparison to mesophilic diatom species. If the reduced acclimation to shade in ice algal communities, as a result of light transmission through ice is enhanced due to a thinning of ice (Arrigo et al. 2012) or shortened ice seasons at the lower latitude limits of sea ice distribution (Taguchi and Takahashi 1993), the ice algal communities at the bottom of the sea ice might have advantage of avoiding strong photoinhibition when cells are exposed to the high light. The F_v/F_m at the end of incubations was also significantly dependent upon the amounts of $DT_{Chl\ a}$ (Fig. 3-17B), which suggest that the photoinhibition could be reduced by enhancement of $DT_{Chl\ a}$ due to the synthesis of $DT^{de\ novo}$ which might be located in the close vicinity to the PSII light-harvesting complexes.

3.4.1.3. Photoprotective ability

The significant negative linear relationships between the relative F_v/F_m and $DT^{XC}_{Chl\ a}$ in the ice algal communities (Fig. 3-7B), which were also observed in the mesophilic diatom species in the Chapter II (Fig. 2-23A in p. 71), indicates that the synthesis of DT through xanthophyll cycle might assist to reduce photodamage and the PSII reaction center could be damaged progressively during the light exposure even if some excess energy is dissipated through xanthophyll cycle. The higher values of S^{XC} in the ice algal communities than those in the mesophilic diatom species (Fig. 3-18A) suggests that the lower efficiency of thermal dissipation through $DT^{XC}_{Chl\ a}$ in the ice algal communities might contribute to increase in the energy arriving at the reaction center. The mechanisms of thermal dissipation through xanthophyll cycle might be not enough to compensate for the excess light energy under the severe environmental stresses such as low temperature, as suggested by Gracía-Plazaola et al. (2012) for plants. The relationship between the relative F_v/F_m

and $DT^{de\ novo}{}_{Chl\ a}$, which is observed only for mesophilic diatoms (Fig. 2-23B in p. 71), suggests that the *de novo* synthesis of DT in the mesophilic diatom species might assist to reduce photodamage. The logarithmical decrease in the relative F_v/F_m with $DT^{de\ novo}{}_{Chl\ a}$ could indicate that no further prevention of photodamage by the synthesis of $DT^{de\ novo}$ should be occurred.

The linear relationship between $DT^{XC}{}_{Chl\ a}$ and NPQ (Fig. 3-8) suggests that NPQ is dependent on the accumulation of DT produced through xanthophyll cycle in ice algal communities. The lower slopes of the relationship between $DT_{Chl\ a}$ and NPQ for the mesophilic diatom species than those of ice algal communities ($p < 0.01$; Fig. 3-18C) suggest the lower quenching efficiency of DT (Goss and Jakob 2010). Furthermore, the significant difference in the slope between ice algal communities and mesophilic diatom species could be explained by distinguishing NPQ to thermal dissipation (NPQ_{Fast}) and photoinhibitory (NPQ_{Slow}) components of NPQ. The larger proportion of NPQ_{Slow} during the DT synthesis in the ice algal communities (Fig. 3-9) than those of the mesophilic diatom species (Fig. 2-25 in p. 73) suggest that the apparent increase in NPQ by the quenching due to photoinbition may therefore contribute to the higher quenching efficiency of DT in the ice algal communities than those of the mesophilic diatoms.

3.4.2. Dark recovery

Following 120 min exposure to high light, the kinetics of the recovery in the F_v/F_m in darkness within 24 hrs (Fig. 3-11) are coincided with the epoxidation of DT to DD (Fig. 3-10A, B) and the relaxation of NPQ (Fig. 3-11). Previous studies have reported a recovery of F_v/F_m can be attributed to relaxation of NPQ by xanthophyll cycle (Domingues et al. 2012). The recovery of F_v/F_m under dark condition is related to the F_v/F_m values at the end of light exposure experiments (Fig. 3-12). These results suggest that the photodamage of PSII recovers in the dark to a level close

to the initial condition when only a small amount of photodamage has occurred.

3.4.3. Conclusions

Photoprotective acclimation of the ice algal communities, which are usually acclimated to shade conditions, to the high light enhances the thermal dissipation through the xanthophyll cycle within minutes to hours. Although there were no difference of the initial rate constant (*k*) of de-epoxidation between mesophilic diatom species and ice algal communities, the activity of xanthophyll cycle in the ice algal communities could be lower for long light exposure time than those in the mesophilic diatoms. The slope of relationship between DT^{XC} and F_v/F_m suggests that the capacity of DT^{XC} to reduce photoinhibition in the ice algal communities might be lower than those of mesophilic diatom. In addition to the low capacity of photoprotection in DT^{XC}, the lack of response of *de novo* DT synthesis might cause the severe damage of PSII reaction centers in the ice algal community under high light conditions. The damaged PSII in the ice algal communities could be repaired under dark condition. Although the ice algal communities could dissipate excess heat by activation of the xanthophyll cycle, damage of PSII, which is mainly caused by the oxidation of the reaction center proteins of PSII at the exposure to high light, is enhanced by the low capacity of photoprotection in DT^{XC} and no *de novo* DT synthesis. Even if the PSII reaction centers in the ice algal communities are severely damaged, the ice algal communities could recover photosynthetic capacity under dark when the repair of PSII is larger than the damage of PSII.

Table 3-1. Freezing period of sea ice, snow and ice thickness, relative PAR between the upper-surface and undersurface of the ice algal layer to PAR in the air, and biomass of ice algal community at the bottom of sea ice at the site of sampling in Saroma-Ko Lagoon. Freezing period of sea ice in day, snow and ice thickness in cm, relative PAR in %, and biomass in Chl *a* mg m^{-3}. Mean ± one standard deviation.

		Freezing	Thickness		%PAR		
Year	Exp.	period	Snow	Ice	Upper	Under	Biomass
2012	Exp. 1	32	9.6 ± 1	40.1 ± 1.4	10.0	2.46	765 ± 47
2013	Exp. 2	51	6.8 ± 0.6	55.4 ± 1.1	3.55	1.08	173 ± 5.4
2013	Exp. 3	51	6.8 ± 0.6	55.4 ± 1.1	3.55	1.08	117 ± 8.6
2014	Exp. 4	30	8.6 ± 1	46.8 ± 1.6	5.09	3.00	145 ± 6.3

Table 3-2. Species composition (%) based on cell volume of ice algal community before high light exposure experiments.

	2012	2013		2014
Species	Exp. 1	Exp. 2	Exp. 3	Exp. 4
Diatoms				
Centric diatom				
Detonula confervacea	8.1	88	82	86
Chaetoceros similis	0	1.6	7.9	0.052
Other centric diatoms	1.2	0	0	0.44
Pennate diatom				
Achnanthes taeniata	3.4	1.3	1.5	0.039
Entomoneis sp.	0	6.07	4.4	7.0
Navicula transitans var. *derasa*	30	0	0	0.24
Pinnularia quadratarea var. *constricta*	52	0	0	0.52
Other pennate diatoms	3.2	3.0	4.1	4.4
Others	2.0	0.16	0	1.7
Centric diatoms: total diatoms	9.5	90	90	88
Pennate diatoms: total diatoms	91	10	10	12

Table 3-3. Total cell volume (μm^3 ml^{-1}) of ice algal community and mesophilic diatoms before high light exposure experiments.

	Total cell volume
Ice algal communities	
Exp. 1	24,777,276
Exp. 2	16,907,128
Exp. 3	11,663,347
Exp. 4	13,986,559
Mesophilic diatom species	
T. weissflogii	42,133,389
C. muelleri	49,499,793
T. pseudonana	6,195,275

Table 3-4. Cellular Chl *a* content per unit volume (Chl a_{vol}) and cellular light absorption per unit volume (a_{vol}) before high light exposure experiments in ice algal community. Chl a_{vol} in fg μm^{-3} and a_{vol} in m^2 μm^{-3}. Mean ± one standard deviation.

Year	Exp.	Chl a_{vol}	a_{vol}
2012	Exp. 1	6.11 ± 0.37	0.381 ± 0.023
2013	Exp. 2	7.01 ± 0.22	0.222 ± 0.0069
2013	Exp. 3	6.82 ± 0.50	0.216 ± 0.034
2014	Exp. 4	3.87 ± 0.17	0.177 ± 0.0059

Table 3-5. Molar ratio of pigment to Chl *a* (mol [100 mol Chl *a*]$^{-1}$) before high light exposure experiments in ice algal communities. Mean ± one standard deviation.

Year	Exp.	Fucoxanthin	Chl *c*	DD	DT	β-carotene
2012	Exp. 1	160 ± 10	67.9 ± 2.4	9.78 ± 1.1	0.577 ± 0.085	0.540 ± 0.13
2013	Exp. 2	71.4 ± 3.2	39.9 ± 1.7	4.55 ± 0.27	0	3.69 ± 0.45
2013	Exp. 3	71.1 ± 1.4	39.3 ± 1.7	8.53 ± 0.32	0.914 ± 0.28	2.79 ± 1.1
2014	Exp. 4	42.6 ± 2.9	32.5 ± 2.4	4.63 ± 0.43	0.0850 ± 0.081	5.20 ± 0.16

Table 3-6. Light-saturation index (E_k), ratio of E_k to PAR, and maximum quantum efficiency (F_v/F_m) before high light exposure experiments in ice algal community. E_k in μmol photons m^{-2} s^{-1}, and E_k/PAR and F_v/F_m in relative unit. Mean ± one standard deviation. No data, nd.

Year	Exp.	E_k	E_k/PAR	F_v/F_m
2012	Exp. 1	nd	nd	0.632 ± 0.026
2013	Exp. 2	59.0	2.09	0.531 ± 0.0059
2013	Exp. 3	144	5.10	0.386 ± 0.014
2014	Exp. 4	95.1	1.36	0.594 ± 0.0030

Table 3-7. PAR (µmol photons m^{-2} s^{-1}) of sunlight during high light exposure experiments with ice algal communities.

Year	Exp.	Maximum	Minimum	Weight average
2012	Exp. 1	1145	520	734
2013	Exp. 2	1691	994	1406
2013	Exp. 3	725	335	579
2014	Exp. 4	1182	426	672

Table 3-8. Initial rate constant (k) of de-epoxidation of DD to DT, maximum $DT^{XC}_{Chl\ a}$, and decrease in F_v/F_m compared to the initial value during light exposure experiments in ice algal communities. k in m^{-1}, $DT_{Chl\ a}$ in mol (100 mol Chl a)$^{-1}$, and decrease in F_v/F_m in %. [a] Mean ± 95% confidence limits. [b] Mean ± one standard deviation.

Year	Exp.	k	$DT^{XC}_{Chl\ a}$	Decrease in F_v/F_m
2012	Exp. 1	0.168 ± 0.32[a]	1.93 ± 0.14[b]	87.1 ± 4.0[b]
2013	Exp. 2	0.198 ± 0.33[a]	1.03 ± 0.19[b]	97.2 ± 2.2[b]
2013	Exp. 3	0.304 ± 0.20[a]	4.50 ± 0.62[b]	74.9 ± 6.8[b]
2014	Exp. 4	0.205 ± 0.017[a]	1.48 ± 0.14[b]	93.4 ± 3.0[b]

Table 3-9. Slope between $DT^{XC}_{Chl\ a}$ and relative F_v/F_m to the initial value (S^{XC} in relative unit) and slope between $DT_{Chl\ a}$ and NPQ (100 mol Chl *a* [mol DT]$^{-1}$) during light exposure experiments in ice algal communities. Mean ± 95% confidence limits.

Year	Exp.	S^{XC}	$DT_{Chl\ a}$ and NPQ
2012	Exp. 1	−62.0 ± 25	2.00 ± 0.49
2013	Exp. 2	−97.0 ± 12	1.43 ± 0.40
2013	Exp. 3	−20.8 ± 5.2	0.424 ± 0.16
2014	Exp. 4	−72.5 ± 14	1.65 ± 0.42

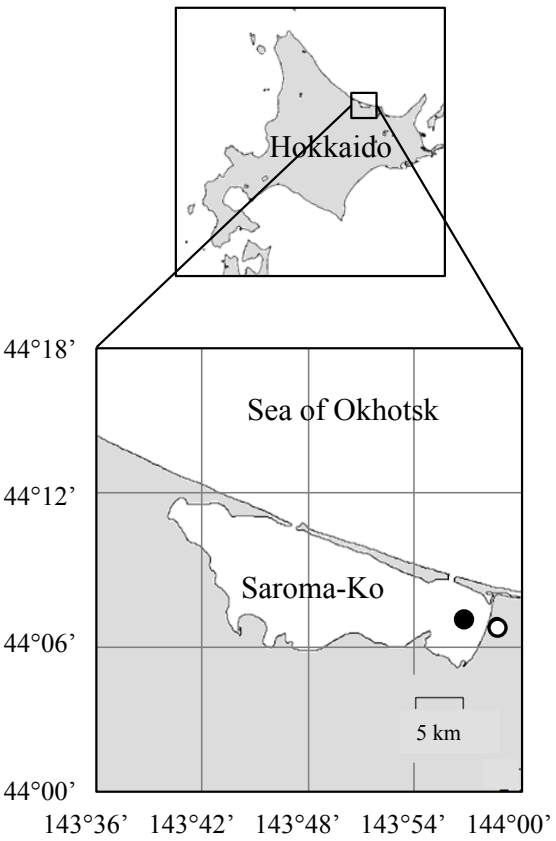

Figure 3-1. Location of ice-core sampling (solid circle) and high light exposure experimental site (open circle). The high light exposure experiment was conducted in front of the Saroma Research Center for Aquaculture.

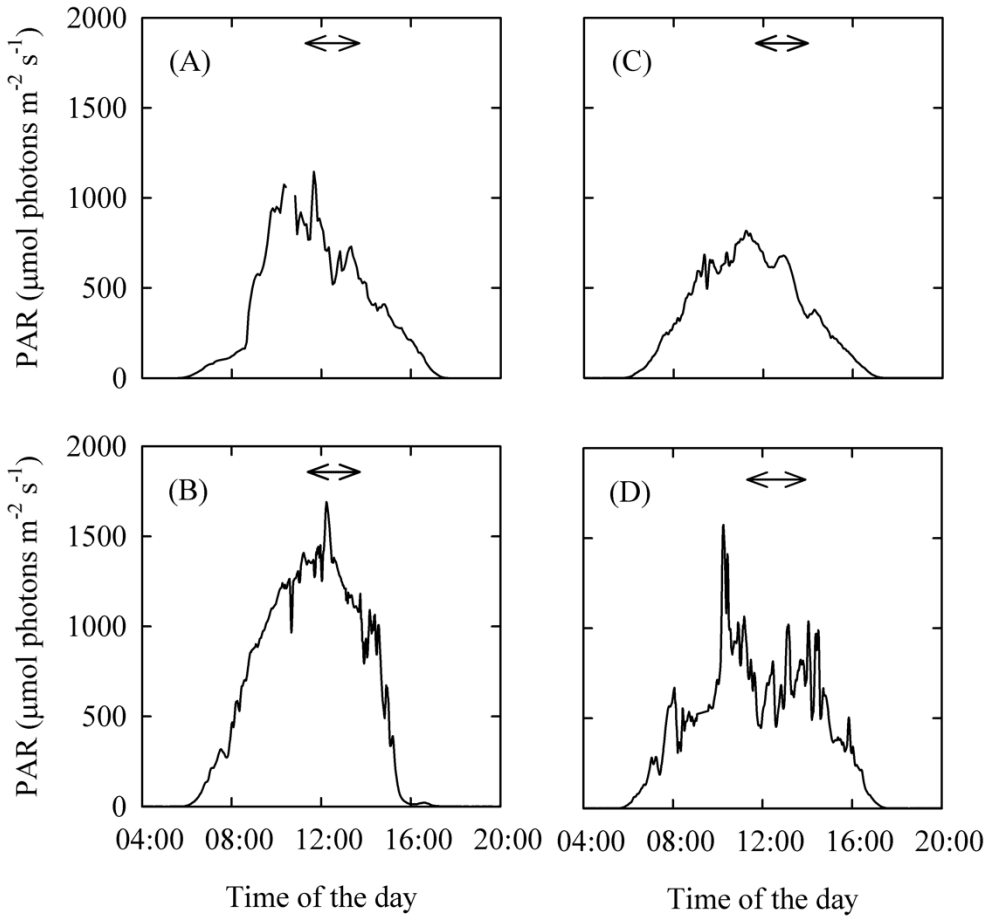

Figure 3-2. Photosynthetic available radiation (PAR) of sunlight at Saroma-Ko Lagoon, Hokkaido on March 7, 2012 (Exp. 1) (A), February 28 (Exp. 2) (B) and March 1, 2013 (Exp. 3) (C), and March 7, 2014 (Exp. 4) (D). The arrows indicate the period of the high light exposure experiments.

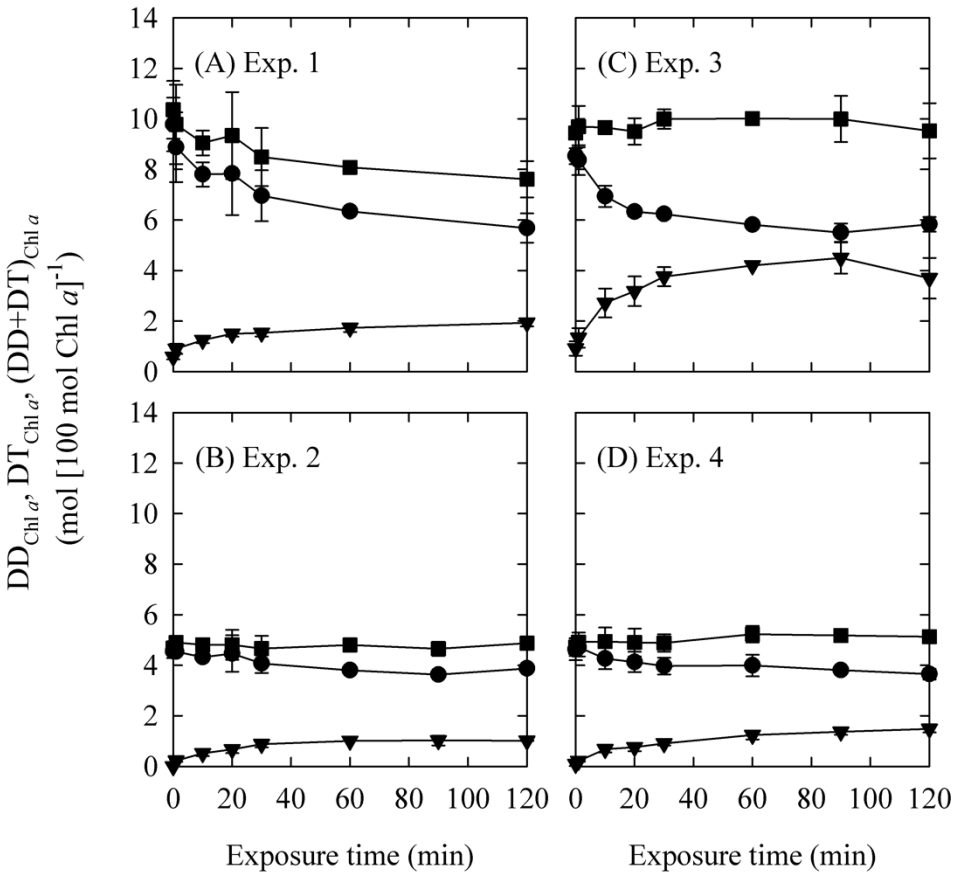

Figure 3-3. Temporal changes in molar ratios of DD (circle), DT (reversed triangle), and DD+DT (square) to Chl *a* in Exp. 1 (A), Exp. 2 (B), Exp. 3 (C), and Exp. 4 (D) after exposure to sunlight. Error bars indicate one standard deviation of the mean.

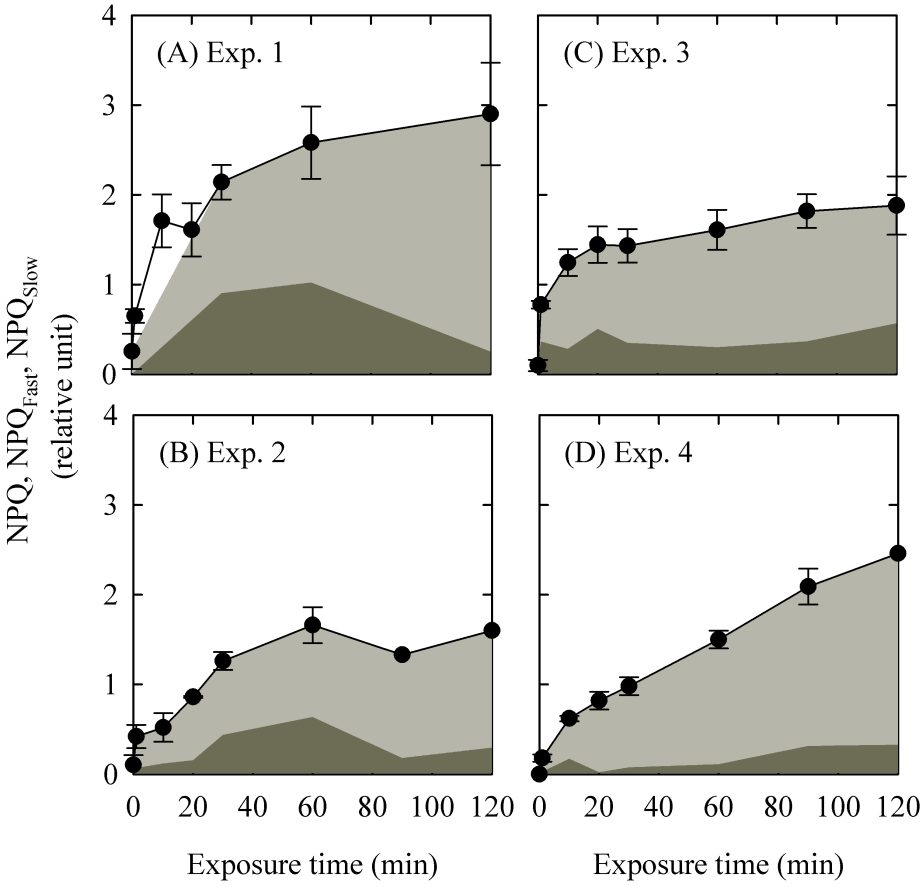

Figure 3-4. Temporal changes in total NPQ (circle) in Exp. 1 (A), Exp. 2 (B), Exp. 3 (C), and Exp. 4 (D) after exposure to sunlight. Areas of dark gray and light gray indicate NPQ_{Fast} and NPQ_{Slow}, respectively. Error bars indicate one standard deviation of the mean.

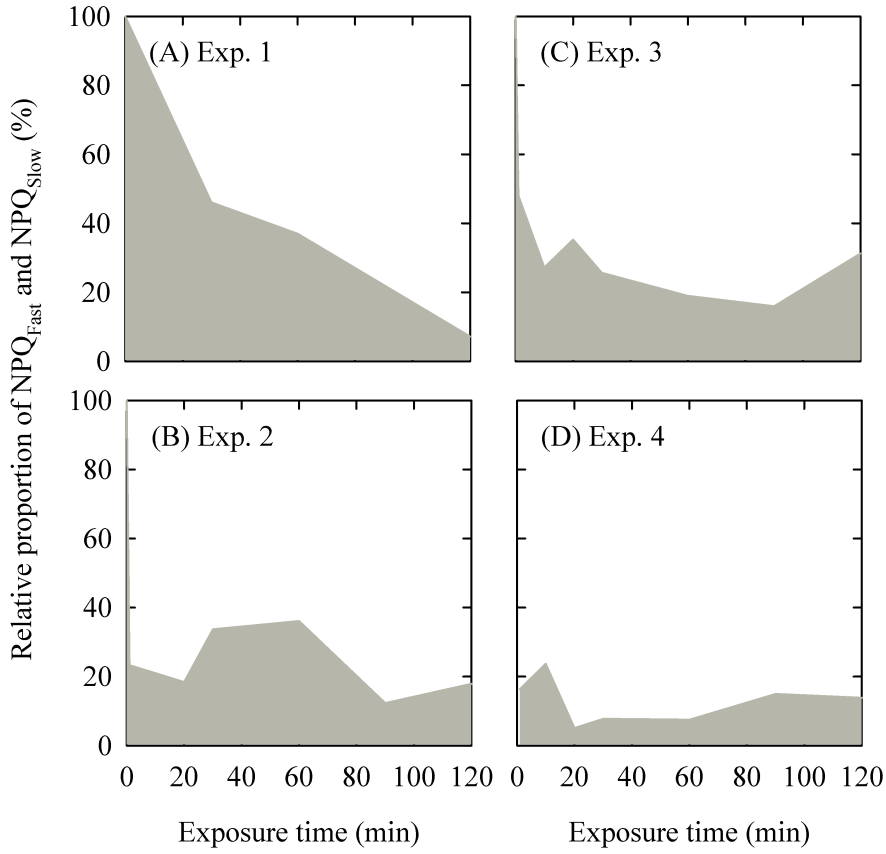

Figure 3-5. Temporal changes in relative proportion of NPQ_{Fast} (gray) and NPQ_{Slow} (white) in Exp. 1 (A), Exp. 2 (B), Exp. 3 (C), and Exp. 4 (D) after exposure to sunlight.

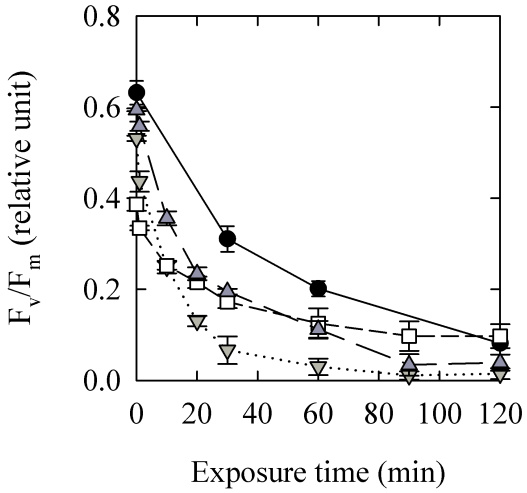

Figure 3-6. Temporal changes in F_v/F_m in Exp. 1 (circle), Exp. 2 (reversed triangle), Exp. 3 (square) in Exp. 4 (triangle) after exposure to sunlight. Error bars indicate one standard deviation of the mean.

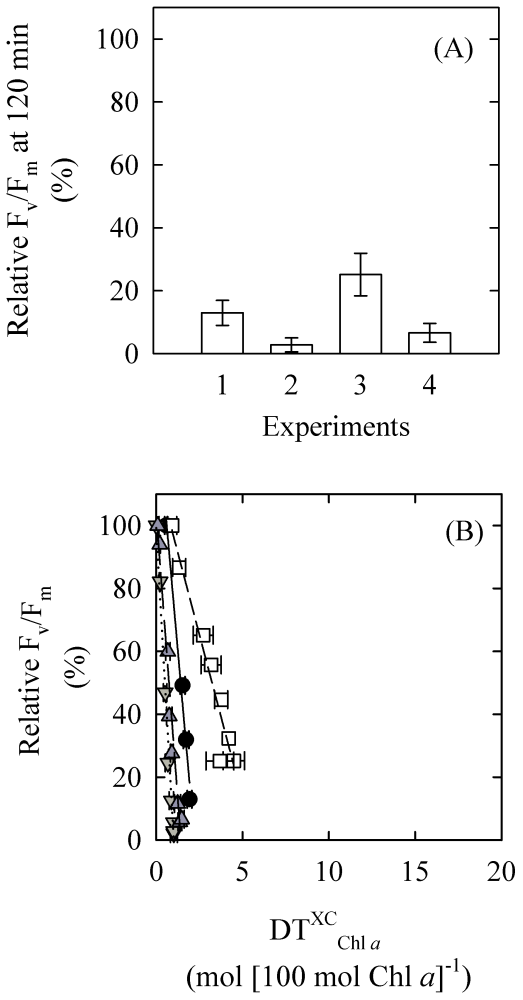

Figure 3-7. Relative F_v/F_m at 120 min exposure to the initial value (A) and relationship between $DT^{XC}_{Chl\ a}$ and relative F_v/F_m to the initial value in Exp. 1 (circle), Exp. 2 (reversed triangle), Exp. 3 (square), and Exp. 4 (triangle) after exposure to sunlight (B). Error bars indicate one standard deviation of the mean. F_v/F_m = –62 $DT^{XC}_{Chl\ a}$ + 137, r = 0.99, in Exp. 1, F_v/F_m = –97 $DT^{XC}_{Chl\ a}$ + 99, r = 0.99, in Exp. 2, F_v/F_m = –21 $DT^{XC}_{Chl\ a}$ + 117, r = 0.97, in Exp. 3, F_v/F_m = –73 $DT^{XC}_{Chl\ a}$ + 104, r = 0.98, in Exp. 4.

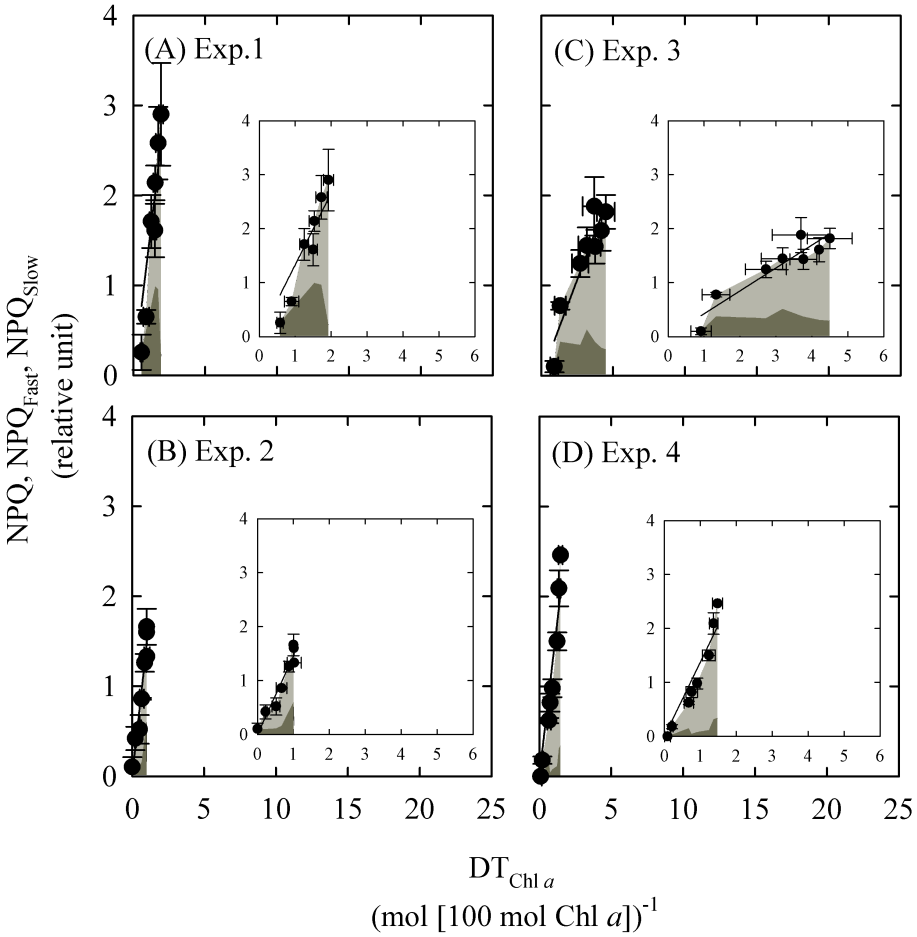

Figure 3-8. Relationship between $DT_{Chl\ a}$ and NPQ (circle) in Exp. 1 (A), Exp. 2 (B), Exp. 3 (C), and Exp. 4 (D) after exposure to sunlight. Areas of dark gray and light gray indicate NPQ_{Fast} and NPQ_{Slow}, respectively. Error bars indicate one standard deviation of the mean. Inset: First 6 mol DT (100 mol Chl a)$^{-1}$ enlarged. NPQ = 2.0 $DT_{Chl\ a}$ – 1.0, r = 0.96, in Exp. 1, NPQ = 1.4 $DT_{Chl\ a}$ + 0.02, r = 096, in Exp. 2, NPQ = 0.42 $DT_{Chl\ a}$ – 0.0004, r = 0.94, in Exp. 3, NPQ = 1.7 $DT_{Chl\ a}$ – 0.31, r = 0.97, in Exp. 4.

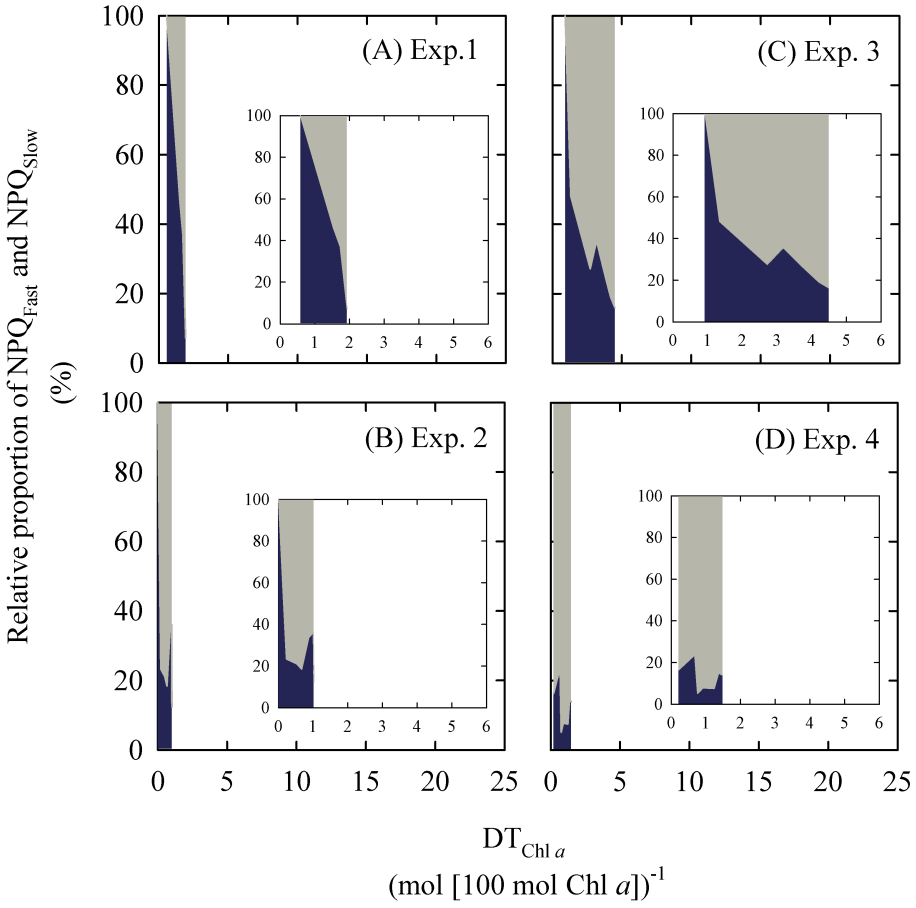

Figure 3-9. Relationship between $DT_{Chl\ a}$ and relative proportion of NPQ_{Fast} (dark gray) and NPQ_{Slow} (light gray) in Exp. 1 (A), Exp. 2 (B), Exp. 3 (C), and Exp. 4 (D) after exposure to sunlight. Inset: First 6 mol DT (100 mol Chl *a*)$^{-1}$ enlarged.

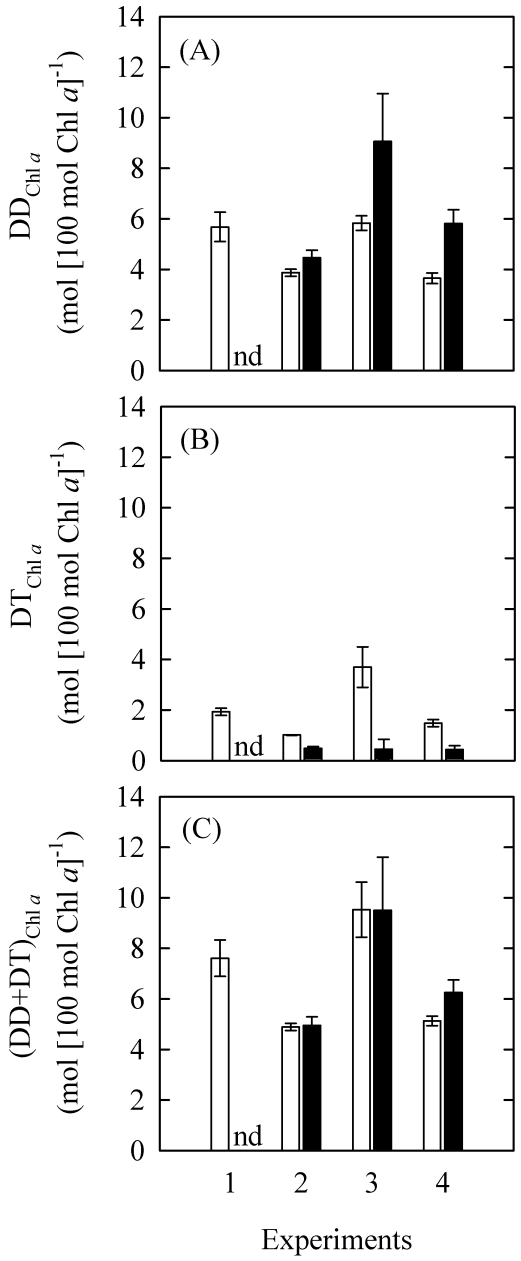

Figure 3-10. Molar ratios of DD (A), DT (B), and DD+DT (C) to Chl *a* before (open bar) and after 24 hrs (solid bar) dark storage in Exp. 1, Exp. 2, Exp. 3, and Exp. 4. Error bars indicate one standard deviation of the mean. No data, nd.

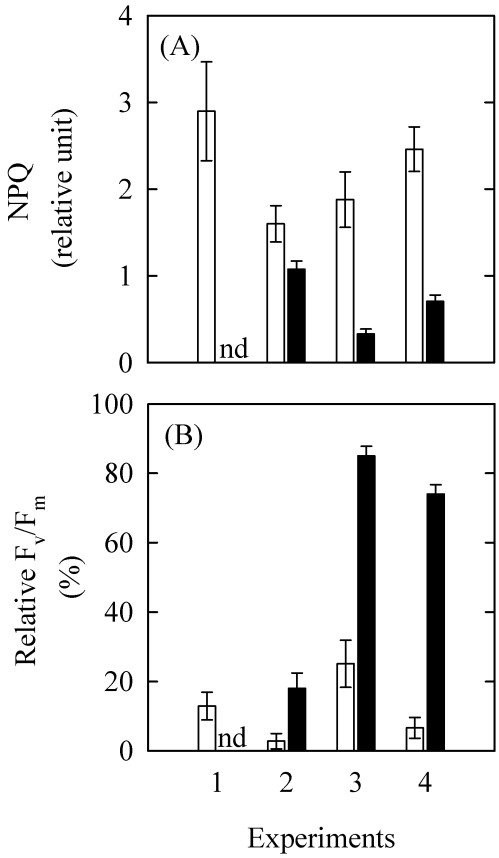

Figure 3-11. NPQ (A) and relative F_v/F_m to the initial values (B) before (open bar) and after 24 hrs dark storage (solid bar) in Exp. 1, Exp. 2, Exp. 3, and Exp. 4. Error bars indicate one standard deviation of the mean. No data, nd.

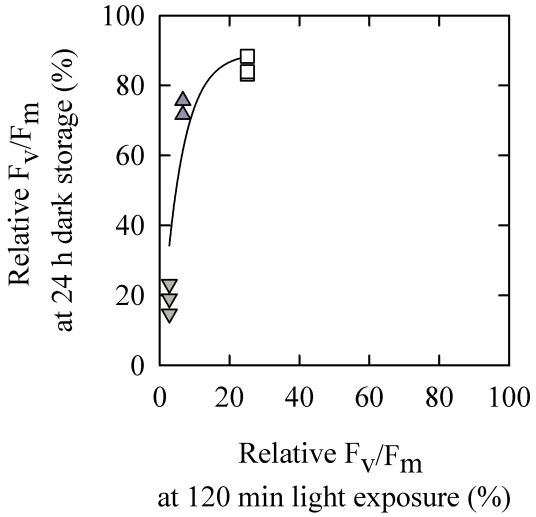

Figure 3-12. The relationship between relative F_v/F_m before and after 24 hrs dark storage in comparison with the initial values in Exp. 2 (reversed triangle), Exp. 3 (square), and Exp. 4 (triangle). [F_v/F_m at 24 h] = 89 × (1 – exp [– 0.18 × {F_v/F_m at 120 min}]), r = 0.92.

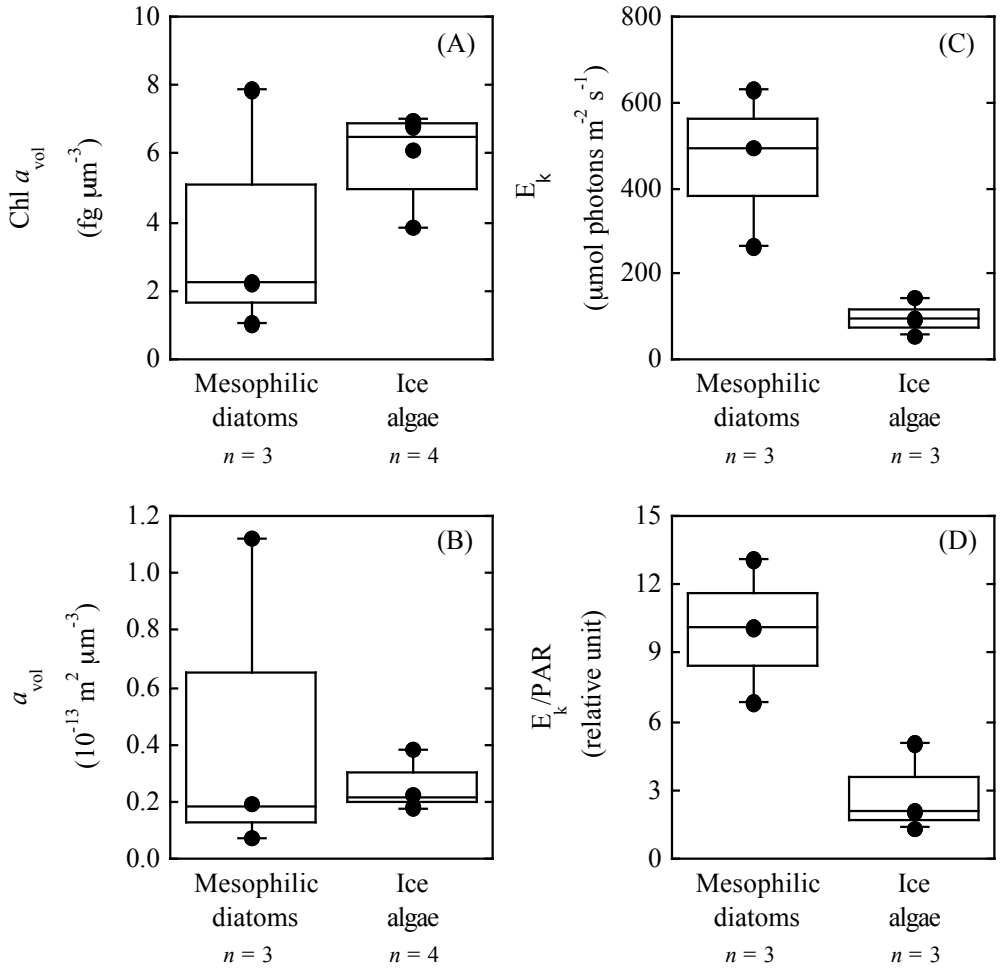

Figure 3-13. Box plots of Chl a_{vol} (A), a_{vol} (B), E_k (C), and E_k/PAR (D) before light exposure experiments between mesophilic diatom species and ice algal communities. The boxes represent the 25% (Q1) and 75% (Q3) quartiles of all data for each algal group and the central line represents median. The whiskers represent the upper and lower limits defined as the value at Q3+1.5(Q3–Q1) for the upper limit and Q1–1.5(Q3–Q1) for the lower limits. Solid circles indicate the observed values in the present study. Circles above the whiskers represent the outliers including the observed values in the present study (solid) and the previously reported values (open).

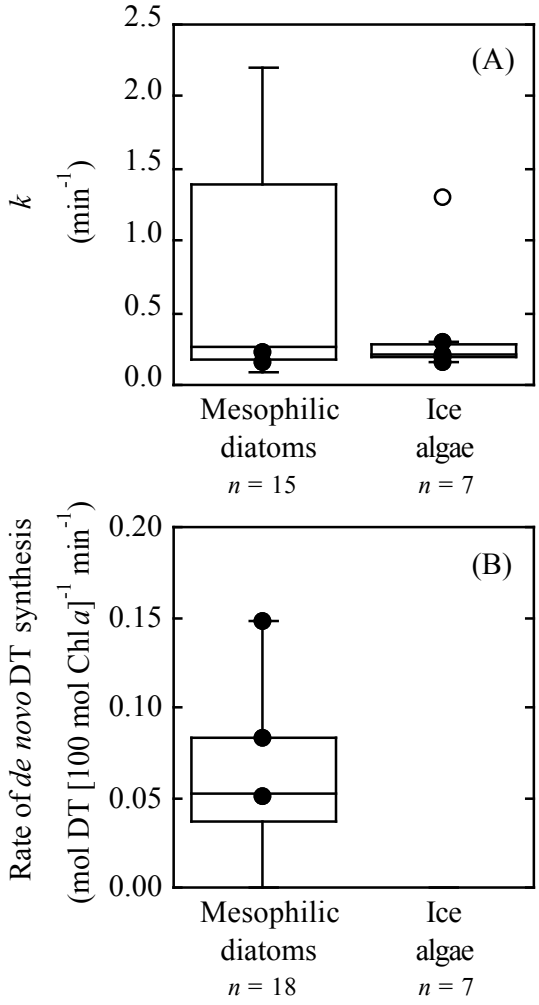

Figure 3-14. Box plots of initial rate constant (k) of de-epoxidation (A) and rate of *de novo* DT synthesis (B) during light exposure experiments between mesophilic diatom species and ice algal communities. See Fig. 3-13 for the boxes and whiskers. Solid circles indicate the observed values in the present study. Circles above the whiskers represent the outliers including the observed values in the present study (solid) and the previously reported values (open). See Appendix 1 for all data.

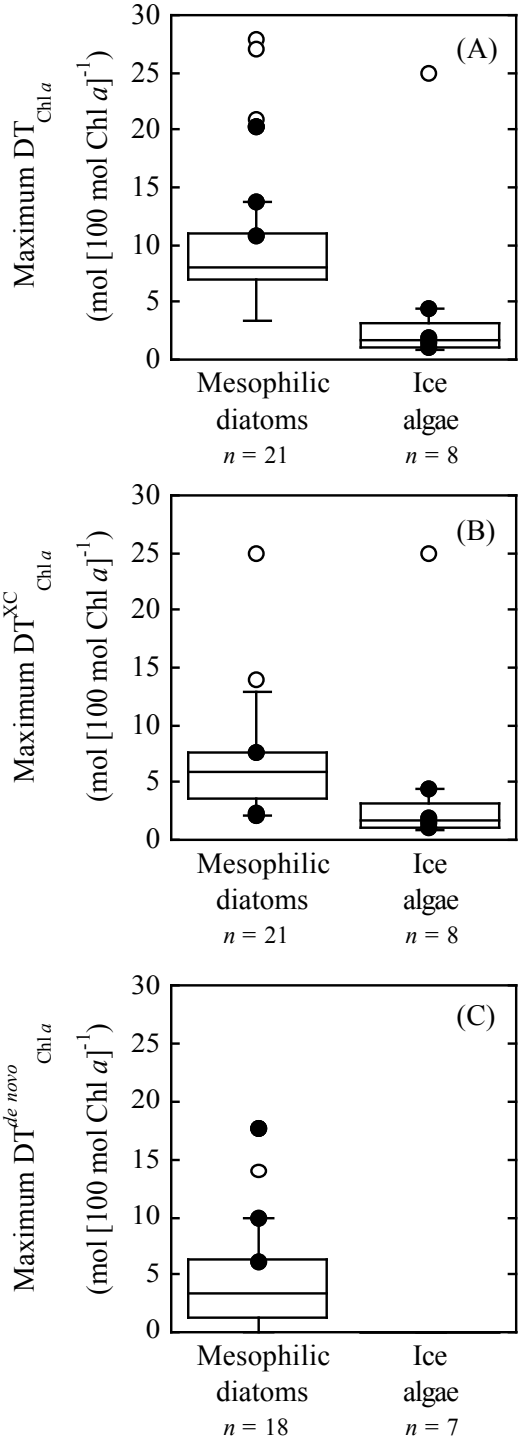

Figure 3-15. Box plots of maximum values of $DT_{Chl\,a}$ (A), $DT^{XC}_{Chl\,a}$ (B), and $DT^{de\ novo}_{Chl\,a}$ (C) during light exposure experiments between mesophilic diatom species and ice algal communities. See Fig. 3-13 for the boxes and whiskers and Fig. 3-14 for the symbols, respectively. See Appendix 1 for all data.

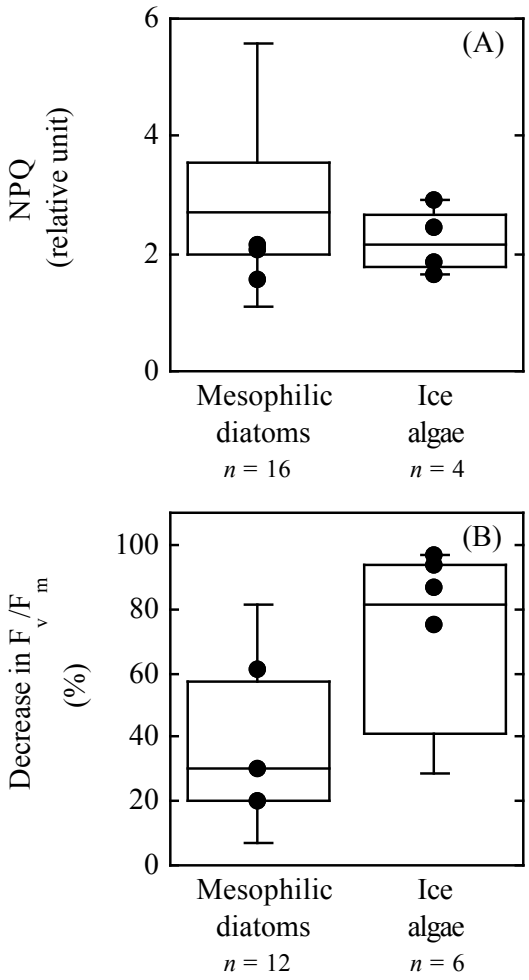

Figure 3-16. Box plots of maximum values of NPQ (A) and decrease in the relative F_v/F_m in comparison with the initial value at the end of light exposure experiments (B) between mesophilic diatom species and ice algal communities. See Fig. 3-13 for the boxes and whiskers and Fig. 3-14 for the symbols, respectively. See Appendix 2 for all data.

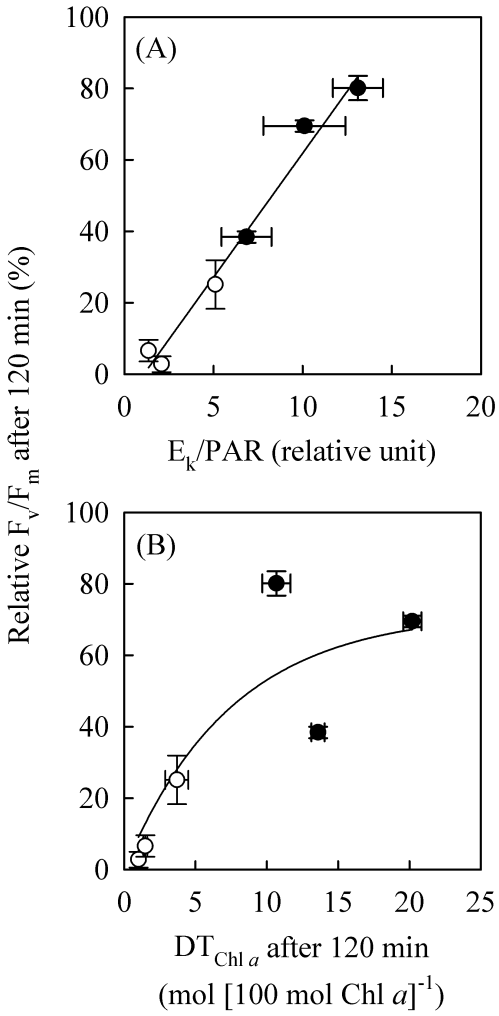

Figure 3-17. Relationship between E_k/PAR before light exposure and relative F_v/F_m to the initial value at the end of light exposure experiment (A) and between $DT_{Chl\ a}$ and relative F_v/F_m to the initial value at the end of light exposure experiment (B) in ice algal communities (open circle) and mesophilic diatom species (closed circle). Error bars indicate one standard deviation of the mean. $F_v/F_m = 7.0 \times DT_{Chl\ a} - 7.6$, $r = 0.99$; $F_v/F_m = 72 \times (1 - \exp[-9.6 \times \{DT_{Chl\ a}/72\}])$, $r = 0.87$.

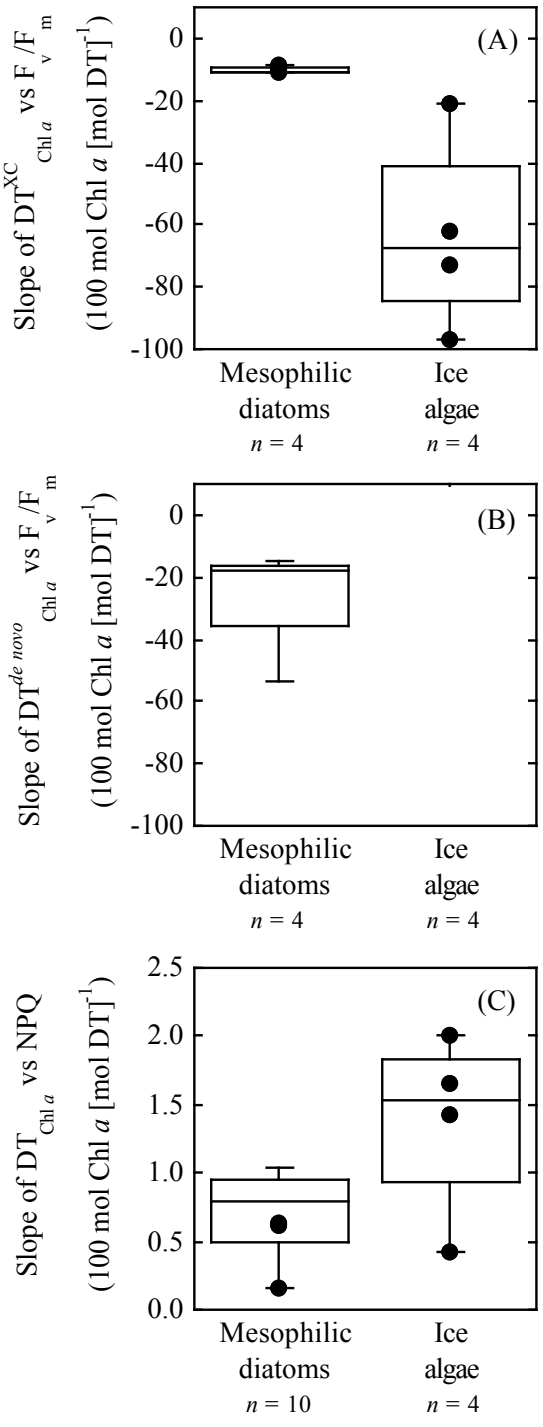

Figure 3-18. Box plots of slope between $DT^{XC}_{Chl\ a}$ and relative F_v/F_m to the initial value (A), between $DT^{de\ novo}_{Chl\ a}$ and relative F_v/F_m to the initial value (B), and between $DT_{Chl\ a}$ and NPQ (C) between mesophilic diatom species and ice algal communities. See Fig. 3-13 for the boxes and whiskers and Fig. 3-14 for the symbols, respectively. See Appendix 2 for all data.

CHAPTER IV

GENERAL CONCLUSIONS

4.1. Thermal dissipation through xanthophyll cycle

Photoprotective acclimations of low- or dark-acclimated mesophilic diatoms and ice algal cells to high light are appeared to enhance the thermal dissipation through the xanthophyll cycle. However, the smaller synthesis of DT through xanthophyll cycle ($DT^{XC}_{Chl\ a}$) in the ice algal communities than those in the mesophilic diatoms with similar initial rate constant (k) of de-epoxidation suggests that the activity of xanthophyll cycle of DD to DT in the ice algal communities could be lower for the second half of the light exposure than those in the mesophilic diatoms, as well as the photoprotective capacity to reduce the damage of PSII in the DT^{XC}.

The relationships between the production of DT and NPQ for the mesophilic diatoms and ice algal communities obtained in the present study showed that NPQ was linearly dependent on the light-induced DT ($DT^{XC}_{Chl\ a}$) without $DT^{de\ novo}_{Chl\ a}$. Therefore, NPQ is linearly dependent on the presence of DT^{XC} in polar or temperate sea habitats. The present study indicated that the slope of the relationship between the molar ratio of DT to Chl *a* ($DT_{Chl\ a}$) and NPQ, reflecting the quenching efficiency of DT (Goss and Jakob 2010), was much influenced by the enhancement of NPQ due to photodamage of PSII reaction centers. Although the quenching efficiency of DT obtained in the present study is comparable to different diatom species previously reported by Goss et al. (2006) and Lavaud et al. (2004), some ice algal cells may be likely to overestimate the quenching efficiency of DT by the enhancement of NPQ by the quenching due to photoinhibition.

4.2. Relaxation of photodamage

The experimental observation presented in the present study demonstrated that the photoinhibition of PSII in the ice algal cells due to high light was severe than those in the mesophilic diatoms, which was related to the shade acclimation prior to the light exposure as well as the amounts of $DT_{Chl\ a}$ produced after the exposure to high light. The presence of the *de novo* DT synthesis in the mesophilic diatoms enhances the synthesis of $DT_{Chl\ a}$. The photoprotective acclimations in the ice algal cells are not appeared to enhance the antioxidant function through the *de novo* DT synthesis. The results presented in the present study showed that the photoprotective capacity of $DT^{de\ novo}$ having the antioxidant protective shield around the PSII (Dall'Osto et al. 2010, Lepetit et al. 2010) might be related to the addressing of $DT^{de\ novo}$. Mesophilic diatoms might relax the photodamage with synthesis of $DT^{de\ novo}$ which are located in the close vicinity to the PSII light-harvesting complexes.

4.3. Conclusions

The present study demonstrated that the activity of xanthophyll cycle at the beginning of the light exposure was regarded as similar regardless of difference in the ecological groups, whereas the activity of xanthophyll cycle at the second half of the light exposure could be lower in the ice algal communities than those in the mesophilic diatoms. Mesophilic diatoms could reduce the photodamage in PSII due to excess light exposure through the *de novo* synthesis of DT as the antioxidant function in addition to the high photoprotective capacity of DT^{XC} as thermal dissipation of excess energy. Consequently, the capability of photoprotective acclimation might be elevated by the synthesis of DT through the xanthophyll cycle and the *de novo* DT synthesis. The information on the photoprotective acclimation of mesophilic diatoms and ice algae should be consider to

understand their dynamics, particularly when advances in the shoaling of surface mixed layer depths and the melting sea ice due to recent global warming will accelerate the exposure of high light condition to them in the future.

4.4. Implication

The present study confirms that marine diatoms have a capability to protect from the high light and simultaneously recover from any damage in the PSII reaction centers caused by the high light. The protection processes is enhanced by the presence of the *de novo* DT synthesis of mesophilic diatoms. The recovery processes dominate under low light or dark conditions. Although the apparent lack of response of the *de novo* DT synthesis to light exposure in the ice algal communities suggests that the *de novo* DT synthesis might be minimal at low temperatures, further work must be performed to characterize how physiological and environmental conditions influence the process of *de novo* DT synthesis in marine diatoms.

In the present study, photoprotective responses of marine diatoms were compared between species level and community level, using the several diatom species and the ice algal communities predominated by diatoms, respectively. The photoprotective responses in marine diatoms at the community level might be influenced by the species-specific differences in the photoprotective responses and/or the cell size of diatom community. Therefore, further studies are required on the photoprotective responses in the dominant species of ice algal community in monoculture.

Absorption bands of the light-harvesting pigments, including Chl *a*, Chl *c*, Fuco, and β-caro, in marine diatoms range mainly from 400 to 500 nm and around 675 nm (Fig. 1A). The irradiances in the high light exposure experiments have different spectra for the mesophilic diatoms

and the ice algal communities in the present study. The solar spectrum is distributed smoothly from 400 to 700 nm, whereas the spectrum of cool fluorescence shows distinct peaks at 406, 436, 545, and 588 nm (Fig. 1B). Therefore, the absorption of light-harvesting pigments might be different between two experiments with the mesophilic diatoms and the ice algal communities, even if the light intensity from 400 to 700 nm is maintained at the similar levels in the both light sources of cool fluorescence tube and sunlight. The artificial light, of which spectral distribution is similar to the solar spectrum, should be used in the light exposure experiments in the laboratory. The actinic light at 655 nm for the measurement of NPQ is located within the red absorption band in Chl *a*, and the light intensity in the exposure experiments is adopted for the intensity of actinic light in the present study for the measurement of NPQ. For example, the energy of wavelength at 440 nm in the red absorption band of Chl *a* is approximately 1.4 times higher than those at 675 nm in the blue absorption band of Chl *a* according to Planck's law. Thus the energy of actinic light at 675 nm might be higher compared with those in which the light from 400 to 700 nm is employed as the actinic light source. Therefore, the response of NPQ might vary depending on the wavelength of actinic light.

In natural environments, the ice algal community is adapted to stable, low light conditions at the undersurface of sea ice. When they are released to a surface water of water column in spring, the transition to high light could damage severely because they perform little the *de novo* DT synthesis. It has been argued for a long time if ice algae released from the sea ice could be a seed population for the ice-edge bloom in spring without definite conclusions. The experimental results obtained in the present study strongly suggest little possibility in the immediate bloom which is seeded by the ice algal cells because the low light acclimated ice algal cells are readily damaged by high light. Instead, ice algal cells seem to have been evolved to aggregate and sink rapidly out of the

surface layer. Therefore, the possibility in survival of the damaged ice algal cells could be predicted under near- or complete darkness in the water column in the shallow coastal waters or stratified waters. Some of the released ice algal cells may be trapped at the stratified water column or may sink out of the water column. In addition to the present study, the previous studies indicate that marine diatoms can survive in continuous dark conditions for weeks to months and they can recover to activate the photosynthetic activity to start dividing when they are exposed to light. Once the ice algal cells survived under near- or complete darkness are transported to the surface water by a vertical water mixing, they may have much opportunities either to be incorporated to new sea ice and may play a significant role in primary production in the high latitudes.

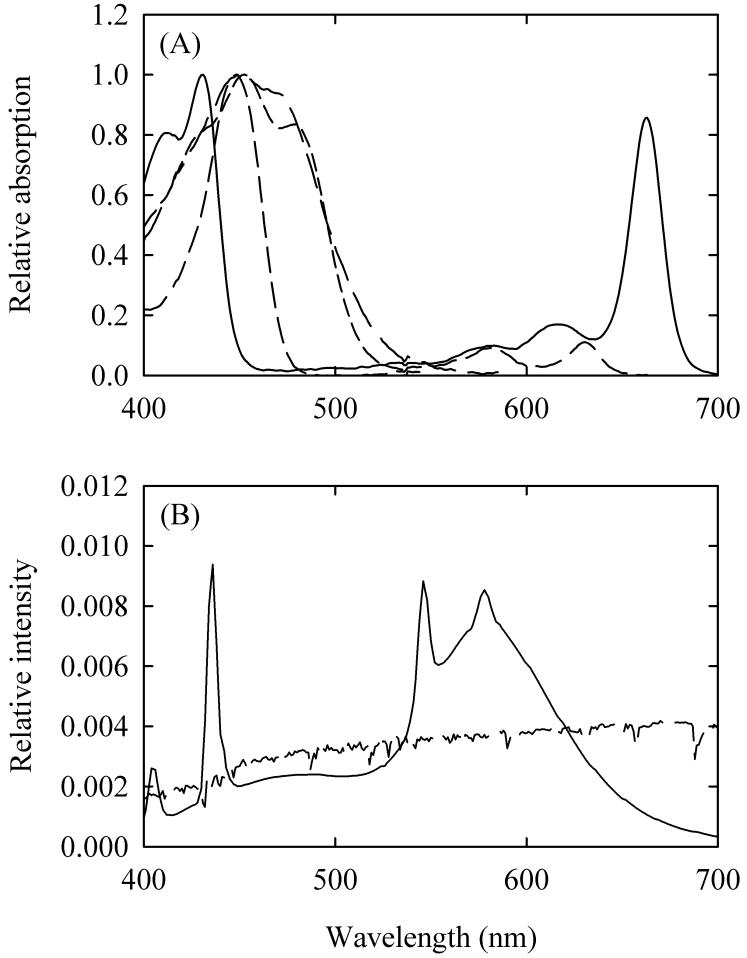

Figure 4-1. Absorption spectra of Chl *a* (solid line), Fuco (long-dashed line), Chl *c* (medium-dashed line), and β-caro (short-dashed line), which were normalized to their absorption maxima (A) and relative intensities of light sources of cool fluorescence tube (solid line) and sunlight (dashed line) compared to total PAR (B).

REFERENCES

Ackley, S. F., Buck, K. R. & Taguchi, S. (1979) Standing crop of algae in the sea ice of the Weddle Sea region. *Deep-Sea Research*, 26: 269–281.

Adams, W. W., Zarter, C. R., Mueh, K. E., Amiard, V. & Demmig-Adams, B. (2006) Energy dissipation and photoinhibition: a continuum of photoprotection. In Demmig-Adams, B., Adams, W. W. & Mattoo, A. K. [Eds.] *Phoroprotection, Photoinhibition, Gene Regulation, and Environment. Advances in Photosynthesis and Respiration*. Springer, Dordrecht, Netherlands, pp. 49–64.

Anderson, O. R. (1975) The ultrastructure and cytochemistry of resting cell formation in *Amphora coffaeformis* (Bacillariophyceae). *Journal of Phycology*, 11: 272–281.

Antia, N. J. (1976) Effects of temperature on the darkness survival of marine microplanktonic algae. *Microbial Ecology*, 3: 41–54.

Armbrust, E. V., Chisholm, S. W. & Olson, R. J. (1990) Role of light and the cell cycle on the induction of spermatogenesis in a centric diatom. *Journal of Phycology*, 26: 470–478.

Arrigo, K. R., Perovich, D. K., Pickart, R. S., Zachary, W., Brown, Z. W., van Dijken, G. L., Lowry, K. E., Mills, M. M., Palmer, M. A., Balch, W. M., Bahr, F., Bates, N. R., Benitez- Nelson, C., Bowler, B., Brownlee, E., Ehn, J. K., Frey, K. E., Garley, R., Laney, S. R., Lubelczyk, L., Mathis, J., Matsuoka, A., Mitchell, B. G., Moore, G. W. K., Ortega-Retuerta, E., Pal, S. M., Polashenski, C. M., Reynolds, R. A., Schieber, B., Sosik, H. M., Stephens, M. & Swift, J. H. (2012) Massive phytoplankton blooms under Arctic sea ice. *Science*, 336: 1408.

Arrigo, K. R., Robinson, D. H. & Sullivan, C. W. (1993) A high resolution study of the platelet ice ecosystem in McMurdo Sound, Antarctica: photosynthetic and bio-optical characteristics of a dense microalgal bloom. *Marine Ecology Progress Series*, 98: 173–185.

Babin, M. & Stramski, D. (2002) Light absorption by aquatic particles in the near-infrared spectral

region. *Limnology and Oceanography*, 47: 911–915.

Bianchi, F., Boldrin, A., Cioce, F., Dieckman, G., Kuosa, H., Larsson, A. -M., Nöthig, E. -M., Sehlstedt, P. -I., Socal, G. & Syvertsen, E. E. (1992) Physiographic distribution in relation to sea ice, hydrography and nutrients in the northwestern Weddle Sea in early spring 1988 during EPOS. *Polar Biology*, 12: 225–235.

Bluhm, B. A., Gradinger, R. R. & Schnack-Schiel, S. B. (2010) Sea ice meio- and macrofauna. In Thomas, D. N. & Dieckmann, G. S. [Eds.] *Sea Ice*, 2nd edition. Wiley Blackwell, Oxford, UK, pp. 357–394.

Büchel, C. & Wilhelm, C. (1993) In vivo analysis of slow chlorophyll induction kinetics in algae: progress, problems and perspectives. *Photochemistry and Photobiology*, 58: 137–148.

Chevalier, E. M., Gévaert, F. & Créach, A. (2010) *In situ* photosynthetic activity and xanthophylls cycle development of undisturbed microphytobenthos in an intertidal mudflat. *Journal of Experimental Marine Biology and Ecology*, 385: 44–49.

Cleveland, J. S. & Weidemann, A. D. (1993) Quantifying absorption by aquatic particles: A multiply scattering correction for glass-fiber filters. *Limnology and Oceanography*, 38: 1321–1327.

Costello, J. C. & Chisholm, S. W. (1981) The influence of cell size on the growth rate of *Thalassiosira weisflogii*. *Journal of Plankton Research*, 3: 415–419.

Cullen, J. J. & Lewis, M. R. (1988) The kinetics of algal photoadaptation in the context of vertical mixing. *Journal of Plankton Research*, 10: 1039–1063.

Dall'Osto, L., Cazzaniga, S., Havaux, M. & Bassi, R. (2010) Enhanced photoprotection by protein-bound vs free xanthophyll pools: a comparative analysis of chlorophyll b and xanthophyll biosynthesis mutants. *Molecular Plant*, 3: 576–593.

Demers, S., Roy, S., Gagnon, R. & Vignault, C. (1991) Rapid light-induced changes in cell fluorescence and in xanthophyll-cycle pigments of *Alexandrium excavatum* (Dinophyceae) and *Thalassiosira pseudonana* (Bacillariophyceae): a photo-protection mechanism.

Marine Ecology Progress Series, 76: 185–193.

Depauw, F. A., Rogato, A., d'Alcalá, M. R. & Falciatore, A. (2012) Exploring the molecular basis of responses to light in marine diatoms. *Journal of Experimental Botany*, 63: 1575–1591.

Dimier, C., Corato, F., Tramontano, F. & Brunet, C (2007) Phoroprotection and xanthophyll-cycle activity in three marine diatoms. *Journal of Phycology*, 43: 937–947.

Dimier, C., Giovanni, S., Ferdinando, T. & Brunet, C. (2009) Comparative ecophysiology of the xanthophyll cycle in six marine phytoplanktonic species. *Protist*, 160: 397–411.

Domingues, N., Matos, A. R., da Silva, J. M., Cartaxana, P. (2012) Response of the diatom *Phaeodactylum tricornutum* to photooxidative stress resulting from high light exposure. *PloS ONE*, 7: e38162.

Duarte, C. M. & Cebrián, J. (1996) The fate of marine autotrophic production. *Limnology and Oceanography*, 41: 1758–1766.

Erga, S. R. & Skjoldal, H. R. (1990) Diel variations in photosynthetic activity of summer phytoplankton in Lindåspollene, western Norway. *Marine Ecology Progress Series*, 65: 73–85.

Falkowski, P. G. (1994) The role of phytoplankton photosynthesis in global biogeochemical cycles. *Photosynthesis Research*, 39: 235–258.

Falkowski, P. G. & Raven, J. A. (2007) *Aquatic photosynthesis*. Princeton University Press, Princeton, New Jersey, USA, 484 pp.

Field, C., Behrenfeld, M. J., Randerson, J. T. & Falkowski, P. (1998) Primary production of the biosphere: integrating terrestrial and oceanic components. *Science*, 281: 237–240.

Franklin, L. A., Osmond, C. B. & Larkum, A. W. D. (2003). Photoinhibition, UV-B and algal photosynthesis. In Larkum, A. W. D., Douglas, S. E. & Raven, J. A. [Eds.] *Photosynthesis in algae*. Kluwer Academic Publishers, Dordrecht, Netherlands, pp. 351–384.

Garrison, D. L. & Buck, K. R. (1986) Organism losses during ice melting: a serious bias in sea ice community studies. *Polar Biology*, 6: 237–239.

Geider, R. J., La Roche, J., Greene, R. M. & Olaizola, M. (1993) Response of the photosynthetic apparatus of *Phaeodactylum tricornutum* (Bacillariophyceae) to nitrate, phosphate, or iron starvation. *Journal of Phycology*, 29: 755–766.

Genty, B., Briantais, J. & Baker, N. R. (1989) The relationship between the quantum yield of photosynthetic electron transport and quenching of chlorophyll fluorescence. *Biochimica et Biophysica Acta*, 990: 87–92.

Gilbert, M., Domin, A., Becker, A. & Wilhelm, C. (2000) Estimation of primary productivity by chlorophyll *a in vivo* fluorescence in freshwater phytoplankton. *Photosynthetica*, 38: 111–126.

Giovagnetti, V., Flori, S., Tramontano, F., Lavaud, J. & Brunet, C. (2014) The velocity of light intensity increase modulates the photoprotective response in coastal diatoms. *PLoS ONE*, 9: e103782.

Goss, R., Ann Pinto, E., Wilhelm, C. & Richter, M. (2006) The importance of a highly active and ΔpH-regulated diatoxanthin epoxidase for the regulation of the PSII antenna function in diadinoxanthin cycle containing algae. *Journal of Plant Physiology*, 163: 1008–1021.

Goss, R. & Jakob, T. (2010) Regulation and function of xanthophyll cycle-dependent photoprotection in algae. *Photosynthsis Research*, 106: 103–122.

Gracía-Plazaola, J. I., Esteban, R., Fernández-Marín, B., Kranner, I. & Porcar-Castell, A. (2012) Thermal energy dissipation and xanthophyll cycle beyond the *Arabidopsis* model. *Photosynthesis Research*, 113: 89–103.

Griffith, G. P., Vennell, R. & Lamare, M. D. (2009) Diadinoxanthin cycle of the bottom ice algal community during spring in McMurdo Sound, Antarctica. *Polar Biology*, 32: 623–636.

Guillard, R. R. L. & Ryther, J. H. (1962) Studies of marine planktonic diatoms: I. *Cyclotella nana* Hustedt, and *Detonula confervacea* (Cleave) Gran. *Canadian Journal of Microbiology*, 8: 229–239.

Guillard, R. R. L. & Siereki, M. S. (2005) Counting cells in cultures with the light microscope. In

Anderson, R. A. [Ed.] *Algal Culturing Techniques*. Elsevier, New York, USA, pp. 239–252.

Harding, L. W. Jr., Meeson, B. W., Prézelin, B. B. & Sweeney, B. M. (1981) Diel periodicity of photosynthesis in marine phytoplankton. *Marine Biology*, 61: 95–105.

Harris, G. N., Scanlan, D. J. & Geider, R. J. (2009) Responses of *Emiliania huxleyi* (Prymnesiophyceae) to step changes in photon flux density. *European Journal of Phycology*, 44: 31–48.

Hartig, P., Wolfstein, K., Lippemeier, S. & Colijn, F. (1998) Photosynthetic activity of natural microphytobenthos populations measured by fluorescence (PAM) and 14C-tracer methods: a comparison. *Marine Ecology Progress Series*, 166: 53–62.

Hasle, G. R. (1978) The inverted microscope method. In Sournia, A. [Ed.] *Phytoplankton Manual. Monographs on oceanographic methodology, No. 6*. UNESCO, Paris, pp. 191–196.

Head, E. J., Horne, E. P. W. (1993) Pigment transformation and vertical flux in an area of convergence in the Northe Atlantic. *Deep-Sea Research II*, 40: 329–346.

Henley, W. J. (1993) Measurement and interpretation of photosynthetic light-response curves in algae in the context of photoinhibition and diel changes. *Journal of Phycology*, 29: 729–739.

Hillebrand, H., Dürselen, C. D., Kirschtel, D., Pollingher, U. & Zohary, T. (1999) Biovolume calculation for pelagic and benthic microalgae. *Journal of Phycology*, 35: 403–424.

Ihnken, S., Eggert, A. & Beardall, J. (2010) Exposure times in rapid light curves affect photosynthetic parameters in algae. *Aquatic Botany*, 93: 185–194.

Iwasawa, K., Murata, A. & Taguchi, S. (2009) Cell shrinkage of Prymnesiophyceae *Isochrysis galbana* during storage with preservatives. *Plankton and Benthos Res*earch, 4: 120–121.

Jakob, T., Goss, R. & Wilhelm, C. (1999) Activation of diadinoxanthin de-epoxidase due to a chlororespiratory proton gradient in the dark in the diatom *Phaeodactylum tricornutum*. *Plant Biology*, 1: 76–82.

Jerlov, N. G. (1976) *Marine Optics*, 2nd edition. Elsevier, New York, USA, 231 pp.

Kashino, Y. & Kudoh, S. (2003) Concerted response of xanthophyll-cycle pigments in a marine diatom, *Chaetoceros gracilis*, to shifts in light condition. *Phycological Research*, 51: 168–172.

Kirst, G. O. & Wiencke, C. (1995) Ecophysiology of polar algae. *Journal of Phycology*, 31: 181–199.

Kishino, M. (1993) Spectral light environment in/under sea ice in Lake Saroma. *Bulletin of Plankton Society of Japan*, 39: 161–163.

Kishino, M., Takahashi, M., Okami, N. & Ichimura, S. (1985) Estimation of the spectral absorption coefficients of phytoplankton in the sea. *Bulletin of Marine Science*, 37: 634–642.

Krause, G. H. & Weis, E. (1991) Chlorophyll fluorescence and photosynthesis: the basics. *Annual Review of Plant Biology*, 42: 313–349.

Kropuenske, L. R., Mills, M. M., van Dijken, G. L., Alderkamp, A. C., Berg, G. M., Robinson, D. H., Welschmeyer, N. A. & Arrigo, K. R. (2010) Strategies and rates of photoacclimation in two major Southern Ocean phytoplankton taxa: *Phaeocystis antarctica* (Haptophyta) and *Fragilariopsis cylindrus* (Bacillariophyceae). *Journal of Phycology*, 46: 1138–1151.

Kudoh, S., Imura, S. & Kashino, Y. (2003) Xanthophyll-cycle of ice algae on the sea ice bottom in Saroma Ko lagoon, Hokkaido, Japan. *Polar Bioscience*, 16: 86–97.

Kudoh, S., Robineau, B., Suzuki, Y., Fujiyoshi, Y. & Takahashi, M. (1997) Photosynthetic acclimation and the estimation of temperate ice algal primary production in Saroma-ko Lagoon, Japan. *Journal of Marine Systems*, 11: 93–109.

Lavaud, J. & Lepetit, B. (2013) An explanation for the inter-species variability of the photoprotective non-photochemical chlorophyll fluorescence quenching in diatoms. *Biochimica et Biophsica Acta*, 1827: 294–302.

Lavaud, J., Materna, A. C., Sturm, S., Vugrinec, S. & Kroth, P. G. (2012) Silencing of the violaxanthin de-epoxidase gene in the diatom *Phaeodactylum tricornutum* reduces

diatoxanthin synthesis and non-photochemical quenching. *PLoS ONE*, 7: e36806.

Lavaud, J., Rousseau, B. & Etienne, A. -L. (2003) Enrichment of the light-harvesting complex in diadinoxanthin and implications for the nonphotochemical fluorescence quenching in diatoms. *Biochemistry*, 42: 5802–5808.

Lavaud, J., Rousseau, B. & Etienne, A. -L. (2004) General features of photoprotection by energy dissipation in planktonic diatoms (Bacillariophyceae). *Journal of Phycology*, 40: 130–137.

Lavaud, J., Rousseau, B., van Gorkom, H. & Etienne, A. -L. (2002) Influence of the diadinoxanthin pool size on photoprotection in the marine planktonic diatom *Phaeodactylum tricornutum*. *Plant Physiology*, 129: 1398–1406.

Lavaud, J., Strzepek, R. F. & Kroth, P. G. (2007) Phoroprotection capacity differs among diatoms: Possible consequences on the spatial distribution of diatoms related to fluctuations in the underwater light climate. *Limnology and Oceanography*, 52: 1188–1194.

Lazzara, L., Nardello, I., Ermanni, C., Mangoni, O. & Saggiomo, V. (2007) Light environment and seasonal dynamics of microalgae in the annual sea ice at Terra Nova Bay, Ross Sea, Antarctica. *Antarctic Science*, 19: 83–92.

Lepetit, B., Volke, D., Gilbert, M., Wilhelm, C. & Goss, R. (2010) Evidence for the existence of one antenna-associated, lipid-dissolved and two protein-bound pools of diadinoxanthin cycle pigments in diatoms. *Plant Physiology*, 154: 1905–1920.

Lewin, J. C. Lewin, R. A. (1960) Auxotrophy and heterotrophy in marine littoral diatoms. *Canadian Journal of Microbiology*, 6: 127-134.

Lippemeier, S., Hartig, P. & Colijn F. (1999). Direct impact of silicate on the photosynthetic performance of the diatom *Thalassiosira weissflogii* assessed by on- and off-line PAM fluorescence measurements. *Journal of Plankton Research*, 21: 269–283.

Lippemeier, S., Hintze, R., Vanselow, K., Hartig, P. & Colijn F. (2001) In-line recording of PAM fluorescence of phytoplankton cultures as a new tool for studying effects of fluctuating nutrient supply on photosynthesis. *European Journal of Phycology*, 36: 89–100.

Lohr, M. & Wilhelm, C. (1999) Algae displaying the diadinoxanthin cycle also possess the violaxanthin cycle. *Proceedings of the National Academy of Sciences of the United States of America*, 96: 8784–8789.

Lohr, M. & Wilhelm, C. (2001) Xanthophyll synthesis in diatoms: quantification of putative intermediates and comparison of pigment conversion kinetics with rate constants derived from a model. *Planta*, 212: 382–391.

Lüder, U. H., Wiencke, C. & Knoetzel, J. (2002) Acclimation of photosynthesis and pigments during and aftersix months of darkness in *Palmaria decipiens* (Rhodophyta): A study to simulate Antarctic winter sea ice cover. *Journal of Phycology*, 38: 904–913.

Mangoni, O., Carrada, G. C., Modigh, M., Catalano, G. & Saggiomo, V. (2009) Photoacclimation in Antarctic bottom ice algae: an experimental approach. *Polar Biology*, 32: 325–335.

Maxwell, K. & Johnson, N. (2000) Chlorophyll fluorescence–a practical guide. *Journal of Experimental Botany*, 51: 659–668.

McMinn, A. & Hattori, H. (2006) Effect of time of day on the recovery from light exposure in ice algae from Saroma Ko lagoon, Hokkaido. *Polar Bioscience*, 20: 30–36.

McMinn, A. & Martin, A. (2013) Dark survival in a warming world. *Proceedings of the Royal Society B*, 280: 20122909

McQuoid, M. R. & Hobson, L. A. (1996) Diatom resting stages. *Journal of Phycology*, 32: 889–902.

Medcof, J. C. (1975) Living animals in ship's ballast water. *Proceedings of the National Shellfisheries Association*, 65: 11–12.

Melis, A. (1999) Photosystem-II damage and repair cycle in chloroplasts: what modulates the rate of photodamage *in vivo*? *Trends in Plant Science*, 4: 130–135.

Meyer, A. A., Tackx, M. & Daro, N. (2000) Xanthophyll cycling in *Phaeocystis globosa* and *Thalassiosira* sp.: a possible mechanism for species succession. *Journal of Sea Research*, 43: 373–384.

Mitchell, B. G. & Kiefer, D. A. (1988) Chlorophyll *a* specific absorption and fluorescence excitation spectra for light-limited phytoplankton. *Deep-Sea Research*, 35: 639–663.

Mitchel, C., Legendre, L. & Taguchi, S. (1997) Coexistence of microalgal sedimentation and water column recycling in a seasonally ice-covered ecosystem (Saroma-ko Lagoon, Sea Okhotsk, Japan). *Journal of Marine Systems*, 11: 133–148.

Moisan, T. A., Olaizola, M. & Mitchell, B. G. (1998) Xanthophyll cycling in *Phaeocystis Antarctica*: changes in cellular fluorescence. *Marine Ecology Progress Series*, 169: 113–121.

Morgan-Kiss, R. M., Priscu, J. C., Pocock, T., Gudynaite-Savitch, L. & Huner, N. P. A. (2006) Adaptation and acclimation of photosynthetic microorganisms to permanently cold environments. *Microbiology and Molecular Biology Reviews*, 70: 222–252.

Nelson, D. M., Tréguer, P., Brzezinski, M. A., Leynaert, A. & Quéguiner, B. (1995) Production and dissolution of biogenic silica in the ocean: revised global estimates, comparison with regional data and relationship to biogenic sedimentation. *Global Biogeochemical cycle*, 9: 359–372.

Obata, M. & Taguchi, S. (2009) Photoadaptation of an ice algal community in thin sea ice, Saroma-Ko Lagoon, Hokkaido, Japan. *Polar Biology*, 32: 1127–1135.

Olaizola, M., La Roche, J., Kolber, Z. & Falkowski, P. G. (1994) Non-photochemical fluorescence quenching and the diadinoxanthin cycle in a marine diatom. *Photosynthesis Research*, 41: 357–370.

Olaizola, M. & Yamamoto, H. Y. (1994) Short-term response of the diadinoxanthin cycle and fluorescence yield to high irradiance in *Chaetoceros muelleri* (Bacillariophyceae). *Journal of Phycology*, 30: 606–612.

Osmond, C. B. (1994) What is photoinhibition? Some insights from comparisons of shade and sun plants. In Baker, N. R. & Bowyer, J. R. [Eds.] *Photoinhibition of Photosynthesis from Molecular Mechanisms to the Field*. BIOS Scientific Publishers, Oxford, England, pp.

1–24.

Owens, T. G. (1986) Light-harvesting function in the diatoms *Phaeodactylum tricornutum*. II. Distribution of excitation energy between the photosystems. *Plant Physiology,* 80: 739–746.

Palmisano, A. C. & Sullivan, C. W. (1982) Physiology of sea ice diatoms. I. Response of three polar diatoms to a simulated summer-winter transition. *Journal of Phycology*, 18: 489–498.

Parkins, R. G., Mouget, J. -L., Lefebvre, S. & Lavaud, J. (2006) Light response curve methodology and possible implications in the application of chlorophyll fluorescence to benthic diatoms. *Marine Biology*, 149: 703–712.

Parsons, T. R., Maita, Y. & Lalli, C. M. (1984) *A manual of Chemical and Biological Methods for Seawater Analysis*, Pergamon Press, Oxford, UK.

Peters, E. (1996) Prolonged darkness and diatom mortality: II. Marine temperate species. *Journal of Experimental Marine Biology and Ecology*, 207: 43–58.

Petrou, K., Hill, R., Brown, C. M., Campbell, D. A., Doblin, M. A. & Ralph, P. J. (2010) Rapid photoprotection in sea-ice diatoms from the East Antarctic pack ice. *Limnology and Oceanography*, 55: 1400–1407.

Popels, L. C., MacIntyre, H. L., Warner, M. E., Zhang, Y. & Hutchins, D. A. (2007) Physiological responses during dark survival and recover in *Aureococcus anophagefferens* (Pelagophyceae). *Journal of Phycology*, 43: 32–42.

Rand, J., & Mellor, M. (1985) Ice-coring augers for shallow depth sampling. No. CRREL-85–21. Cold Regions Research and Engineering Lab, Hanover.

Riebesell, U., Schloss, I. & Smetakek, V. (1991) Aggregation of algae released from melting sea ice: implications for seeding and sedimentation. *Polar Biology*, 11: 223–229.

Ruban, A. V., Lavaud, J., Rousseau, B., Guglielmi, G., Horton, P. & Etienne, A. -L. (2004) The super-excess energy dissipation in diatom algae: comparative analysis with higher plants.

Photosynthesis Research, 82: 165–175.

Ruban, A. V., Johnson, M. P. & Duffy, C. D. P. (2012) The photoprotective molecular switch in the photosystem II antenna. *Biochimica et Biophysica Acta*, 1817: 167–181.

Saito, H. & Taniguchi, A. (1978) Phytoplankton communities in the Bering Sea and adjacent seas. II. Spring and summer communities in seasonally ice-covered area. *Astarte*, 11: 27–35.

Satoh, H., Yamaguchi, Y., Watanabe, K., Tanimura, A., Fukuchi, M. & Aruga, Y. (1989) Photosynthetic nature of ice algae and their contribution to the primary production in lagoon Saroma Ko, Hokkaido, Japan. *Proceedings of the NIPR Symposium on Polar Biology*, 2: 1–8.

Scharek, R., Smetacek, V., Fahrbach, E., Gordon, L. I., Rohardt, G. & Moore, S. (1994) The transition from winter to early spring in the eastern Weddell Sea, Antarctica: Plankton biomass and composition in relation to hydrography and nutrients. *Deep-Sea Research*, 41: 1231–1250.

Scheer, H. (2003) The pigments, In Green, B. R. & William, W. P. [Eds] *Light-Harvesting Antennae in Photosynthesis*. Kluwere Academic Publisher, Netherlands, pp. 29–81.

Schellenberger Costa, B., Jungandreas, A., Jakob, T., Weisheit, W., Mittag, M. & Wilhelm, C. (2013) Blue light is essential for high light acclimation and photoprotection in the diatom *Phaeodactylum tricornutum*. *Journal of Experimental Botany*, 64: 483–493.

Schindler, C. & Lichtenthaler, H. K. (1994) Is there a correlation between light-induced zeaxanthin accumulation and quenching of variable chlorophyll a fluorescence? *Plant Physiology and Biochemistry*, 32: 813–823.

Schreiber, U., Schliwa, U. & Bilger, W. (1986) Continuous recording of photochemical and non-photochemical chlorophyll fluorescence quenching with a new type of modulation fluorometer. *Photosynthesis Research*, 10: 51–62.

Schumann, A., Goss, R., Jakob, T. & Wilhelm, C. (2007) Investigation of the quenching efficiency of diatoxanthin in cells of *Phaeodactylum tricornutum* (Bacillariophyceae) with different

pool size of xanthophyll cycle pigments. *Phycologia*, 46: 113–117.

Shirasawa, K., Leppäranta, M., Saloranta, T., Kawamura, T., Polomoshnov, A. & Surkov, G. (2005) The thickness of coastal fast ice in the Sea of Okhotsk. *Cold Region Science and Technology*, 42: 25–40.

Sicko-Goad, L., Stoermer E. F., Kociolek, J. P. (1989) Diatom resting cell rejuvenation and formation: Time course, species records and distribution. *Journal of Plankton Research*, 11: 375–389.

Smayda, T. J. (1958) Biogeographical studies of marine phytoplankton. *Oikos*, 9: 29–32.

Smayda, T. J. (1980) Phytoplankton species succession. In Morris, I. [Ed.] *The Physiological Ecology of Phytoplankton*. University of California Press, California, USA, pp. 493–570.

Smith, W. O. & Nelson, D. (1986) Importance of ice edge phytoplankton production in the Southern Ocean. *BioScience*, 36: 251–257.

Suzuki, R. & Ishimaru, T. (1990) An improved method for the determination of phytoplankton chlorophyll using N, N-dimethylformamide. *Journal of Oceanographical Society of Japan*, 46: 190–194.

Taguchi, S. & Takahashi, M. (1993) Ecosystem of Lake Saroma under sea ice covered condition in winter: Summary of the plankton colloquim. *Bulletin of the Plankton Society of Japan*, 39: 152–514.

Takahashi, K., Nagao, N. & Taguchi, S. (2015) Diel distribution and feeding habits of Neomysis mirabilis under seasonal sea ice in a subarctic lagoon or northern Japan. *Aquatic Biology*, 23: 183–190.

Tomas, C. R. (1997) *Identifying marine phytoplankton*. Academic Press, San Diego, USA.

Van de Poll, W. H., Alderkamp, A. -C., Janknegt, P. J., Roggeveld, J. & Buma, A. G. J. (2006) Photoacclimation modulates excessive photosynthetically active and ultraviolet radiation effects in a temperate and an Antarctic marine diatom. *Limnology and Oceanography*, 51: 1239–1248.

Van de Poll, W. H., Lagunas, M., de Vries, T., Visser, R. J. W. & Buma, A. G. J. (2011) Non-photochemical quenching of chlorophyll fluorescence and xanthophyll cycle responses after excess PAR and UVR in *Chaetoceros brevis*, *Phaeocystis antarctica* and coastal Antarctic phytoplankton. *Marine Ecological Progress Series*, 426: 119–131.

Walters, R. G. & Horton, P. (1991) Resolution of components of non-photochemical chlorophyll fluorescence quenching in barley leaves. *Photosynthesis Research*, 27: 121–133.

Webb, W. L., Newton, M. & Starr, D. (1974) Carbon dioxide exchange of *Alnus rubra*: a mathematical model. *Oecologia*, 17: 281–291.

White, A. J. & Critchley, C. (1999) Rapid light curves: A new fluorescence method to assess the state of the photosynthetic apparatus. *Photosynthesis Research*, 59: 63-72.

Wilhelm, C., Büchel, C., Fisahn, J., Goss, R., Jakob, T., LaRoche, J., Lavaud, J., Lohr, M., Riebesell, U., Stehfest, K., Valentin, K. & Kroth, P. G. (2006) The regulation of carbon and nutrient assimilation in diatoms is significantly different from green algae. *Protist*, 157: 91–124.

Wu, H., Roy, S., Alami, M., Green, B. R. & Campbell, D. A. (2012) Photosystem II photoinactivation, repair, and protection in marine centric diatoms. *Plant Physiology*, 160: 464–476.

Wulff, A., Roleda, M., Zacher, K. & Wiencke, C. (2008) Exposure to sudden light burst after prolonged darkness-a case study on benthic diatoms in Antarctica. *Diatom Research*, 23: 519–532.

Young, A. J., Phillip, D., Ruban, A. V., Horton, P. & Frank, H. A. (1997) The xanthophyll cycle and carotenoid-mediated dissipation of excess excitation energy in photosynthesis. *Pure and Applied Chemistry*, 69: 2125–2130.

APPENDICES

Appendix 1. The parameters of DT in the Chapter III. [a] The value of *k* was estimated during the first 3 min. [b] The rate of de novo DT synthesis was estimated from 0 min to the end of light exposure. [c] The maximum values of $DT^{XC}_{Chl\ a}$ and $DT^{de\ novo}_{Chl\ a}$ were estimated from the value of rate of *de novo* DT synthesis.

Group or location	Major species	Temp. (°C)	Light exposure		DT						References
			Intensity (μmol photons m^{-2} s^{-1})	Period (min)	*k* (min^{-1})	Maximum $DT_{Chl\ a}$ (mol DT [100 mol Chl *a*]$^{-1}$)	Maximum DT/(DD+DT) (%)	Rate of *de novo* DT synthesis (mol DT [100 mol Chl *a*]$^{-1}$ min]$^{-1}$)	Maximum $DT^{XC}_{Chl\ a}$ (mol DT [100 mol Chl *a*]$^{-1}$)	Maximum $DT^{de\ novo}_{Chl\ a}$ (mol DT [100 mol Chl *a*]$^{-1}$)	
Mesophilic diatoms											
	Chaetoceros gracilis	20	400	180	0.2	10.5	75	0	10.5	0	Kashino and Kudoh (2003)
	Chaetoceros muelleri	24	1500	30	1.60	10.2	40	0.14[b]	6.0[d]	4.2[c]	Olaizola and Yamamoto (1994)
	Chaetoceros muelleri	20	900	120	0.151	10.7	48.2	0.0836	2.15	10.0	Present study
	Cylindrotheca fusiformis	20	2000	60	1.2	3.3	46	0.026	2.7[d]	0.78[c]	Lavaud et al. (2004)
	Ditylum brigthwellii	20	2000	60	1.2	3.8	44	0.024	2.6[d]	1.2[c]	Lavaud et al. (2004)
	Phaeodactylum tricornutum	20	800	15	—	7.0	—	—	7.0	—	Goss et al. (2006)
	Phaeodactylum tricornutum	20	450	60	1.4	—	—	0.027	—	—	
		20	2000	60	2.2	6.1	55	0.054	4.5[d]	1.6[c]	Lavaud et al. (2004)
	Phaeodactylum tricornutum	20	700	30	0.262	28	87	0.10[b]	25[e]	3.1[c]	Lohr and Wilhelm (1999)
	Phaeodactylum tricornutum	18	415	120	0.131	11	35	0.0428	8.7[d]	5.1[c]	Olaizola et al. (1994)
		18	750	120	0.089	21	51	0.0593	13[d]	7.1[c]	
		18	1500	120	0.105	27	71	0.113	14[d]	14[e]	
	Phaeodactylum tricornutum	18	2000	60	—	5.9	—	—	5.9	—	Lavaud and Lepetit (2013)
	Skeletonema costatum	20	2000	120	1.7	7.2	53	0.059	5.4[d]	1.8[c]	Lavaud et al. (2004)
	Skeletonema costatum	18	2000	60	—	7.0	—	—	7.0	0	Lavaud and Lepetit (2013)
	Thalassiosira pseudonana	20	800	15	—	7.4	—	—	7.4	—	Goss et al. (2006)
	Thalassiosira pseudonana	12	450	90	—	8.1	50	0.044[b]	4.6[d]	3.9[c]	Wu et al. (2012)
		18	450	90	—	7.6	52	0.053[b]	2.8[d]	4.8[c]	
		24	450	90	—	8.7	61.0	0.041[b]	5.0[d]	3.7[c]	
	Thalassiosira pseudonana	20	900	120	0.234	13.7	72.1	0.0509	7.60	6.10	Present study
	Thalassiosira weissflogii	20	2000	60	1.4	4.9	41	0.036	3.7[d]	1.2[c]	Lavaud et al. (2004)
	Thalassiosira weissflogii	20	900	120	0.232	20.2	72.7	0.148	2.43	17.8	Present study
Ice algal communities											
Antarctic	*Fragilariopsis curta*	−1.8	200	300	—	—	39.0	—	—	—	Petrou et al. (2011)
McMurdo Sound	*Berkelaya adeliense*	−1.8	200	60	1.3	2	31	0	2	0	Griffith et al. (2009)
McMurdo Sound	*Berkelaya adeliense*	−1.8	200–800	240	0.21	25	84	0	25	0	Griffith et al. (2009)
Terra Nova Bay	—	<0	925	120	—	0.8	43	—	0.8	—	Mangoni et al. (2009)
Saroma-Ko Lagoon	—	<0	100	120	0.25[a]	0.9	25	0	0.9	0	Kudoh et al. (2003)
Saroma-Ko Lagoon	*Pinnularia quadratarea* var. *constricta*	−1	520–1145	120	0.168	1.93	25.4	0	1.93	0	Present study
	Detonula confervacea	−1	994–1691	120	0.198	1.03	21.9	0	1.03	0	
		−1	335– 725	120	0.304	4.50	44.9	0	4.50	0	
		−1	426–1182	120	0.205	1.48	28.9	0	1.48	0	

Appendix 2. The parameters of NPQ and F_v/F_m in the Chapter III. [a] Slopes for mesophilic diatoms were determined by light exposure for 5 min at varying light intensity and 60 min at fixed high light intensity as shown below.

Group or location	Major species	Temp. (°C)	Light exposure		NPQ		F_v/F_m			References
			Intensity (μmol photons m^{-2} s^{-1})	Period (min)	Maximum NPQ (relative unit)	Slope of $DT_{Chl\ a}$ vs NPQ (100 mol Chl *a* [mol DT]$^{-1}$)	Decrease in F_v/F_m (%)	Slope of $DT^{XC}_{Chl\ a}$ vs F_v/F_m (100 mol Chl a [mol DT]$^{-1}$)	Slope of $DT^{de\ novo}_{Chl\ a}$ vs F_v/F_m (100 mol Chl a [mol DT]$^{-1}$)	
Mesophilic diatoms										
Chaetoceros gracilis		20	400	180	—	—	—	—	—	Kashino and Kudoh (2003)
Chaetoceros muelleri		24	1500	30	2.4	—	65	−11	—	Olaizola and Yamamoto (1994)
Chaetoceros muelleri		20	900	120	2.06	0.609	19.9	− 8.62	−14.4	Present study
Cylindrotheca fusiformis		20	2000	60	3.7	0.96[a]	—	—	—	Lavaud et al. (2004)
Ditylum brigthwellii		20	2000	60	4.1	1.04[a]	—	—	—	Lavaud et al. (2004)
Phaeodactylum tricornutum		20	800	15	1.9	—	—	—	—	Goss et al. (2006)
Phaeodactylum tricornutum		20	450	60	—	—	—	—	—	
		20	2000	60	4.5	0.95[a]	—	—	—	Lavaud et al. (2004)
Phaeodactylum tricornutum		20	700	30	—	—	—	—	—	Lohr and Wilhelm (1999)
Phaeodactylum tricornutum		18	415	120	1.1	—	30	—	—	Olaizola et al. (1994)
		18	750	120	2.3	—	53	—	—	
		18	1500	120	3.4	—	81	—	—	
Phaeodactylum tricornutum		18	2000	60	5.6	0.95	—	—	—	Lavaud and Lepetit (2013)
Skeletonema costatum		20	2000	120	3.0	0.49[a]	—	—	—	Lavaud et al. (2004)
Skeletonema costatum		18	2000	60	3.0	0.49	—	—	—	Lavaud and Lepetit (2013)
Thalassiosira pseudonana		20	800	15	1.4	—	—	—	—	Goss et al. (2006)
Thalassiosira pseudonana		12	450	90	—	—	—	—	—	Wu et al. (2012)
		18	450	90	—	—	—	—	—	
		24	450	90	—	—	—	—	—	
Thalassiosira pseudonana		20	900	120	2.17	0.155	61.6	−10.3	−53.8	Present study
Thalassiosira weissflogii		20	2000	60	3.3	0.99[a]	—	—	—	Lavaud et al. (2004)
Thalassiosira weissflogii		20	900	120	1.57	0.634	30.5	−10.7	−17.9	Present study
Ice algal communities										
Antarctic	*Fragilariopsis curta*	−1.8	200	300	—	—	29	—	—	Petrou et al. (2011)
McMurdo Sound	*Berkelaya adeliense*	−1.8	200	60	—	—	—	—	—	Griffith et al. (2009)
McMurdo Sound	*Berkelaya adeliense*	−1.8	200–800	240	—	—	—	—	—	Griffith et al. (2009)
Terra Nova Bay	—	<0	925	120	—	—	—	—	—	Mangoni et al. (2009)
Saroma-Ko Lagoon	—	<0	100	120	—	—	—	—	—	Kudoh et al. (2003)
Saroma-Ko Lagoon	*Pinnularia quadratarea* var. *constricta*	−1	520–1145	120	2.90	2.00	87.1	−62.0	—	Present study
	Detonula confervacea	−1	994–1691	120	1.66	1.43	97.2	−97.0	—	
		−1	335– 725	120	1.88	0.424	74.9	−20.8	—	
		−1	426–1182	120	2.46	1.65	93.4	−72.5	—	